Z-scan and Degenerate Four Wave Mixing Studies in Certain Photonic Materials

Unnikrishnan K P

International School of Photonics
Cochin University of Science & Technology
Cochin – 682 022, India

Ph D Thesis submitted to
Cochin University of Science & Technology
in partial fulfillment of the requirements for the
Degree of Doctor of Philosophy

March 2003

G 85 12

Z-scan and Degenerate Four Wave Mixing Studies in Certain Photonic Materials
Ph. D Thesis in the field of Photonic Materials

Author
Unnikrishnan. K. P
Research Fellow, International School of Photonics
Cochin University of Science & Technology, Cochin – 682 022, India
kpu@cusat.ac.in; kpunnikrishnan_1999@yahoo.com

Research Supervisor
Dr. C. P. Girijavallabhan
Professor, International School of Photonics
Director, Centre for Excellence in Lasers & Optoelectronic Sciences
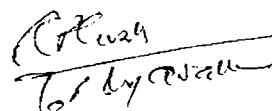Cochin University of Science & Technology, Cochin – 682 022, India
vallabhan@cusat.ac.in

CERTIFICATE

Certified that the work presented in the thesis entitled *"Z-scan and degenerate four wave mixing studies in certain photonic materials"* is based on the original work done by Mr. Unnikrishnan K P, under my guidance and supervision at the International School of Photonics, Cochin University of Science & Technology, Cochin - 682 022, India and it has never been included in any other thesis submitted previously for award of any degree.

Cochin - 682 022

March 10, 2003

Prof. C. P. Girijavallabhan

DECLARATION

Certified that the work presented in this thesis entitled *"Z-scan and degenerate four wave mixing studies in certain photonic materials"* is based on the original work done by me under the guidance and supervision of Dr. C P Girijavallabhan, Professor, International School of Photonics, Cochin University of Science & Technology, Cochin - 682 022, India and it has not been included in any other thesis submitted previously for award of any degree.
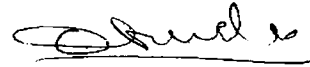
Cochin - 682 022

March 10, 2003
                                     Unnikrishnan. K. P

Preface

Observation of second harmonic generation (SHG) by P A Franken in 1961 marked the birth of nonlinear optics as a new discipline of laser matter interaction. Nonlinear optics is the study of phenomena that result from light induced modifications in the optical properties of the materials. This branch of science explores the coherent coupling of two or more electromagnetic fields in a nonlinear medium to generate new frequencies that are sum or difference of coupling frequencies. Franken attributed the new result to coherent mixing of two optical fields at 694 nm to produce an optical field at 347 nm.

Since then nonlinear optics has been an important area of science and technology. Interest in the study of nonlinear laser matter interactions arises because of two main reasons: (1) it is an effective method of understanding the nonlinear optical (NLO) properties of materials as well as spatial and temporal evolution of the nonlinearity and (2) a number of technological application have been realized and many others have been proposed using NLO effects. In this context investigation of NLO properties of certain important photonic materials was chosen as the topic of research outlined in the proposed thesis. Third order NLO effects are particularly interesting partly because third order effects have greater technological relevance and partly because third order effects are present, in varying degree of strength, in all materials irrespective of symmetry of materials. Organic materials, nanomaterials and photonic band gap materials are among the NLO materials of recent interest. Phthalocyanines (Pcs) and naphthalocyanines (Ncs) are typical organic NLO materials. They form one class of materials investigated here. The other type of material studied in this work is silver nanosol, aqueous solution of silver nanoparticles, which may be considered as a representative of nanomaterials. Origin and dynamics of linear as well as nonlinear optical properties of nanoparticles are completely different from those of organic compounds like Pcs and thus two distinct class of materials have been

investigated. Degenerate four wave mixing and Z-scan were chosen as the experimental techniques for the present investigation. The proposed thesis contains seven chapters. The content of each chapter is described briefly.

Chapter 1: In this chapter, the basic concepts and salient features of nonlinear optics are described. Some of the important nonlinear optical effects like optical limiting, optical phase conjugation (OPC) and second harmonic generation (SHG) are mentioned and a few applications of these phenomena in technology are explained. A brief survey of important NLO materials such as organic materials, nanoparticles, nanotubes, quantum wires, quantum dots, photonic band gap (PBG) materials is also given. Emphasis is given to organic materials like Pcs and metal nanoparticles, which are the materials of present investigation. The motivation for the present work as well as concise description important results obtained during this work is given at the end.

Chapter 2: This chapter contains the relevant theory and experimental details of the degenerate four wave mixing (DFWM) and Z-scan techniques. Back scattering geometry of DFWM was used for the experiments. Variants of Z-scan techniques and other possible configurations of DFWM are mentioned. Specifications of excitation sources and other instruments used for making the measurements are also given.

Chapter 3: This chapter contains the results obtained from open aperture Z-scan experiments carried out in solutions of metal substituted phthalocyanines and naphthalocyanines at a fixed wavelength (532nm). Nonlinear absorption coefficient was measured and optical limiting property of these samples was analyzed. All these samples were found to exhibit reverse saturable absorption (RSA) at this wavelength. Samples selected include metal mono phthalocyanines (LaPc, MoOPc) metal subsituted naphthalocyanines (ZnNc, MgNc) , metal substituted bis – phthalocyanines [Eu(Pc)$_2$, Sm(Pc)$_2$, Nd(Pc)$_2$] and a bis- naphthalocyanine Eu(Nc)$_2$. It may be noted that the samples selected cover different structural variants of phthalocyanines.

Besides, metal ions are also different. Among (mono) MPcs, LaPc was found to be better nonlinear absorber. Among bis-Pcs, Eu(Pc)$_2$ was found to be better nonlinear absorbing material. Pcs in solution form can exhibit negative nonlinear refraction due to thermal lensing effect. Closed aperture measurements were taken in solutions of Pcs and exhibited thermal nonlinearity as expected.

Chapter 4: Studies on wavelength dependence of nonlinear absorption in bis-Pcs are too few. In this chapter, a comparative study of wavelength dependence of nonlinear absorption in three bis - Pcs viz. Eu(Pc)$_2$, Sm(Pc)$_2$ and Nd(Pc)$_2$ in the blue side of their Q-band is given. Objective of the work was to find out the upper wavelength limit for reverse saturable absorption. Such studies help to know whether these samples exhibit optical limiting property over a wide spectral range. Besides, saturation intensity I$_s$, nonlinear absorption coefficient β and imaginary part of third order susceptibility Im[$\chi^{(3)}$] were measured and resonant enhancement of Im[$\chi^{(3)}$] was also investigated. It was observed that magnitude of resonant enhancement is different in these samples. Nd(Pc)$_2$ exhibited resonant enhancement of two orders of magnitude but in other two samples, resonant enhancement was not as intense as in the case of Nd(Pc)$_2$. While Eu(Pc)$_2$ and Nd(Pc)$_2$ exhibited reverse saturable absorption at 604nm, Sm(Pc)$_2$ exhibited a clear saturable absorption at this wavelength. Since all these samples have similar structures, small but experimentally observable differences between these samples might be arising from slightly varying influence of these metal ions.

Chapter 5: This chapter contains the results of degenerate four wave mixing studies carried out in solutions of metal substituted phthalocyanines and naphthalocyanines. Polarizations of interacting beams were so chosen that formation of thermal grating is prevented so that the response we get is entirely electronic. Third order susceptibility $\chi^{(3)}$, figure of merit of third order nonlinearity F = $\chi^{(3)}$/α and isotropically averaged second hyperpolarizability $\langle\gamma\rangle$ were measured. Samples selected include metal mono

phthalocyanines (LaPc, MoOPc, FePc), metal subsituted naphthalocyanines (ZnNc, MgNc, VoONc), metal substituted bis – phthalocyanines [Eu(Pc)$_2$, Sm(Pc)$_2$] and a bis- naphthalocyanine Eu(Nc)$_2$. It may be noted that the samples selected covers different structural variants of Pcs with different levels of π electron conjugation. Moreover metal substituents in these samples also vary. Level of π electron conjugation, nature of metal substituent and dimensionality of the molecules significantly influence the $\langle\gamma\rangle$ values. The measurements were carried out with view to exploring the combined influence of these factors on $\langle\gamma\rangle$. The results obtained were explained by taking in to account the level of π electron conjugation, nature of metal substituent and dimensionality of the samples.

Chapter 6: The results of nonlinear absorption studies in silver nanosol using open aperture Z-scan technique at selected wavelengths near plasmon band are included in this chapter. Nanosol exhibited surface plasmon resonance (SPR) peak around 416nm. An interesting result of this investigation is that this material could act as a reverse saturable absorber and a saturable absorber at the same wavelength, depending entirely on the incident intensity. The results were explained in terms of plausible effects of SPR bleach and photochemical change induced absorption. Besides, closed aperture Z-scan experiments were also performed at 532nm, but result was negative. Divided Z-scan curve did not reveal any sign of positive or negative refraction. Possible reasons for this negative result are also mentioned.

Chapter 7: This chapter contains a brief description of future prospects along with summary and conclusions.

Most of the results included in this thesis have been published / communicated for publication, details of which are given below.

Publications (in journals)

1. Third order nonlinear optical studies in europium naphthalocyanine using degenerate four wave mixing and Z-scan **K P Unnikrishnan**, Jayan Thomas, V P N Nampoori, C P G Vallabhan, Opt. Commun. **204** (2002) p. 385 – 390

2. Degenerate four wave- mixing in some metal phthalocyanines and naphthalocyanines by **K P Unnikrishnan**, Jayan Thomas, V P N Nampoori, C P G Vallabhan, Chem. Phys. **279** (2002) p. 209-213

3. Wavelength dependence of nonlinear absorption in a bis-phthalocyanines studied using Z-scan technique. **K P Unnikrishnan**, Jayan Thomas, V P N Nampoori and C P G Vallabhan, App. Phys. B. **75** (2002) p. 871-874

4. Nonlinear absorption in certain metal phthalocyanines at resonant and near resonant wavelengths. **K P Unnikrishnan**, Jayan Thomas, V P N Nampoori, C P G Vallabhan, Opt. Commun. **217** (2003) p. 269 - 274

5. Nonlinear absorption and optical limiting in solutions of some rare earth substituted phthalocyanines. **K P Unnikrishnan**, Jayan Thomas, Binoy Paul, Achamma Kurian, Pramod Gopinath, V P N Nampoori and C P G Vallabhan, J. of Non. Opt. Phys. & Mater. **10**. No. 1(2001) p. 113-121

6. Second hyperpolarizability of certain phthalocyanines and naphthalocyanines. **K P Unnikrishnan**, Jayan Thomas, V P N Nampoori and C P G Vallabhan, Submitted to Synthetic Metals

7. Nonlinear optical absorption silver nanosol: **K P Unnikrishnan**, V P N Nampoori, V Ramakrishnan and M Umadevi and C P G Vallabhan. Communicated to J. Physics. D. App. Phys.

In conference proceedings

1. Nonlinear absorption and optical limiting in solutions of a bis-phthalocyanine. **K P Unnikrishnan**, B Paul, A Kurian, P Gopinath, V P N Nampoori and C P G Vallabhan, Proceedings of the National Laser Symposium – 2000 (NLS- 2000). A Malik, K N Srivastava and S Pal (Eds). Allied Publishers Ltd. New Delhi. p. 167

2. Degenerate four wave mixing in some metal phthalocyanines; **K P Unnikrishnan**, V P N Nampoori and C P G Vallabhan, Proceedings of National Laser Symposium(NLS-2001) p. 279 Allied Publishers (New Delhi)

3. Nonlinear optical absorption in silver nanosol. **K P Unnikrishnan**, V P N Nampoori, M Umadevi, V Ramakrishnan and C P G Vallabhan, Proceedings of the National Laser Symposium – 2002 (NLS- 02). Allied Publishers Ltd. New Delhi. p. 550

4. Nonlinear absorption in a bis-phthalocyanine: $Sm(Pc)_2$. **K P Unnikrishnan**, Jayan Thomas, V P N Nampoori and C P G Vallabhan, Proceedings of International Conference in on Fibre Optics and Photonics (in CD form). PHOTONICS - 2002 held at TIFR, Mumbai, India

ACKNOWLEDGEMENT

who helped me in one way or other for the successful completion of my research work.

I would like to remember with deep sense of gratitude the support received from the parents during the present work

Unnikrishnan K P

Contents

Chapter 3: Nonlinear absorption in phthalocyanines and naphthalocyanines at a fixed wavelength (532 nm)

1

Introduction
Nonlinear optics and nonlinear optical materials

Abstract

The fundamentals of nonlinear optics are introduced in this chapter. Physical origin of optical nonlinearity and the concept of phase matching are explained. A few important applications of nonlinear optical effects are also described briefly. An over view of important nonlinear optical (NLO) materials is given. A few of the materials investigated in this thesis viz., phthalocyanines, naphthalocyanines and nanoparticles, are described in detail.

1. Introduction

Observation of the second harmonic generation (SHG) by P A Franken in 1961 marked the birth of nonlinear optics as a new discipline in the area of laser-matter interaction. Franken observed that light of 347.1 nm could be generated when a quartz crystal was irradiated with light of 694.2 nm, obtained from a ruby laser. He attributed this novel result to the coherent mixing of two optical fields at 694.1 nm in the crystal to produce 347.1 nm [1]. Nonlinear optics is essentially concerned with the study of phenomena that result from field induced modifications in the optical properties of the materials. This branch of science explores the coherent coupling of two or more electromagnetic fields in a nonlinear medium. During these coupling processes, new frequencies can be generated that are the sum or the difference of the coupling frequencies. Though the discovery of SHG marked the birth of nonlinear optics as a new branch of experimental investigation, SHG was not the first nonlinear optical (NLO) effect to be observed. Optical pumping is a nonlinear optical phenomenon, which was known prior to the invention of laser [2]. A brief description of NLO interactions and NLO materials is given in the following sections.

2. Nonlinear polarization

Light is transverse electromagnetic (EM) wave. EM field is a vector field. Therefore, in principle, when interaction of light with matter is formulated, the effect of both the electric field ($\bar{E}$) and magnetic field ($\bar{B}$) as well as their directional nature must be considered. Besides, spatial and temporal variation of $\bar{E}$ & $\bar{B}$ is also to be taken into account [2]. However, light-matter interaction in nonmagnetic materials is described in terms of $\bar{E}$ only. In non-magnetic materials, $\bar{B}$ is neglected [3]. Magnitude of $\bar{B}$ is less than that of $\bar{E}$. In fact, $\bar{B}$ is related to $\bar{E}$ through the velocity of light, c by the relation

$$\bar{B} = \bar{E}/c \qquad (1.1)$$

Based on the concept of harmonic oscillator, the basic physics of the light-matter interaction can be summarized briefly as follows. $\bar{E}$ of light can interact with charged particles in the matter, mainly electrons, and hence distort the equilibrium charge distribution, which results in the separation of unlike charges to produce an electric polarization. The polarization thus generated is related to externally applied electric field through a characteristic property of the medium, called optical susceptibility [χ] [2]. It determines the magnitude as well as the direction of induced electric polarization for a given field strength, at a particular wavelength. The magnitude of optical susceptibility depends on various factors such as molecular and atomic structure of the materials, wavelength of excitation and intensity of light [2]. It has been found that when excitation intensity is increased, induced polarization becomes a nonlinear function of applied electric field strength [2,4-6]. The consequence of the nonlinear relationship between $\bar{E}$ and $\bar{P}$ is that, at very high values of intensity, a number of new and interesting phenomena begin to manifest macroscopically.

In this context, it is highly desirable to examine the strength $\bar{E}$ associated with light obtained from various sources used for optical excitation and compare the same with interatomic field. $\bar{E}$ associated with conventional light sources such as Xenon lamp and Mercury lamp, which were mainly used to excite samples in the pre-laser era, is very low in comparison with interatomic electric field. Because of its low electric field strength, light from conventional sources cannot appreciably perturb the molecular charge distribution. For instance, atomic field is of the order of 10^8 or 10^9 Vcm^{-1} [2, 6, 7], whereas electric field strength associated with conventional sources is $10^2 - 10^5$ Vcm^{-1}. Under the action of such a low electric field, electrons bound to the nucleus are displaced only by about 10^{-18} m, which is very small in comparison with interatomic distance, of the order of 10^{-10} m [4]. Therefore, it can be said that this small displacement is within the elastic limit and hence, there is no unharmonicity in the oscillations of induced polarization. Hence, measurements using conventional

light sources gave a polarization $\vec{P}$, which is linearly dependent on electric field strength. $\vec{P}$, in this case can be written as [6]

$$\vec{P} = \varepsilon_0 \chi^{(1)} \vec{E} \tag{1.2}$$

where ε_0 is the susceptibility of vacuum. This domain of interaction of electric field with matter is referred to as linear optics. Linear effects, also called first order effects, include linear optical properties such as linear refractive index, linear absorption, and birefringence.

With invention of lasers, which has high degree of spectral purity, coherence and directionality, it has become possible to irradiate atoms and molecules with an $\vec{E}$ that is comparable to interatomic field. This is because of the fact that lasers can be focussed to a very small spot size, of the order of its wavelength, giving very large intensity and consequently extremely high electric field strength, at the focal region. This results in a considerable distortion of the equilibrium charge distribution, which gives rise to a large displacement of electrons with respect to their equilibrium position. Consequently, vibration of the electrons becomes highly unharmonic. It is also interesting to note that, when laser beam is tightly focussed photon density at the focal region approaches atomic density. In such cases, the potential which electrons experience cannot be approximated to a parabolic one. Consequence of this unharmonicity is that unlike in eq.(1.2), induced polarization becomes a function of higher powers of electric field too, i.e. nonlinear dependence on electric field strength. In such cases the polarization is expressed as a power series in the applied field as [8]

$$\vec{P}_{NL} = \varepsilon_0 \left(\chi^{(1)} E + 2D_2 \chi^{(2)} E_1 E_2 + 4D_3 \chi^{(3)} E_1 E_2 E_3 + \cdots \cdots \right) \tag{1.3}$$

Here, $\chi^{(2)}$ and $\chi^{(3)}$ correspond to second order and third order susceptibilities respectively. D_1, D_2 etc. are related to degeneracy [8]. In the nonlinear optical regime, a number of interesting phenomena that are conspicuous by their absence in linear regime, emerge. One significant difference between linear and nonlinear optical interactions is that unlike in the linear case, in nonlinear optical processes two light beams can interact and exchange energy through induced nonlinear polarization of the medium [2]. In the case of very intense laser beams, even air itself can act as nonlinear medium. It is well known that femtosecond laser pulses get self-focussed in air [9]. One of the best examples of nonlinear process is the generation of super continuum (white light), which occurs when some materials are irradiated with terra watts of power. Many of these nonlinear optical effects have important scientific and technological relevance. Therefore, study of nonlinear effects is very important. It helps us to understand the mechanism of nonlinearity as well as its spatial and temporal evolution. Besides, detailed knowledge of NLO processes and their dynamics is also essential for the implementation of these techniques in appropriate areas of technology such as optical switching [10], optical communication [11], passive optical power limiting [12-14], data storage [15] and design of logic gates [16,17].

The wavelength at which nonlinear parameters are measured is also important. If the wavelength of excitation is close to one, two or three-photon resonance, resonant enhancement of nonlinearity will occur. At and near resonant frequencies, refractive index becomes a complex quantity. If wavelength of the light interacting with matter is at or near resonance, the power series expansion as in eq.(1.3) is not relevant. In the case of resonant excitation [2] (one photon, two-photon or three-photon), the nonlinear susceptibility term corresponding to resonant absorption can have enormously large magnitude. Generally, resonant nonlinearity has large magnitude but slow response, whereas non-resonant nonlinearity has very fast response but low in magnitude. Usually, observed nonlinear susceptibility is due to the response of

weakly bound outer most electrons of atoms or molecules. If $\bar{E}_a$ is the average electric field experienced by such electrons due to nucleus and neighboring electrons, we can consider the expansion in eq.(1.3) in terms of a dimensionless quantity, $\bar{E}/\bar{E}_a$. If the wavelength of excitation is far away from resonance, order of magnitude of nonlinear susceptibility terms can then be written as $\langle \chi^{(2)} \rangle \approx \langle \chi^{(1)} \rangle / E_a$ and $\langle \chi^{(3)} \rangle \approx \langle \chi^{(1)} \rangle / E_a^2$ and so on [2]. However, if the wavelength of excitation is very close to any of resonant frequency, magnitude of nonlinearity can be much higher. If the expansion of nonlinear polarization as power series in electric field is valid, the corresponding nonlinearity is called weak nonlinearity. On the other hand, if the frequency of excitation is very close to resonance, power series expansion as in eq. (1.3) is not correct. Such nonlinearity is called strong nonlinearity [2].

3. Some important nonlinear effects

All the nonlinear optical effects can be broadly classified into two categories; one is concerned with frequency conversion and the other one is concerned with optical modulation [18]. Examples of frequency conversion processes are sum and difference frequency generations. Processes concerned with optical modulation include Kerr effect, self phase modulation etc. In optical modulation processes, light modulates some property of the medium like refractive index. Generation of new frequencies in frequency conversion processes is due to the oscillations of induced nonlinear polarization at appropriate frequency. Obviously, frequency conversion processes are instantaneous and take place in a time scale as short as the inverse of the frequencies involved ($\approx v^{-1}$). However, common practice is to broadly classify the NLO effects on the basis of the susceptibility term involved like second order, third order etc.

All the nonlinear optical interactions consist of two successive processes; (1) intense light beam induces a nonlinear response (i.e. nonlinear polarization) in the medium and (2) the medium reacts on the light, which induced the nonlinear polarization, and modifies the light in a nonlinear way [2,8]. The first process is governed by the

constitutive equations, which are general relations between external field and induced polarization, written in terms of optical susceptibility $\chi^{(n)}$. The second process is governed by Maxwell's equations, which describe the generation of new frequencies in presence of nonlinear polarization. It is to be noted that the nonlinear polarization acts as a source term in Maxwell's equations [2,8].

All the nonlinear interactions should satisfy certain conditions called "phase matching condition" for macroscopic manifestation of NLO effects [2]. Physically, this corresponds to the necessary condition for the constructive interference of new waves generated in the interaction length. Mathematically, phase matching condition can be written as

$$\vec{k}_f - \vec{k}_i = \Delta\vec{k} = 0 \qquad (1.4)$$

i.e. change in wave vector must be zero. If this condition is not satisfied, we will not be able to observe any nonlinear effects macroscopically, even if the medium is nonlinear. Phase matching condition depends on a number of factors such as polarization of the light, symmetry of the sample etc.

As indicated earlier, propagation of EM waves in a nonlinear medium is governed by Maxwell's equation [2]

$$\nabla^2 \vec{E} = \sigma\mu \frac{\partial \vec{E}}{\partial t} + \mu\varepsilon \frac{\partial^2 \vec{E}}{\partial t^2} + \mu \frac{\partial^2}{\partial t^2} \vec{P}_{NL}(r,t) \qquad (1.5)$$

Here σ, μ and ε are conductivity, magnetic permeability and susceptibility of the medium respectively. It is interesting to point out here that while Maxwell's equation explains how new frequencies are generated in a nonlinear medium in presence of nonlinear polarization, it does not tell how a nonlinear polarization is generated. The later part is described solely by constitutive equations.

3.1 Second order effects

Second order effects which are related to $\chi^{(2)}$, correspond to all three wave mixing phenomena such as second harmonic generation (SHG) $\chi^{(2)}(2\omega; \omega, \omega)$, optical rectification $\chi^{(2)}(0; \omega, -\omega)$, parametric mixing $\chi^{(2)}(\omega_1 \pm \omega_2; \omega_1, \pm \omega_2)$, Pockel's effect $\chi^2(\omega;\omega, 0)$ [8]. Constitutive equation for typical second order process, under dipole approximation, is given by [5]

$$P_i^{(2\omega)} = \sum_{j,k=x,y,z} d_{ijk}^{2\omega} E_j^{(\omega)} E_k^{(\omega)} \qquad (1.6)$$

Summation over repeated index is assumed. Centro symmetric materials posses inversion symmetry i.e. $V(r) = V(-r)$. Eq. (1.6) can satisfy this requirement only if $d_{ijk}^{(2\omega)}$ vanishes completely. Hence, second order effects appear only in non-centro symmetric materials. The most popular second order effect is SHG. Efficiency of SHG is proportional to phase mismatch Δk as given by the relation [5]

$$\eta_{SHG} \propto \frac{\sin^2(\Delta kl/2)}{(\Delta kl/2)^2} \qquad (1.7)$$

It is obvious that as Δk deviate from zero, the conversion efficiency steadily decreases.

3.2 Third order effects

Third order effects involve all four wave-mixing phenomena. Some of the important third order effects are third harmonic generation (THG) $\chi^{(3)}(3\omega; \omega, \omega, \omega)$, non degenerate four wave mixing $\chi^{(3)}(\omega_1 + \omega_2 \pm \omega_3; \omega_1, \omega_2, \pm \omega_3)$, Raman scattering $\chi^{(3)}$ $(\omega \pm \Omega; \omega, -\omega, \omega \pm \Omega)$, instantaneous AC Kerr effect (degenerate four wave mixing) $\text{Re}\chi^{(3)}(\omega; \omega, \omega, -\omega)$, Brillouin scattering $\chi^{(3)}$ $(\omega \pm \Omega; \omega, -\omega, \omega \pm \Omega)$, DC Kerr effect

Re $\chi^{(3)}(\omega; \omega, 0, 0)$, two photon absorption $\text{Im}[\chi^{(3)}(\omega; \omega, -\omega, \omega)]$ and electric field induced second harmonic generation $\chi^{(3)}(2\omega; \omega, \omega, 0)$ [8].

Unlike $\chi^{(2)}$, $\chi^{(3)}$ is present in all the materials [2], irrespective of their symmetry. Therefore, third order nonlinearity is the lowest order universally occurring nonlinearity. Real part of third order nonlinearity is responsible for optical switching applications while imaginary part is responsible for optical limiting or nonlinear absorption. Therefore, third order nonlinear optical effects are very important in the context of technological applications. The general constitutive equation for the third order process can be written, neglecting nonlocal terms, as

$$\vec{P}_i^{(3)}(r,t) = \sum_{a,d,c} \chi_{ijkl}^{(3)}(\omega_a + \omega_b + \omega_c, \omega_a, \omega_b, \omega_c) E_j(\omega_a, \vec{r}) E_k(\omega_b, \vec{r}) E_l(\omega_c, \vec{r})$$

(1.8)

3.3. Cascaded nonlinearity

Cascaded nonlinearity refers to a situation where a few lower order effects occur in a sample successively to produce an effective higher order nonlinear process. There are many occasions where first order and second order effects or first order and third order nonlinear effects occur successively. For example, in degenerate four-wave mixing experiments (DFWM) if two-photon absorption (TPA) is present, the optical phase conjugate (OPC) signal is related to pump beam intensity through its fifth power, instead of normal cubic dependence [19,20]. Photorefractive effect is also an example for cascaded nonlinear effect. In this case, initially linear absorption (first order phenomenon) takes places in the sample, which is followed by the occurrence of quadratic electro-optic effect, which is a second order phenomenon [21,22]. Therefore, it need to be ensured that in the experiments involving NLO effects, no unintended cascaded nonlinear effects does interfere with measurements.

3.4 Susceptibility tensor and hyperpolarizability

In isotropic materials, orientation of induced polarization $\vec{P}$ or electric induction vector $\vec{D}$, given by eq. (1.9), [23]

$$\vec{D} = \varepsilon\vec{E} = \varepsilon_0\vec{E} + \vec{P} \qquad (1.9)$$

is along the direction of external electric field. But in anisotropic materials, electric induction vector is not oriented along the direction of inducing field alone, but it can have components in other directions as well. Magnitude of different components is usually different. Since refractive index (and hence velocity of light) is related to polarization, non-parallelism between the cause (excitation) and the response (polarization) gives rise to optical anisotropy. Therefore, susceptibility is generally a tensor. Optical double refraction is the most familiar example of optical anisotropy. In the case of solids, the origin of non-parallelism between the response and excitation can be found in the crystalline nature of matter. In this type of materials, the vectorial nature of light is very important [23].

The nth order susceptibility $\chi^{(n)}_{i_1..i_n}$ is a tensor of rank (n+1) with $3^{(n+1)}$ components. However, when symmetry conditions are applied, the number of independent components may be reduced. In certain experiments, it is possible to select different components by properly choosing the polarizations of interacting beams. The susceptibility tensors satisfy symmetry relationship, as shown below [2]:

$$
\left.
\begin{aligned}
&[\chi^{(2)}_{ijk}(\omega_1 + \omega_2, \omega_1, \omega_2)]^* = \chi^{(2)}_{ijk}(-\omega_1 - \omega_2, -\omega_1, -\omega_2) \\[6pt]
&[\chi^{(3)}_{ijkl}(\omega_1 + \omega_2 + \omega_3, \omega_1, \omega_2, \omega_3)]^* = \chi^{(2)}_{ijk}(-\omega_1 - \omega_2 - \omega_3, -\omega_1, -\omega_2, -\omega_3) \\[6pt]
&\chi^{(2)}_{ijk}(\omega_1 + \omega_2, \omega_1, \omega_2) = \chi^{(2)}_{ikj}(\omega_1 + \omega_2, \omega_2, \omega_1) \\[6pt]
&\chi^{(3)}_{ijkl}(\omega_1 + \omega_2 + \omega_3, \omega_1, \omega_2, \omega_3) = \chi^{(3)}_{ikjl}(\omega_1 + \omega_2 + \omega_3, \omega_2, \omega_1, \omega_3)
\end{aligned}
\right\} \qquad (1.10)
$$

For isotropic non dissipative media, there are only three independent components as is evident from following equations [2].

$$\left.\begin{aligned}
&\chi_{xxxx} = \chi_{yyyy} = \chi_{zzzz} \\
&\chi_{yyzz} = \chi_{zzyy} = \chi_{zzxx} = \chi_{xxzz} = \chi_{xxyy} = \chi_{yyxx} \\
&\chi_{yzyz} = \chi_{zyzy} = \chi_{zxzx} = \chi_{xzxz} = \chi_{xyxy} = \chi_{yxyx} \\
&\chi_{yzzy} = \chi_{zyyz} = \chi_{zxxz} = \chi_{xzzx} = \chi_{xyyz} = \chi_{yxxy}. \\
&\chi_{xxxx} = \chi_{xxyy} + \chi_{xyxy} + \chi_{xyyx}
\end{aligned}\right\} \qquad (1.11)$$

Nonlinear susceptibility $\chi^{(n)}$ is a macroscopic quantity, which corresponds to the response of bulk material. Corresponding microscopic quantity is the atomic polarizability $\alpha^{(n)}$. In very dilute media, where dipole-dipole interaction can be neglected, $\chi^{(n)}$ is related to $\alpha^{(n)}$ by the equation [2]

$$\chi^{(n)} = N\alpha^{(n)} \qquad (1.12)$$

where, N is the number of molecules per unit volume. In presence of induced dipole-dipole interaction

$\chi^{(n)} = L^4 N\alpha^{(n)}$ where L, the local field correction factor, is given by $L = \dfrac{(n^2 + 2)}{3}$

(n is the refractive index)

4. Applications

As indicated earlier, there are a number of applications for NLO effects in various fields of technology and basic research [10-17]. Hence, study of NLO effects is highly relevant and desirable. Apart from the magnitude of nonlinearity, other parameters relevant to the applications of NLO effects are its (1) sign, (2) response time and (3) nature (real or imaginary) of the nonlinearity at the wavelength of excitation. In this section, a few important NLO effects are described briefly.

4.1 Frequency mixing

High power lasers in different spectral regions can be obtained by sum and difference frequency generations. For example, lasers in the infrared region can be obtained by difference frequency generation, whereas laser beams in the visible and UV regions can be obtained from sum frequency generations. Frequency doubled YAG laser is the most popular source of green light. Frequency tripled YAG laser is used for fusion applications. Optical parametric oscillators, which work on the principle of parametric wave mixing, are now used to get continuously tunable laser output from 400 nm to 2000 nm [24].

4.2 Optical short pulse generation and measurement

Optical pulses having pulse width less than nanosecond can be obtained only by using nonlinear techniques. Picosecond pulses can be obtained by mode locking technique [5]. Among different mode locking techniques, passive mode locking using nonlinear saturable absorbers is preferred due to intrinsic speed limit of active mode locking techniques using acousto-optic & electro-optic modulators [6]. Organic films, dye jets, bulk semiconductor quantum wells etc are some of the nonlinear media used for this purpose [25]. Pulse width of less than one picosecond is usually measured by autocorrelation technique which utilizes SHG [5]. Frequency resolved optical grating (FROG) is a nonlinear optical technique used for measuring the time dependant intensity and phase of a femtosecond pulses [26]. Thus, generation and characterization of ultra short pulses is possible only with appropriate nonlinear processes.

4.3 Nonlinear optical effects in optical communications

The sign of the refractive nonlinearity determines whether self-focussing or self-defocusing will occur in a medium when intense light propagates through it [2]. In communication, Stimulated Brillioun Scattering, Stimulated Raman Scattering etc. are detrimental effects, as they can cause optical loss and also frequency shift during

propagation of laser beams through fibers. Fiber amplifiers are used to compensate the attenuation. Stimulated Brillioun Scattering is particularly important in single mode fibers. Self phase modulation is also an important nonlinear phenomenon in optical fiber communications as it can effect pulse broadening. Today's fiber communication employs optical/ eletrical/optical converters at the transmitter and receiver ends. The bandwidth of optical signal is very much higher than that of electronics and therefore, the optical/ eletrical/optical conversion processes act like a bottleneck in the exploitation of full bandwidth of optics. This bottleneck can be removed if all optical devices are fabricated using NLO effects [27,28].

4.4 Optical switching

Organic materials with large and fast nonlinearity are promising candidates for optical switching [10]. The response time of the nonlinearity depends on the mechanism of evolution of nonlinearity. Therefore, it determines the operating speed of the devices. Refractive nonlinearity is responsible switching [29].
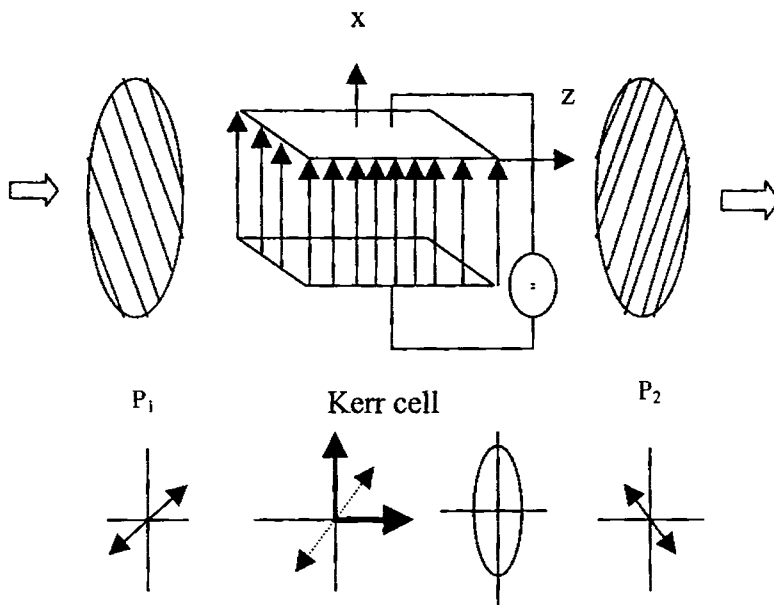
Fig. 1. Working of an optical switch

Schematic diagram of optical switching is shown in fig. 1. Ultimate goal is the design and fabrication of switches, wires, transistors and gates made of single field responsive molecule connected by photonic wires [30]. The difference between an electronic wire and a photonic wire is that the latter supports excited energy transfers rather than electron/hole transfer process [31]. Absorption of a photon as input by a chromophore at one end, causes emission of a photon at other end as out put. Optical switching by third order effects (e.g. optical Kerr effect) has advantages over linear electro-optic effect. The former has instantaneous response (response time around a picosecond) while the latter's response time can be higher [4]. This is because of the fact that electro-optic effects involve charge separation and hence the speed of switching is determined by the mobility of carries [26]. All optical switching requires a phase shift of more than π to be induced by light intensity through refractive index modulation [29].

4.5 Optical limiting

Passive optical power limiters are used to protect sensors, including human eyes, from intense laser light [12-14]. An ideal optical limiter [fig.2] will have a linear transmission upto a threshold input fluence I_{th} value, which can vary for different materials.
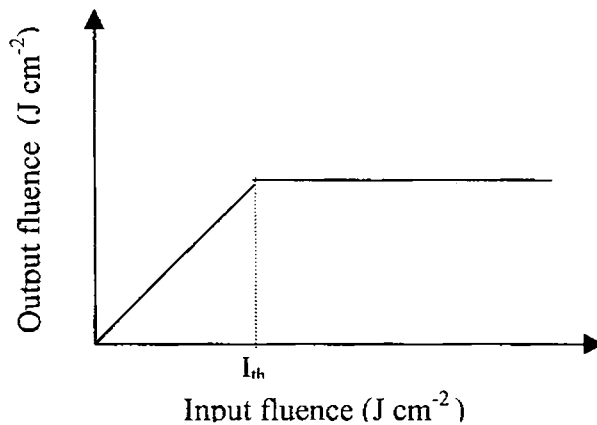
Fig. 2. Ideal optical limiting curve

If incident fluence is increased beyond I_{th}, transmittance remains constant. Optical limiting occurs mostly due to absorptive nonlinearity, which corresponds to imaginary part of third order susceptibility [32]. The two important mechanisms of optical limiting are TPA [14] and excited state absorption (ESA) [33]. The other possible mechanism of optical power limiting is nonlinear scattering. Optical limiting in carbon black suspension is a good example for nonlinear scattering [34,35].

5. NLO materials

Implementation of NLO effects in appropriate areas of technology invariably requires availability of suitable materials. Materials, which possess large and fast non-resonant nonlinear response, are the requirement of photonic technology, except for optical limiting. There is, in fact, a symbiotic relationship between the availability of suitable materials and growth of technology. In this context, a lot of materials have been synthesized and their NLO properties have been studied in detail. These materials include inorganic [36,37] as well as organic compounds [38-40]. Inorganic compounds are generally used in frequency conversion processes [18]. For example, KDP is the most popular SHG crystal. It has been observed that organic materials are promising candidates for NLO effects involving optical modulation, particularly for third order processes [18]. Advantage of organic molecules is that they contain a number of π electrons and hence organic compounds are considered to be good nonlinear optical (NLO) materials. In the recent past, some new classes of nonlinear materials such as nanoparticles [41], carbon nanotubes [42] and photonic band gap materials [43] have also been identified to be very useful for many applications. A description of certain important third order organic NLO materials is given below.

5.1. Organic materials

Loosely bound π electrons of organic molecules are easily polarizable. They also posses ultrafast response time (of the order of a few picoseconds). A number of organic materials have been studied for their NLO properties. Polymers,

phthalocyanines and naphthalocyanines (Pcs and Ncs), porphyrins, fullerenes etc. are some of them. Here, polymers are discussed very briefly. Pcs and Ncs, which form a class of compounds investigated in this thesis, are discussed in detail. As far as their NLO properties are concerned, porphyrins closely resemble Pcs and Ncs, though the structure of the former is different from Pcs and that of Ncs.

5.1.1. Polymers

One-dimensional organic molecules like polydiacetylene (PDA) were initially investigated for their third order NLO properties. PDA has the largest known nonresonant nonlinearity. Although NLO properties depend on the extent of π electron conjugation, it must be said that in one-dimensional organic compounds, NLO coefficients do not increase indefinitely with respect to increase in conjugation. It has been observed that their nonlinearity gets saturated after a definite length, called conjugation length [43,44]. Theoretical work reveals that in linear chain polymers, a strong TPA can occur at nearly half the energy of band gap [45]. Two photon resonances limit their applicability in device fabrication, by effecting severe loss in optical fibers made of polymers. Different types of polymers have been synthesized. Zwitterionic polymers [46], ladder polymers [47] and push-pull polymers are some of them [48]. Polymers can also act as the host to other NLO materials like phthalocyanines and fullerenes [49]. Significance of NLO materials embedded solid matrix is that technology requires solid materials rather than liquids.

5.1.2. Phthalocyanines and naphthalocyanines

Two-dimensional macromolecules like Pcs and Ncs are also good NLO materials. Pcs and Ncs have the added advantage of being chemically and thermally stable as well as synthetically flexible. Besides, these materials can be easily processed into thin films [31,50,51]. These materials are organic compounds, with extensive π electron delocalization, closely resembling naturally occurring photosynthetic materials viz., chlorophyll. Pcs can be used as pigments and they are also the models for biologically

important materials like hemoglobin. They can also serve as active element in chemical sensors [52] and also of greater importance in the fabrication of optoelectronic devices [53]. Pcs are semiconductors and photoconductors also [54,55]. Their intrinsic conductivity (in undoped condition) is due to the presence of π electrons. The conductivity present in Pcs is called hole conductivity. The energy gap which, these molecules must traverse, is related to the energy required to make an electron to pass from the highest filled to the lowest unfilled energy levels of the molecule [56]. Owing to the presence of easily polarizable π electrons, Pcs possess fairly good optical nonlinearity with a response time, of the order of picoseconds. In the light of the importance of Pcs and Ncs as NLO materials, they form one class of materials investigated, as a part of the present research.

The common structural feature of Pcs is a basic unit consisting of four pyrrole units linked in a circular manner by four azamethine bridges. Each Pc unit contains 18 π electrons [31,38,50,51,57]. The center hydrogen atom of free base Pcs has a lone-pair electrons, which make these compounds weakly acidic. The hole in the center of these macromolecules can accommodate hydrogen or metals ions. Accordingly, they are called metal free Pc (H_2Pc) or metal Pc (MPc) [58]. Fig. 3 a. shows the structure of a metal substituted Pc (MPcs) [38,50]. Nearly 60 metals ions have been incorporated at the center of Pc ring [38]. Idealized molecular structures, found in solutions, are used to classify the molecular structures. These structures show the highest symmetry (D_{4h} and C_{4v}) [57]. Ncs are the compounds with higher degree of π electron conjugation than Pcs. It can be seen that there are four additional benzene rings in Ncs so that the extent of π electron conjugation is higher in Ncs. Fig. 1 b shows the structure of a metal Nc (MNc) [59]. Lanthanide and actinide metal ions can form homo dimers of Pcs and Ncs; $M(Pc)_2$ and $M(Nc)_2$ [60,61] respectively. Such compounds are called bis-Pcs or bis-Ncs. Fig. 4. a and fig. 4. b show the structures of typical bis-Pcs and bis-Ncs respectively [38].
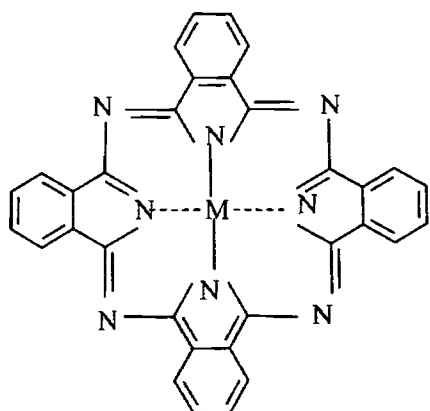
Fig.3 a. Structure of MPcs
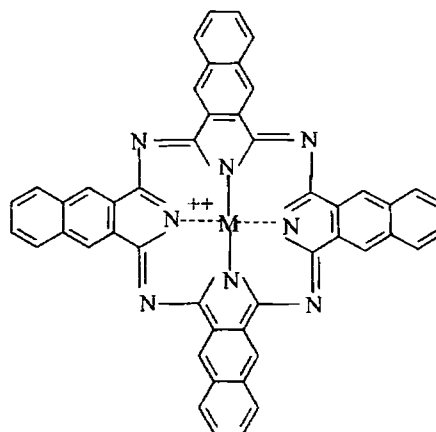
fig. 3. b. Structure of MNcs
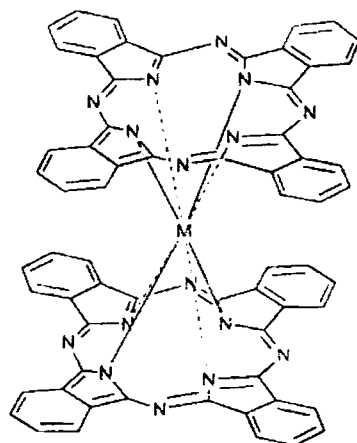
Fig. 4. a Structure of bis-Pcs
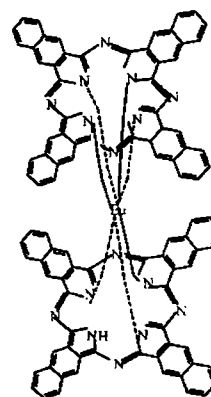
Fig. 4. b. Structure of bis-Ncs

In this thesis, (mono) MPcs investigated are molybdenum oxy phthalocyanine (MoOPc), LaPc and FePc. (Mono) Ncs selected for the study include MgNc, ZnNc

and VONc. In the case of MoOPc and VONC, the oxygen atom may be considered as an axial substituent, as it projects out of the Pc plane. Therefore, MoOPc and VONC have a pyramidal-type structure [62]. Fe^{2+}, MoO^{2+}, VO^{2+} and Zn^{2+} are transition metal ions. All these transition metal ions, except Zn^{2+}, possess partially filled d-shells. Pcs and Ncs, which contain transition metal ions with partially filled d-shells, can exhibit a number of charge transfer (CT) mechanisms [63]. Besides, transition metals with incomplete d-shells can enhance intersystem crossing rate through spin-orbit coupling [64-66]. All these aspects have been discussed in detail in chapters 3, 4 and 5.

From figures 3 and 4, it can be seen that the structures of bis-Pcs and bis-Ncs are different from those of (mono) Pcs and (mono) Ncs. Bis-Pcs and bis-Ncs have a sandwich structure where, the metal atom lie in between two Pc planes, rotated by a staggering angle α [50]. Therefore bis-Pcs and bis-Ncs are not planar like mono Pcs and mono Ncs. In the case of bis-Pcs and bis-Ncs, the central metal is coordinated to all of the isoindole nitrogen atoms of Pc or Nc macrocycles. The staggering angle depends on both the height of coordination polyhedron (distance between the best planes of the two Pc macrocycles) and the crystal structure. Dependence of the staggering angle on the crystal structure is evident from the fact that similar structures have similar staggering angles. It is also known that some metals can form several bis-Pcs with different staggering angles [50,60,61]. There are a number of important structural parameters for Pcs and Ncs. Some of these parameters are; (1) location of inner hydrogen in metal free Pcs, (2) coordination chemistry of the central metal ions in MPcs, (3) staggering angle in bis-Pc, (4) deformation in solid state molecular structures (5) linear and slipped stacking [50]. Pcs are sometimes classified as type I or type II. Type I molecules have identically (or similarly) shaped sides and are symmetrical in respect of Pc plane. Two distinguishable sides characterize molecules of the type II. One side of type II complexes is the Pc macrocycle, while the other side is characterized by an extra– coordinated metal ion or additional axial ligand [50].

Typical absorption spectrum of all the Pcs consists of two intense bands; one known as Q- band, around 600-800 nm in the visible region and the other one, known as S band (Soret band), around 300-400 nm region [57]. The Q band, which arises from π-π* transition, is composed of at least seven smaller bands. Intense absorption occurs between 600 nm and 700 nm. The Q-band of the absorption spectrum is the characteristic of a particular Pc compound. Introduction of metal into phthalocyanine molecules has a variable effect on the intensity and spacing of its absorption spectrum, however, the general features of the phthalocyanine spectrum remain intact [56]. Fig. 5 shows the absorption spectra of the (mono) MPcs investigated here.
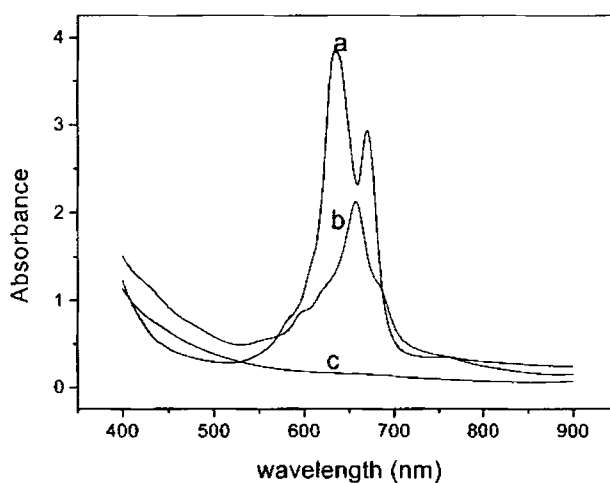
Fig. 5. Absorption spectra of MPcs
a. LaPc; b. MoOPc; c. FePc

On introduction of the metal ions at the centre, the weakest absorption bands disappear and the spectrum gets shifted to lower wavelengths. The extent of the spectral shift is proportional to the atomic number of the central atom. Fig. 6 shows the absorption spectrum of bis-Pcs investigated here. It may also be noted that with respect to increase in π electron conjugation, Q-band gets red shifted. Fig. 7 shows the absorption spectrum of (mono) Ncs and bis-Ncs studied in this thesis. The red

shift of the Q-band of Ncs, which have high degree of conjugation with respect to Pcs, is evident from a comparison of fig 7 with fig. 5 and fig. 6.
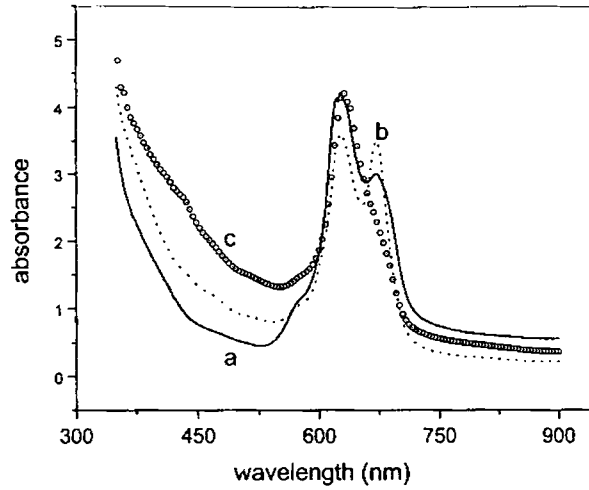
Fig. 6. Absorption spectra of bis-Pcs

a.   Eu(Pc)$_2$; b. Sm(Pc)$_2$; c. Nd(Pc)$_2$
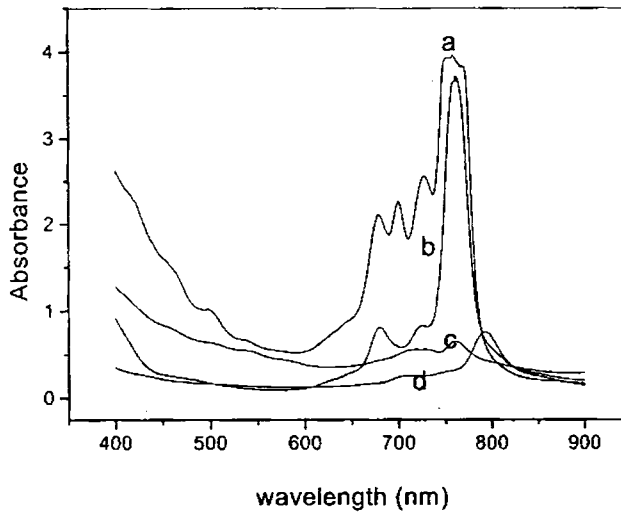
Fig. 7. Absorption spectra of Ncs

a. ZnNc; b. MgNc; c. Eu(Nc)$_2$; d. VONc

Apart from their chemical and thermal stability, they have the advantage of synthetic flexibility. Owing to synthetic flexibility, their structures can be easily tailored to suit the requirement of specific applications, without compromising their other properties. Apart from metal ion, a number of axial and peripheral substituents can also be incorporated into the Pc ring. These substituents can modify electronic and optical properties considerably. Some chemical species like amino group (NH_2) can donate electrons to the Pc ring, while some other chemical groups like –COOH can withdraw electrons from the Pc ring. Therefore, if an electron withdrawing group and an electron-donating group are attached to the opposite ends of an organic system, we get systems, called push-pull compounds, which have relatively high values of polarizability [66,67]. The enhancement of polarizability in push-pull compounds can be explained as follows. The donor pushes electrons into the Pc ring while the acceptor pulls the electrons. The push and pull result in increased charge separation. However, enhancement of polarizability depends not only on the charge separation but also on the amount of communication between the donor and acceptor, intermolecular charge transfer processes (ICT), through the π electron systems [67].

Recently, Pc- azacrown- fullerene and Pc-fullerene multi component systems have been synthesized and their photo-physical properties have been studied [68,69]. Using molecular beam epitaxy, we can get crystalline films of Pcs. Crystalline forms of Pcs exhibit polymorphism. Some of the main differences between the polymorphic structures are different stacking angles of Pc molecules with the stacking axis or different stacking modes or different overlapping arrangements or different hydrogen-bonding pattern. In Susich's nomenclature, polymorphs are called α, β or γ forms with β form being the stable one [50]. As mentioned earlier, monomer absorption spectra can be obtained from dilute solutions of Pcs. In concentrated solutions, Pcs usually form dimers or trimers [70-72]. Dimer and trimer formations occur through hydrogen bonding. Evidently probability of the dimer formation is higher in polar solvents. If there is fairly good electrostatic shielding between solute molecules in the

solution i.e. if dielectric constant of the solvent is high, there is only very low probability of dimer formation [71]. Formation of dimers manifests in their absorption spectra as broadening of the characteristic Q band. Similar broadening has been reported in the case of crystalline, polycrystalline and amorphous thin films of Pcs. The broadening is attributed to the intermolecular interaction induced splitting of the energy levels [71,72].

A different class of compound, which closely resembles Pcs, is sub-Pcs [73,74]. Sub-Pcs are cone-shaped macrocycles, composed of three isoindole units. These samples can be used as the intermediates for synthesis of unsymmetrical Pc derivatives. Sub-Pcs, which contains 14 π electrons, have C_3 symmetry. Like Pcs, sub-Pcs also have fairly good thermal stability [73].

5.2. Nanoparticles

Nanoparticles are relatively new class of photonic materials. Nanoparticles are the materials having a size less than or about 100 nm. Properties of nanoparticles are considerably different from those of the bulk. The unique electric and optical properties of nanoparticles are the result of quantum and dielectric confinement effects that arise on reduction in particle size down to nanometer scale [75]. Amongst metal nanoparticles, noble metal nanoparticles are of particular interest because of their potential applications in fabrication of nanodevices [36]. Characteristic feature of nanoparticles is the presence of surface plasmon band (in the case of metal nanoparticles) or exciton bands (in the case of semiconductor nanoparticles) in their absorption spectra. Surface plasmon is the collective oscillation of free electrons in the conduction band, which occupy states immediately above the Fermi level [76]. In this thesis, nonlinear optical absorption exhibited by silver nanosol, i.e. aqueous solution of silver nanoparticles, is investigated at selected wavelengths near the plasmon band. Linear and nonlinear properties of nanoparticles are discussed in detail in chapter 6.

24

6. Merit factors

It must be said that, mere observation of high nonlinearity is not sufficient for the fabrication of all optical devices, which can perform optical switching, logic operations etc. The material must have very fast response, preferably less than picoseconds. Optical losses due to linear and nonlinear absorption should also be a minimum. Material dispersion should not result in pulse brake up. Besides, system performance has to be stable at operating peak and average powers levels without optical and thermal damage. An important parameter is maximum nonlinear phase shift achievable over a single or multi photon absorption length. This condition can be expressed by the expression [77]

$$W = \frac{n_2 I_s}{\alpha \lambda} \gg 1 \text{ and } T = \frac{\beta \lambda}{n_2} \ll 1 \qquad (1.13)$$

where α and β are linear and nonlinear absorption coefficient respectively, I_s is the saturation intensity and λ is the wavelength.

7. Present work

The results of experimental studies on third order NLO properties carried out in a number of MPcs and MNcs as well in silver nanosol are included in this thesis. Degenerate four wave mixing (DFWM) and Z-scan were used as experimental techniques to probe NLO properties. Second hyperpolarizability $\langle \gamma \rangle$ was measured for a number of MPcs and MNcs and the results were explained in terms of their structure and spectroscopic properties. Nonlinear absorption at 532 nm was studied in these Pcs. Wavelength dependence of nonlinear absorption was investigated in certain bis-Pcs. Besides, nonlinear absorption in a representative metal nanoparticle system viz. silver nanosol was also investigated at well chosen wavelengths near plasmon band.

References:

[1] J A Miragliotta. Johns Hokins APL Technical Digest. **16** (1995) p. 348

[2] The principles of nonlinear optics, Y R Shen, John Wiley and Sons (1991) New York.

[3] Polarization of light in nonlinear optics. Yu P Svirko and N J Zheludev. John Wiley & Sons (1998) Chichester

[4] Nonlinear optics. E G Sauter. Johm Wiley & Sons Inc (1996) New York

[5] Optical Electronics In Modern Communications. A Yariv. Oxford University Press (1997) New York

[6] Nonlinear Optics. G L Wood and E J Sharp. Electro-Optic hand Book. (Eds) R E Fischer and W J Smith (1994) McGraw Hill Inc. New York

[7] Nonlinear Optics in Signal Processing. Robert W Easu and Alan Miller. Chapman & Hall (1993) London

[8] Optical Phase Conjugation. R A Fisher (Ed.) Academic press (1983) New York

[9] T W Yau, C H Lee and J Wang. J. Opt. Soc. Am. B. **17** (2000) p. 1626

[10] B L Davies and M Samoc. Current Opinion in Solid State and Material Science (1997) p. 213

[11] O Aso, M Tadakuma, S Namiki. Furukawa Review No. 19 (2000) p.63

[12] J S Shirk, R G S Pong, F J Bartoli and A W Snow. Appl. Phys. Lett. **63** (1993) p. 1880

[13] D Dini, M Barthel and M Hanack. Eur. J. Org. Chem. (2001) p. 3759

[14] G H He, C Weder, P Smith and P N Prasad. IEEE J. OE **34** (1998) p.2279

[15] H Ditlbacher, J R Krenn, B Lamprecht, A Leitner and F R Aussenegg. Opt. Lett. **25** (2000) p. 563

[16] A Bhardwaj, P O Hedekvist and K Vahala. J. Opt. Soc. Am. B **18** (2001) p. 657

[17] P O Hedekvist, A Bhardwaj, K Vahala and H anderson. Appl. Opt. **40** (2001) p. 1761

[18] H Hashimoto, T Nakashima, K Hattori, T Yamada, T Mizoguchi, Y Koyama and T Kobayashi. Pure Appl. Chem. **71** (1999) p. 2225

[19] S Wu, X C Zhang and R L Fork. Appl. Phys. Lett. **61** (1992) p. 919

[20] M Zhao, Y Cui, M Samoc, P N Prasad, M R Unroe, and B A Reinhardt. J. Chem. Phys. **95** (1991) p. 3991

[21] P Cheben, F del Monte, D J Worsfolds, D J Carrisson, C P Grover and J D Mackenzle. Nature. **408** (2000) p. 64

[22] R Ryf, A Lotscher, C Bosshard, M Zgonik and P Gunter. J. Opt. Soc. Am. B **15** (1998) p. 989

[23] Polarization of Light. S Huard (1997) John Wiley & Sons. (1997) Chichester

[24] Instruction Manual MOPO 700 Series. Spectra Physics Lasers Inc. (1997) CA, USA

[25] J O Gorman, A F J Levi, T T Ek and R A Logan. Appl. Phys. Lett. **59** (1991) p. 16

[26] Th. Schneider, D Wolfframm, R Mitzner, J Reif. Appl. Phys. B **68** (1999) p. 749

[27] Nonlinear Fiber Optics. Chapter 1, G P Agrawal (1995) Academic Press San Diego

[28] Optical Fiber Communications. p. 488. G Keisser (2000)Mac-Graw Hill Boston

[29] M Samoc, A samoc, B L Davies, Z Bao, L Yu, B Hsieh and U Scherf. J. Opt. Soc. Am. B **15** (1998) p. 817

[30] K S Suslick, N A Rakow, M E Kosal and J H Chou. J. Porphyrins and Phthalocyanines. **4** (2000) p. 407

[31] J H Chou, M E Kosal, H S Nalwa, N A Rakow and K S Suslick. Applications of Porphyrins and Metalloporphyrins to Materials Chemistry from Porphyrin Handbook K Kadish, K Smith, K Guilard (Eds). Academic Press (2000) New York vol 7. ch. 41.

[32] F M Quereshi, S J Martin, X Long, D D C Bradley, F Z Heneri, W J Balu, E C Smith, C H Wang, A K Kar and H L Anderson. Chem. Phys. **231** (1998) p. 87

[33] T Xia, D J Hagan, A Dogariu, A A said and Eric W Van Stryland. Appl. Opt.. **36** (1997) p. 4110

[34] Kamjou Mansour, M J Soileau and E W V Stryland. J. Opt. Soc. Am B **9** (1992) p. 1100

[35] Ya Ping, J E Riggs, K B Henbest and R B Martin. J. Non. Opt. Phys. Mat. **9** (2000) p. 481

[36] N K Chacki, M Aslam, J Sharma and K Vijayamohan. Proc. Indian Acad. Sci. (Chem. Sci) **113** (2001) p. 659

[37] W F Zhang, Y B Huang, M S Zhang and Z G Liu. Appl. Phys. Lett. **76** (2000) p. 1003

[38] G de la Torre, P Vazquez, F A Lopez and T Torres. J Mater. Chem. **8** (1998) p. 1671

[39] S R Marder, W E Torruellas, M B Desce, V Ricci, G I Stegeman, S Gilmour, J L Bredas, Jun Li, G U Bublitz, S G Boxer. Science **276** (1997) p. 1233

[40] M Albota, D Beljonne, J L Bredas, J E Ehrlich, Jia Ying Fu, Ahmad A Heikal, S E Hess, T Kogej, M D Levin, S R Marder, D M Maughon, J W Perry, H Rockell, M Rumi, G Subramaniam, W W Webb, X L Wu, C Xu. Science **281** (1998) p. 1653

[41] M El Kouedi and C A Foss, Jr. J. Phys. Chem. B **104** (2000) p. 4031

[42] S R Mishra, H S Rawat, S C Mehendale, K C Rustagi, A K Sood, R Bandhopadhyay, A Govindaraj, C N R Rao. Chem. Phys. Lett. **317** (2000) p. 510

[43] T Hattori, N Tsurumachi, N Muroi, H Nakatsuka and E Ogino. Pergamon. Prog. Crystal Growth and Charat. **33** (1996) p. 183

[44] Ifor D W Samuel, I Ledoux, Corinne Deiporte. D L Pearson and J M Tour. Chem. Mater. **8** (1996) p. 819

[45] P A Gass, I Abraham, R Raj and M Schott. J. Chem. Phys. **100** (1994) p. 88

[46] C Combellas, F Kajzar, G Mathey, M A Petit, A Thiebault. Chem. Phys. **252** (2000) p. 165

[47] J Pospisil, M Samoc and J Zieba. Eur. Polym. J. **34** (1998) p. 899

[48] V Chernyak, S Tretiak, S Mukamel. Chem. Phys **319** (2000) p. 261

[49] J E Riggs and Y P Sun. J Phys. Chem. A **103** (1999) p. 485

[50] M K Engel, Report Kawamura Inst Chem. Res1996 (1997) p. 11-54

[51] G de la Torre, M Nicolau, T Torres: " Phthalocyanines: Systhesis, Supermolecular, Organizattion and Physical Properties" in Supermolecular Photosensitive and Electroactive Materials. H S Nalwa (Ed.) (2001) Academic Press, San Diego. P. 1-111

[52] M S John, K P Unnikrishnan, J Thomas, P Radhakrishnan, V P N Nampoori and C P G Vallabhan. Proceedings of PHOTONICS – 2002. S K Lahiri, R Gangopadyay, B K Mathur, A K Dutta, S K Ray and S Das (Eds). Allied Publishers Ltd. (2000) New Delhi

[53] S A Jenekhe and Shujian Yi. Adv. Mater. **12** (2000) p. 1274

[54] M Umeda, M Mohamedi, T Itoh and I Uchida. J. Appl. Phys. **90** (2001) p. 3984

[55] R D Gould and T S Shafai. Superficies Vacio **9** (1999) p. 226

[56] Phthalocyanine Compounds. F H Moser and A L Thomas. Reinhold Publishing Corporation. (1963) New York

[57] C Li, L Zhang, M Yang, H Wang, Y Wang. Phys. Rev A **49** (1994) p. 1149

[58] R Kubiak, J Janczak. Cryst. Res. Technol. **36**(2001) p. 1095

[59] G R J Williams. J. Molecular Structure (Theochem) **332** (1995) p. 137

[60] N Ishikawa, Y Kaizu. Coord. Chem. Revs. **226** (2002) p. 93

[61] N Kobayashi. Coord. Chem. Revs. **227** (2002) p. 129

[62] A Yamashita, S Matsumoto, S Sakata and T Hayashi., H Kanbara J. Phys. Chem. B **102** (1998) p. 5165

[63] K Kandasamy, S-J Shetty, P N Puntambekar, T S Srivastava, T Kundu and B P Sing. J. Porphyrins and Phthalocyanines. **3** (1999) p. 81

[64] M Koshino, H Kurata, S Isoda and T Kobayashi. ICR Annual Report. 7 (2000) p. 6

[65] V S Williams, S Mazumdar, N R Armstrong, Z Z Ho and N Peyhgambarian. J. Phys. Chem. **96** (1992) p. 4500

[66] K S Suslick, C Ti Chen, G R Meredith and L T Cheng. J. Am. Chem. Soc. **114** (1992) p. 6929

[67] A Sastre, M A D Garcia, B del Rey, C Dhenaut, J Zyss, I ledoux, F A Lopez and T Torres. J. Phys. Chem. A **101** (1997) p. 9773

[68] A Sastre, A Gouloumis, P Vazquez, T Torres, Vinh Doan, B J Schwartz, F Wuld, L Echegoyen and J Rivera. Org. Lett. **1** (1999) p. 1809

[69] B Kessler. Appl. Phys. A **67** (1998) p. 125

[70] M T M Choi, P P S Li and D K P Ng. Tetrahedron **56** (2000) p. 3881

[71] W J Schutte, M S Rehbach and J H Sluyters. J Phys. Chem. **97** (1993) p. 6069

[72] A W Snow and N L Jarvis. J. Am. Chem. Soc. **106** (1984) p. 4706

[73] S H Kang, Y S Kang, W C Zin, G Olbrechts, K Wostyn, K Clays, A Persoons and K Kim. Chem. Commun. (1999) p. 1661

[74] M A D Garcia, F A Lopez, A Sastre, T Torres, W E Torruellas and G I Stegeman. J. Phys. Chem. **99** (1995) p. 14988

[75] N D Fatti, F Valle, C Flytzanis, Y Hamanaka, A Nakamura. Chem. Phys. **251** (2000) p. 215

[76] T S Ahmadi, S L Logunov and M A El-Sayed. J. Phys. Chem. **100** (1996) p.8053

[77] M Samoc, A samoc, B L Davies. Synthetic Metals. **109** (2000) p. 79

2

Experimental techniques and theory

Abstract

Z-scan and degenerate four wave mixing (DFWM) are the two specific experimental techniques used for nonlinear optical measurements presented in this thesis. Details of these two techniques are described in this chapter along with relevant theory. Besides, the specifications and characteristics of the laser sources and those of other instruments utilized for the measurements are also included in this chapter.

1. Z–scan technique

Z-scan technique was originally introduced by Sheik Bahae et. al [1,2]. This is a simple and sensitive single beam technique to measure the sign and magnitude of both real and imaginary part of third order nonlinear susceptibility, $\chi^{(3)}$. In the original single beam configuration, the transmittance of the sample is measured, as the sample is moved, along the propagation direction of a focussed gaussian laser beam. A laser beam propagating through a nonlinear medium will experience both amplitude and phase variations. If transmitted light is measured through an aperture placed in the far field with respect to focal region, the technique is called closed aperture Z-scan experiment [1,2]. In this case, the transmitted light is sensitive to both nonlinear absorption and nonlinear refraction. In a closed aperture Z-scan experiment, phase distortion suffered by the beam while propagating through the nonlinear medium is converted into corresponding amplitude variations. On the other hand, if transmitted light is measured without an aperture (in this case the entire light is collected), the mode of measurement is referred to as open aperture Z-scan [2]. In this case, the throughput is sensitive only to the nonlinear absorption. Closed and open aperture Z-scan graphs are always normalized to linear transmittance i.e. transmittance at large values of $|z|$. Closed aperture Z-scan and open aperture Z-scan experiments respectively yield the real and imaginary parts $\chi^{(3)}$ [2]. Usually closed aperture Z-scan data is divided by open aperture data both measured simultaneously, to cancel the effect of nonlinear absorption contained in the closed aperture measurement [2]. The new graph, called divided Z-scan graph, contains information on nonlinear refraction alone. In a Z-scan measurement, it is assumed that sample is thin, i.e. the sample length is much less than Rayleigh's range z_0. [$z_0 = k\omega_0^2/2$ where k is the wave vector and ω_0 is the beam waist]. This is essential to ensure that beam profile does not vary appreciably inside the sample. Experimental setup for single beam Z-scan technique is given in fig.1. Photodetector (PD1) monitors the input laser energy. PD2 and PD3 give open and closed aperture measurements respectively.
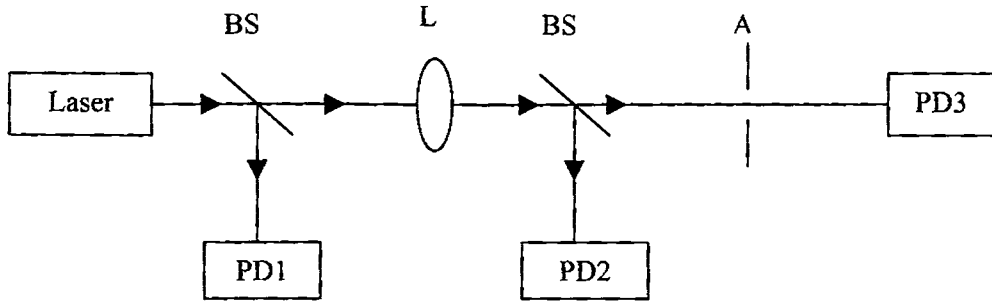
Fig.1. Schematic diagram of Z-scan set up

A: aperture; L: lens; BS: beam splitters

Different variants of this technique such as eclipsing Z-scan [3] and two colour Z-scan [4, 5] have also been introduced. In non degenerate (two colour) Z-scan, the effect of nonlinear refraction and absorption induced by a strong excitation beam at a frequency ω_e on a weak probe beam at a different frequency ω_p i.e. $\Delta n(\omega_e, \omega_p)$ and $\Delta\alpha(\omega_e, \omega_p)$, are measured. [$\Delta n$ refers to the change in refractive index and $\Delta\alpha$ refers to the change in absorption coefficient]. Non degenerate Z-scan technique has some advantages over conventional single beam technique [4]. The frequency difference $(\omega_p - \omega_e)$ can be exploited to get information about the dynamics of the nonlinear response with time resolution much less than the laser pulse width. With two colour Z-scan technique, it is possible to make time resolved measurements by suitably delaying the probe pulse with respect to pump beam. Investigation of non-degenerate nonlinearity has technological importance in the area of dual wavelength all optical switching applications, where cross phase modulation is very important [4]. In eclipsing Z-scan technique, the far field aperture is replaced with an obscuration disk [3], which blocks most of the beam. This modification of the Z-scan technique enhances sensitivity to induced wave front distortion to an order of $\lambda/10^4$. Two colour eclipsing Z-scan technique has also been suggested [6]. Measurements presented in this thesis have been made using single beam open aperture Z-scan technique.

Z-scan technique is highly sensitive to the profile of beam and also to the thickness of the samples [1,2,7]. Any deviation from the gaussian profile of the beam and also from thin sample approximation will give rise to erroneous results. Therefore, some modifications have been suggested to overcome these disadvantages. One such modification is the use of non apertured multi channel Z-scan method, where the total far field beam profile distortion is recorded using a two dimensional CCD camera [8,9]. By image processing, the distorted beam for a given cell position is compared with undistorted beam (i.e. in the absence of nonlinearity). The module of the intensity variation over each pixel of CCD camera is then summed to define the total profile distortion signal (TPDS), which is proportional to nonlinear phase shift. This method has some advantages [9] like (a) the entire far field distribution of both signal and reference beams can be recorded simultaneously (b) after data acquisition the image recorded can be digitized and stored in a computer and the image is ready for further processing and analysis and (c) the dynamic range of a CCD detector is very high. Z-scan measurements can also be made using astigmatic gaussian beams [10] and top hat beams [11]. In the case of astigmatic gaussian beam, a slit is used instead of a (circular) aperture [10]. Z-scan measurement for non gaussian beams with arbitrary sample thickness [12] and arbitrary aperture [13] have also been suggested. In the case of the former, nonlinear parameters are measured in comparison with a standard sample, mostly CS_2 [11].

1.1. Open aperture Z-scan

Nonlinear absorption of a sample is manifested in the open aperture Z-scan measurements. For example, if nonlinear absorption like two-photon absorption (TPA) is present, it is manifested in the measurements as a transmission minimum at the focal point [2]. On the other hand, if the sample is a saturable absorber, transmission increases with increase in incident intensity and results in a transmission maximum at the focal region [14-16]. It has been shown that the model originally developed by Bahae et. al for pure TPA can also be applied to excited state

absorption (ESA) [17]. ESA is a sequential TPA process, where two photons are successively absorbed [18]. However, in this case nonlinear absorption coefficient β is renamed β_{eff}, the details of which are discussed in chapter 3.

1.2. Theory of open aperture Z-scan technique

In the absence of an aperture, transmitted light measured by the detector, in a Z-scan experiment, is not sensitive to phase variations of the beam and hence it can be neglected. The theory of Z-scan experiment given here is same as that in [2]. Only transmitted intensity need to be considered. The intensity dependent nonlinear absorption coefficient $\alpha(I)$ can be written in terms of linear absorption coefficient α and TPA coefficient β as [2]

$$\alpha(I) = \alpha + \beta I \qquad (2.1)$$

The irradiance distribution at the exit surface of the sample can be written as

$$I_r(z,r,t) = \frac{I(z,r,t)e^{-\alpha l}}{1+q(z,r,t)} \qquad (2.2)$$

where $\qquad q(z,r,t) = \beta I(z,r,t)L_{eff} \qquad (2.3)$

L_{eff} is the effective length and is given, in terms of sample length l and α by the relation

$$L_{eff} = \frac{(1-e^{-\alpha l})}{\alpha} \qquad (2.4)$$

The total transmitted power P(z, t) is obtained by integrating eq. (2.2) over z and r and is given by

$$P(z,t) = P_1(t)e^{-\alpha l} \frac{\ln[1 + q_0(z,t)]}{q_0(z,t)} \qquad (2.5)$$

$P_1(t)$ and $q_0(z, t)$ are given by the equations (2.6) and (2.7) respectively.

$$P_1(t) = \frac{\pi \omega_0^2 I_0(t)}{2} \qquad (2.6)$$

$$q_0(z,t) = \frac{\beta I_0(t) L_{eff} z_0^2}{z^2 + z_0^2} \qquad (2.7)$$

For a pulse of gaussian temporal profile, eq.(2.5) can be integrated to give the transmission as

$$T(z) = \frac{C}{q_0 \sqrt{\pi}} \int_{-\infty}^{\infty} \ln(1 + q_0 e^{-t^2}) dt \qquad (2.8)$$

Nonlinear absorption coefficient is obtained from fitting the experimental results to the eq. (2.8).

If $|q_0| < 1$, the eq. (2.8) can be simplified as

$$T(z, S = 1) = \sum_{m=0}^{\infty} \frac{[-q_0(z,0)]^m}{(m+1)^{1/2}} \qquad (2.9)$$

Saturable absorption (SA) occurs when a sample is excited at its resonant wavelengths. In this case, as indicated earlier, absorption in the sample decreases as input intensity is increased. Therefore, nonlinear absorption coefficient may be considered as negative. SA takes place because of the depletion of the ground state population. This type of phenomenon is characterized by a parameter called

saturation intensity I_s [15]. In such cases, we cannot directly apply the eq.(2.8), which was derived for TPA. The simplest model to explain SA is a two-level model [16]. Assuming that SA occurs due to depletion of ground state population, steady state can be expressed by the equation

$$\frac{dN}{dt} = \frac{\sigma I}{h\upsilon}\left(N_g - N\right) - \frac{N}{\tau} = 0 \qquad (2.10)$$

Here N is the concentration of the excited state molecules, N_g is the undepleted ground state concentration, σ is the absorption cross section, hv is the photon energy and τ is the life time of the excited state. Absorption coefficient α is proportional to ground state population we can be written as

$$\alpha = \sigma\left(N_g - N\right) \qquad (2.11)$$

In presence of SA, intensity dependent absorption coefficient $\alpha(I)$ can be written as

$$\alpha(I) = \alpha_0 \frac{1}{1 + \frac{\sigma I}{h\upsilon}} = \alpha_0 \frac{1}{1 + \frac{I}{I_s}} \qquad (2.12)$$

where $h\upsilon/\sigma\tau = I_s$, the saturation intensity.

1.3. Closed aperture Z-scan

Closed aperture Z-scan is an example of self–refraction phenomenon or self phase modulation in space. In the absence of nonlinear absorption, a well-defined peak and valley are observed [1,2]. If the nonlinear refractive index n_2 of the sample is negative, the beam gets converged in the pre-focal region to get focussed closer to the aperture. Consequently, the beam diameter decreases near the aperture, resulting in

large amount of throughput at the detector. This results in a peak in the pre focal region. In the post focal region, the same phenomenon results in the divergence of the beam, which results in the decreased transmission through the aperture. Hence, a valley appears in the post-focal region. If the sample has positive nonlinear refraction, we have just the opposite result (pre focal valley and post focal peak.). The former is called self-defocusing and the later is called self-focussing. One of the mechanisms of self-focussing is optical Kerr effect [19], which has instantaneous response. In this case the electric field of a light beam exerts a torque on anisotropic molecules by coupling to oscillating dipole induced in the molecule by the field itself. Resulting light induced molecular reorientation is the main mechanism for optical nonlinearity in transparent liquids. Nonlinear refractive index depends linearly on light intensity. The other mechanism of optical Kerr effect includes off resonant excitation of narrow band absorbers and consequent distortion of electronic distribution among energy levels in the materials. The resultant intensity dependant refractive index is responsible for self-focussing or self-defocusing. In self-focusing beam collapses upon itself spatially. Kerr like nonlinearity has very fast response time, of the order of picoseconds.

All the measurements mentioned in this thesis have been made in samples taken in solution form under nanosecond excitation. Therefore closed aperture measurements, in the present experimental conditions, can give only thermal response [20,21], which is not of interest in the scope of the present work. Therefore closed aperture Z-scan measurements were not attempted in detail. It may also be noted that the theory of closed aperture Z-scan experiments developed for Kerr type nonlinearity is not applicable for thermal nonlinear refraction.

2. Degenerate four-wave mixing (DFWM)

Four wave mixing refers to interaction of three input waves in a nonlinear medium through the nonlinear polarization corresponding to $\chi^{(3)}(\omega; \omega_1, \omega_2, \omega_3)$, to produce a

fourth wave, at the resultant frequency and wave vector of the input fields [22]. If the frequencies of all the waves are the same (their wave vectors can be different) it is called DFWM. This is a sensitive interferometric method to determine magnitude of $\chi^3(-\omega; \omega, \omega, -\omega)$. In the present case, standard back scattering geometry of DFWM, which gives rise to optical phase conjugation, is used to measure nonlinear coefficients $\chi^{(3)}(-\omega; \omega, \omega,-\omega)$. Schematic diagram of DFWM is shown in fig.2.
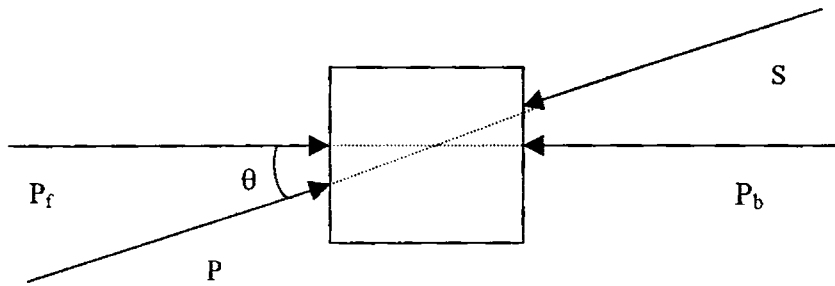
Fig .2. Schematic diagram of DFWM

P_f. forward pump beam; P_b. backward pump beam; P. probe beam

S. OPC signal; θ: angle between pump and probe beams
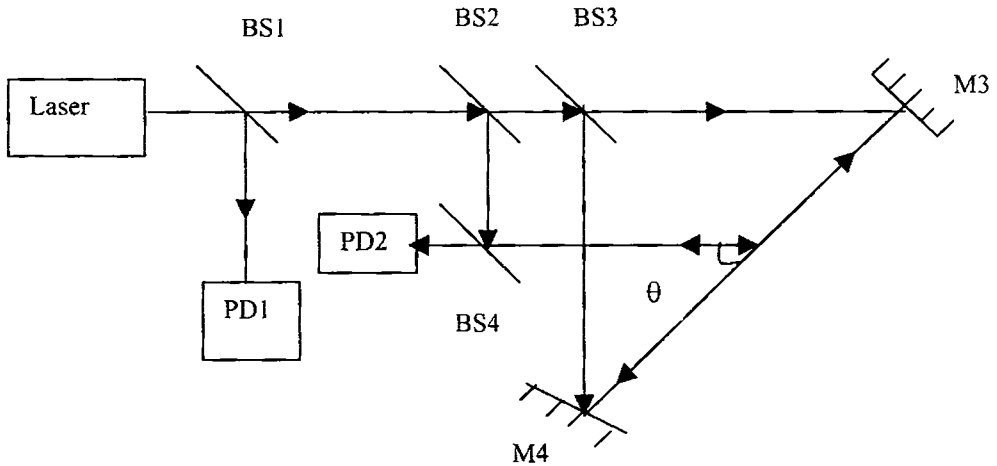
Fig .3. Experimental setup of DFWM

BS: Beam splitters; PD: Photo-detectors; M: Mirrors; θ: Pump-probe beam angle

In the experimental setup, two beams of equal intensity generally called forward and backward pump beams, are made exactly counter propagating. Therefore, sum of their wave vector is zero ($k_f + k_b = 0$). The actual experimental setup for DFWM is given in fig.3. A third beam (called probe beam), which has an intensity less than those of the pump beams, make a small angle with respect to one of the pump beams (in the present case $\approx 8°$) as shown in the fig. 3. Pump-probe intensity ratio was about five. The generated fourth wave is called phase conjugated beam, because its amplitude remains every where the complex conjugate of the probe beam. From phase matching condition ($\Delta k = 0$) it can be seen that wave vector of the phase conjugate beam $k_c = - k_p$, i.e. phase conjugate light retraces the path of the probe beam.
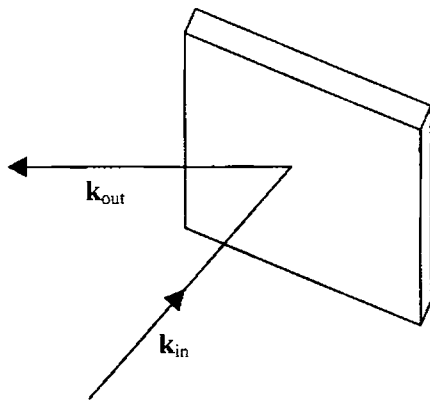
Fig. 4. a	Fig. 4. b
a. Reflection (ordinary mirror)	b. Reflection (phase conjugate mirror)
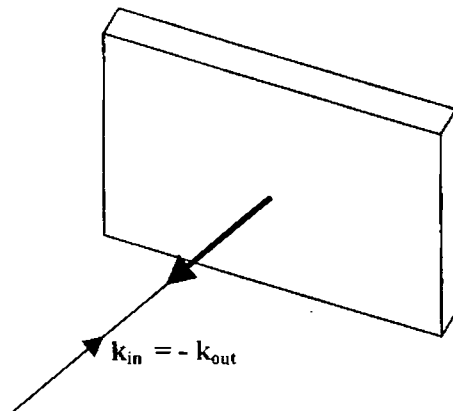
It is to be noted that in a phase conjugate reflection, the wave vector of the incident beam is totally reversed, whereas in an ordinary reflection, only normal component of the wave vector component is reversed. Thus phase conjugate reflection does not obey the Snell's law. Reflection from a phase conjugate mirror and that from an ordinary mirror are illustrated in the fig.4 [22, 23].

Generation of phase conjugate light can be understood as diffraction of one of the input beams from a grating formed by interference of the other two input beams [24-27]. Grating essentially means spatial (or temporal) modulation of certain properties of the medium. Therefore, DFWM is also called real time holography (simultaneous writing and reading of the hologram). In an isotropic medium the vector form of nonlinear polarization is by [24]

$$\vec{P}_{NL} = \frac{1}{2}\left[a\left(\vec{E}_f \cdot \vec{E}_p^*\right)\vec{E}_b + b\left(\vec{E}_b \cdot \vec{E}_p^*\right)\vec{E}_f + c\left(\vec{E}_f \cdot \vec{E}_b\right)\vec{E}_p^*\right] + cc... \qquad (2.13)$$

The first term corresponds to the static grating formed by interference of forward pump beam (P_f) and probe beam (P). Backward pump beam (P_b) is Bragg diffracted from this grating. This is called transmission grating (fig.5.a). The second term corresponds to the static grating formed by the interference of backward pump beam (P_b) and probe beam (P).
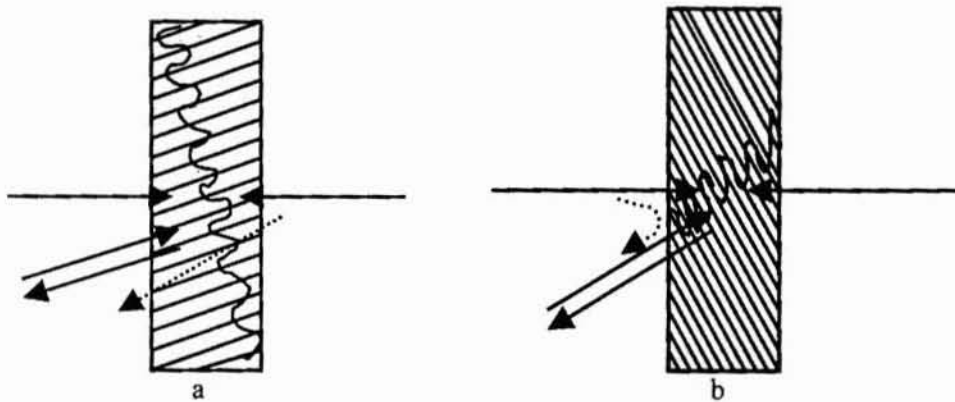
Fig. 5

a. Transmission grating   b. Reflection grating

The forward pump beam (P_f) appears to be reflected from this grating and hence this grating is called reflection grating (fig.5.b) The grating vector for transmission

grating and reflection grating are given by $(k_f - k_p)$ and $(k_b - k_p)$ respectively. These two vectors are orthogonal. Hence, only one of them will dominate. The last term corresponds to a temporally modulated grating (at frequency 2ω), which is stationary in space. The probe beam is diffracted from this grating. This grating is free from wash out effects. It is also to be noted that temporal grating does not have a holographic analogue. The eq. (2.14) gives the grating spacing [24] in terms of the wavelength λ, refractive index of the medium n and the angle between the beams θ.

$$\Lambda = \frac{2\pi}{k_G} = \frac{\lambda}{2n\sin(\theta/2)} \qquad (2.14)$$

Periodic modulation of any material property can be considered as a grating. Nature of the grating formed depends on the characteristics of medium as well as those of interacting fields. The gratings formed as a result of the interference of the beams may be classified into a number of categories like population grating [28], orientational grating [29], thermal grating, polarization grating [26,27] etc. Population grating is formed in an absorptive medium due to electronic excitation of the molecules. Orientational gratings are formed by induced reorientation of anisotropic molecules in presence of electromagnetic fields. Absorption of light and subsequent nonradiative de-excitation results in temperature rise, which leads to the formation of thermal grating [26, 27].

An advantage of DFWM is that we can select a particular susceptibility component of $\chi^{(3)}$ by suitably choosing the polarizations of input fields [24]. In the context of this thesis, we are interested in measuring the pure electronic contribution to nonlinearity. Therefore, polarizations of the interacting beams were adjusted such that the two pump beams are s-polarized (vertical polarization) and the probe beam is p-polarized (horizontal polarization). In this configuration a polarization grating is formed in the sample and $\chi^{(3)}$ component measured is $\chi^{(3)}_{xyyx}$. It is also to be noted that, while

formation of polarization grating, orientational grating etc. solely depends on local field (local response), thermal grating and the gratings formed in the photorefractive effect have nonlocal response [30].

Apart from back scattering geometry of DFWM, there are many other configurations for DFWM. Folded boxcar geometry and forward scattering geometry are a few of them [25].

2.1. Theory of DFWM

The theory of degenerate four wave mixing is based on coupled mode equations, which govern the spatial and temporal evolution of the signal under slowly varying amplitude approximation (SVAP) [23,25,31]. Using SVAP, second order Maxwell's equations can be reduced to first order differential equation. Practically, this approximations implies that growth of the signal with a particular frequency and wave vector, is determined only by the nonlinear polarization having the same modulation frequency and wave vector. This follows from the fact that power transferred to electric field is given by the volume integral of **E** & **P**. If **E** & **P** do not have the same frequency and wave vector, their volume integral will vanish because they are orthogonal functions. Mathematically SVAP is given by the inequality

$$\left|k^2 E\right| >> \left|k\frac{\partial E}{\partial z}\right| >> \left|\frac{\partial^2 E}{\partial z^2}\right| \tag{2.15}$$

It is assumed that two pump beams are of equal intensity and there is no pump depletion: i.e. $|E_1| = |E_2| =$ a constant. Therefore probe beam and phase conjugate beam are only considered. Nondestructive buildup of the signal occurs when nonlinear polarization (the source term in Maxwell's equation) is given by the relation

$$P_i(\omega = \omega + \omega - \omega) = 6\chi_{ijkl}(-\omega, \omega, \omega, -\omega)E_{1j}(\omega)E_{2k}(\omega)E_{p1}^*(\omega)\exp[-i(K_1 + K_2 - K_p) \cdot R]$$

(2.16)

The interaction between probe beam and phase conjugate beam are given by

$$\frac{dE_p}{dz} = -i\kappa^* E_c^* \qquad \frac{dE_c}{dz} = i\kappa^* E_p^* \qquad (2.17)$$

where κ is the coupling constant, given by eq. (2.18)

$$\kappa^* = (2\pi\omega / cn)\chi^{(3)}E_1 E_2 \qquad (2.18)$$

The solution to above equations are given by

$$E_c(0) = -i\left[\left(\frac{\kappa^*}{|\kappa|}\right)\tan(|\kappa|l)\right]E_p^* \qquad (2.19)$$

Eq. (1.18) shows that the phase conjugate signal is the complex conjugate of E_p. [Here we have used the boundary condition that $E_p(0)$ is finite and $E_c(l) = 0$]. If the ratio of the intensities of the pump and probe beams is always constant (i.e. if all the three beams are taken from a parent source) intensity of the phase conjugate signal is given by the relation

$$I(\omega) \propto \left(\frac{\omega}{2\varepsilon_0 cn^2}\right)^2 |\chi^{(3)}|^2 l^2 I_0^3(\omega) \qquad (2.20)$$

Third order susceptibility $\chi^{(3)}$ is usually measured with respect to a standard sample CS_2. In absence of linear absorption, third order susceptibility is given by

$$\chi^{(3)} = \chi_{ref}^{(3)} \left[\frac{\left(\frac{1}{I_0^3} \right)}{\left(\frac{1}{I_0^3} \right)_{ref}} \right]^{\frac{1}{2}} \left[\frac{n}{n_{ref}} \right]^2 \frac{l_{ref}}{l} \qquad (2.21)$$

If sample has linear absorption, eq. (2 21) has to be modified by considering the effect of linear absorption. It is assumed that optical density of the sample (i.e. αl, where α is the linear absorption coefficient and l is the sample length) is much less than one. In presence of linear absorption, susceptibility is given by the following equation

$$\chi^{(3)} = \chi_{ref}^{(3)} \left[\frac{\left(\frac{1}{I_0^3} \right)}{\left(\frac{1}{I_0^3} \right)_{ref}} \right]^{\frac{1}{2}} \left[\frac{n}{n_{ref}} \right]^2 \frac{l_{ref}}{l} \frac{\alpha l}{\left(1 - e^{-\alpha l} \right) e^{-\alpha l/2}} \qquad (2.22)$$

The reflectivity of the phase conjugate mirror R, is defined as the ratio of phase conjugate intensity to probe beam intensity.

$$R = \frac{I_c}{I_p} \qquad (2.23)$$

Eq. (2.23) can be written in terms of the coupling coefficient κ as in eq. (2. 24).

$$R = \tan^2 \left(|\kappa| l \right) \qquad (2.24)$$

2.2. Effects of absorption and pump depletion

In presence of pump beam depletion, phase conjugate reflectivity exhibit deviation in its behaviour from the eq. (2. 24). In such cases phase conjugate reflectivity is given by

$$R = \left| \frac{\kappa^* \tan(Bl)}{B + (\alpha / 2) \tan(Bl)} \right|^2 \qquad (2.25)$$

where
$$B = \left[|\kappa|^2 - (\alpha/2)^2\right]^{1/2} \qquad (2.26)$$

In the presence of pump depletion, the reflectivity becomes a multi-valued function of κ. This arises from the fact that energy is transferred from the pump beam to conjugate beam such that the total energy is invariant. In the case of one photon resonance, it is the imaginary part of the susceptibility, which contributes to the formation of grating, unlike in the non resonant case (where only real part contributes to the grating formation). If $\chi^{(3)}$ has an imaginary part of considerable magnitude, resonant TPA can take place at high intensities, giving rise to formation of thermal grating, concentration grating, free carrier gratings etc, depending on the sample. Net effect of TPA is to produce effective fifth order nonlinearity through cascading $\chi^{(3)}$: $\chi^{(1)}$ processes. Cascading is a situation where a few successive lower order linear or nonlinear effects are combined to produce an effective higher order nonlinear process. In such occasions, the phase conjugate signal may be fitted to an equation of the form [32]

$$I_c = b_3 I_{pump}^3 + b_5 I_{pump}^5 \qquad (2.27)$$

$\chi^{(3)}$ can also be calculated from the fitted value of b_3 of eq. (2. 27).

In the case of instantaneous response like optical Kerr effect, the pulse width of the phase conjugate signal will be 57.77% of the input pulse width for a gaussian pulse. This is approximately true in the case of hyperbolic secant squared pulse also. Therefore, presence of phase conjugate signal temporally broader than 57.71% of incident laser pulse width is an indication of the presence of slower process getting mixed up with instantaneous response. In some cases cascaded effects will imitate a third order process. Such effects have been reported in non-centrosymmetric materials. A few examples are concurrent processes of optical rectification and linear

electro optic effects. It has also been reported that piezoelectric effects can also give rise to signal in DFWM [33].

3. Instruments specifications:

Specifications of the laser sources, photodiodes and laser energy meters used for making measurements are given below.

3.1. Pulsed Nd: YAG laser [34]

Model and Make	: Quanta Ray. GCR: 170
Wavelength	: 532nm
Pulse energy (maximum)	: 450mJ
Pulse width	: 6 – 7 ns
Pulse repetition frequency	: 10 Hz
Spatial mode	: Gaussian (70%)

3.2. MOPO [35]

Model and make	: Quanta Ray MOPO – 710
Wavelength	: 410 – 690 nm (signal)
	: 730 – 2000 nm (idler)
Beam profile	: Gaussian (70%)
Pulse width	: 4 – 5 ns
Beam shape	: Beam shape (round ± 20%)

3.3. Photodiodes [36,37]

Model and make	: Newport 818 UV
Spectral range	: 190nm – 1100nm
Active area	: $1cm^2$
Model and make	: Melles Griot, 13DAS 007
Active area	: $0.1cm^2$

Spectral range	: 350 nm – 1100 nm
Breakdown Voltage	: 20 V
Dark current (at 1V)	: 10 nA

3.4. Oscilloscope [38]

Model and make	: Tektronix TDS 360
Rise time	: 1.75 ns
Input resistance	: 1 MΩ
Sensitivity	: 2 mV/division to 10 V/division

3.5. Energy meter
Detector head (Pyroelectric)

: Rjp – 7620 Energy Ratiometer
: Rjp - 735

3. 6. Spectrophotometer [39]

Model and Make	: Jasco 570
Wavelength range	: 190 nm to 2500
Resolution	: 0.1 nm (UV/Visible region)
	: 0.5 nm (NIR region)

References:

[1] M S Bahae, A A Said and E W Van Stryland, optics Opt. Lett. **14** (1989) p.955

[2] M S Bahae, A A Said, T H Wei, D J Hagan, E W V Stryland. IEEE J. Quantum Electroinics **26** (1990) p. 760

[3] T Xia, D J Hagan, M S Bahae and E W Van Stryland Opt. Lett. **19** (1994) p. 317

[4] M S Bahae, J. Wang, R De Salvo, D J Hagan and E W Van Stryland, Opt. Lett. **17** (1992) p.258

[5] H Ma and C B de Araujo. Appl. Phys. Lett. **66** (1995) p. 1581

[6] A Marcano O and F E Hernandez and A D Sena J. opt. Soc. Am. B **14** (1997) p. 3363

[7] F E Hernandez, A Marcano O, H Maillotte, Optics. Commun.**134** (1997) p.529

[8] A Marcano O, H Maillotte, D Gindre and D Metin. Opt. Lett. **21** (1996) p .101

[9] P Chen, D A Quilanov, I V Tomov and P M Rentzepis, J. Appl. Phys. **85** (10) (1999) p. 7043

[10] Yong-Liang Huang and Chi-Kuang Sun, J. Opt. Soc. Am. B **17** (1) (2000) p.43

[11] Robert E Bridges, George L Fischer and Robert W Boyd Opt. Lett. **20** (17) 1995 p. 1821

[12] P B Chapple, J Staromlynska and R G McDuff. J. Opt. Soc. Am. B **11** (1994) p. 975

[13] J A Herman, T McKay and R G McDuff. Opt. Commun. **154** (1998) p. 225

[14] K P Unnikrishnan, Jayan Thomas, V P N Nampoori and C P G Vallabhan. App. Phys. B **75** (2002) p. 871

[15] O V Przhonska, J H Lim, D J Hagan, E W V Stryland, M V Bondar and Y L Slominsky. J. Opt. Soc. Am. B **15** (1998) p.802

[16] M samoc, A Samoc, B L davies, H Reisch and U Scherf. Opt. Lett. **23** (1998) p. 1295

[17] S Couris, E Koudoumas, A A Ruth and S Leach. Phys. B At. Mol. Opt. Phys. **28** (1995) p. 4537

[18] T Xia, D J Hagan, A Dogariu, A A said and E W V Stryland. Appl. Opt. **36** (1997) p. 4110

[19] T Hattori and T Kobayashi. J. Chem. Phys. **94** (1991) p. 3332

[20] M D I Castillo, J J S Mondragon, S I Stepanov. Optic. **100** (1995) p. 49

[21] S J Bentley, R W Boyd, W E Butler and A C Melissions. Opt. Lett. **25** (2000) p. 1192

[22] Y R Shen Principles of Nonlinear Optics. John Wiley & Sons (SEA) Pte. Ltd. (Singapore)

[23] A Yariv. Optical Electronic in Modern Communications. Oxford University Press (1997) New York.

[24] Jun Ichi Sakai. Phase Conjugate Optics. Mc. Grow Hills New York

[25] R A Fischer (Ed.) Optical Phase Conjugation. Academic Press (1983) New York

[26] J A Nunes, W G Tong, D W Chandler, and L A Rahn. J. Phys. Chem. A **101** (1997) p. 3279

[27] D W Neyer, L A Rahn, D W Chandler, J A Nunes and W G Tong. J. Am. Chem. Soc. **119** (1997) p. 8293

[28] P C de Souza, G Nader, T catunda, M Muramatsu and R J Horowicz. Opt. Commun. **163** (1999) p. 44

[29] M F Yung and X Y Wong. Appl. Phys. B **66** (1998) p. 585

[30] P Cheben, F del Monte, D J Worsfold, D J Carlsson, C P Grover and J D Mackenzle. Nature **408** (2000) p. 64

[31] A Yariv and D M Pepper. Opt. Lett. **1** (1997) p. 16

[32] M Zhao, Y Cui, M Samoc and P N Prasad. J. Chem. Phys. **95** (1991) p. 3991

[33] I Biaggio. Phys. Rev. Lett. **82** (1999) p. 193

[34] User Manual, GCR Series. Spectra Physics Lasers Inc. (1997) CA, USA

[35] Instruction Manual MOPO 700 Series. Spectra Physics Lasers Inc. (1993) CA, USA.

[36] 818-UV Detector Calibration Report, Newport Corporation, CA, USA

[37] Melles Griot Catalogue 1997-98, Melles Griot Inc, USA

[38] User Manual TDS 360. Tektronix Inc. (1995) Wilsonville,

[39]Hardware Manual. Jasco 570, Jasco Corporation, Tokyo, Japan

3

Nonlinear absorption in phthalocyanines and naphthalocyanines at a fixed wavelength (532 nm)

Abstract

Nonlinear absorption in a number of phthalocyanines and naphthalocyanines viz., MoOPc, LaPc, Eu(Pc)$_2$, Sm(Pc)$_2$, Nd(Pc)$_2$ and Eu(Nc)$_2$ was investigated using open aperture Z-scan experiment at 532 nm using nanosecond pulses. Effective nonlinear absorption coefficient was measured. Nonlinear absorption was explained in terms of five-level model. The fluence level for nonlinear absorption in Eu(Nc)$_2$ was found to be around 0.4 Jcm^{-2}, which was about four times those of other samples. Among these samples, Eu(Pc)$_2$ was found to be a better nonlinear absorber.

1. Introduction

The amount of light absorbed in most of the absorbing materials increases linearly with input irradiance, giving rise to a constant transmittance. This is referred to as linear absorption. In such cases, absorption in a sample can be fully described by Beer– Lambert law. If α is the linear absorption coefficient, transmitted intensity I_t is related to input intensity I_0 by the relation

$$I_t = I_0 e^{-\alpha l} \qquad (3.1)$$

where l is the sample length. Obviously, α is independent of intensity and depends only on the wavelength of excitation [1].

Any deviation in the behaviour of absorption from eq.(3.1) is called nonlinear absorption. In such cases, absorption coefficient α can increase or decrease with respect to incident intensity. Thus, it is evident that in presence of nonlinear absorption, α becomes a function of intensity also and hence, it is usually written as $\alpha(I, \lambda)$. For a given wavelength, if $\alpha(I)$ increases with intensity, the corresponding phenomenon is called reverse saturable absorption (RSA) [2], which is the main topic of discussion in this chapter. On the other hand, if $\alpha(I)$ decreases with intensity, the process is called saturable absorption (SA), which is elaborated elsewhere. In the case of RSA, when incident intensity is increased, the sample becomes more opaque, whereas for SA, an increase in incident intensity makes the sample more transparent. Both RSA and SA have important technological applications. For example, RSA is exploited in passive optical power limiting to protect optical sensors, including human eye, from intense laser pulses [3-5]. SA is used in the passive mode locking of lasers [6]. A variety of materials have been synthesized and their nonlinear absorption studies have been reported by earlier researchers [7-17]. It has been found that phthalocyanines (Pcs) and their derivatives are a class of materials, which exhibit

RSA in the spectral region between Q-band and S–band of their ground state electronic absorption spectrum [18-20]. These materials can exhibit RSA under nanosecond and picosecond excitation [21]. Considering the importance of Pcs as nonlinear optical (NLO) materials with good optical limiting property, nonlinear absorption studies in certain Pcs have been carried out at 532nm and the results are included in this chapter. Samples selected for the study include mono Pcs, viz., LaPc, MoOPc; bis-Pcs viz., $Sm(Pc)_2$, $Eu(Pc)_2$ and $Nd(Pc)_2$ and a bis-Ncs viz. $Eu(Nc)_2$. Structures and absorption spectra of these samples have been discussed in chapter 1. There are two absorptive mechanisms effecting RSA, viz., instantaneous two photon absorption (ITPA) [17] and sequential two-photon absorption (STPA) [9]. STPA is also called excited state absorption (ESA). In addition, these samples are also known to exhibit nonlinear refraction. Measurements presented here were carried out in samples taken in solution form using nanosecond pulses. Hence, nonlinear refraction studies will give only thermal effects [22,23], which is negative in nearly all the cases. Thermal nonlinearity is not of our interest and hence detailed study of thermal effects have not been carried out.

2. Experimental

Z-scan is a simple and highly sensitive technique to study nonlinear absorption. All the measurements presented in this chapter were made using 532 nm of a frequency doubled Nd:YAG laser. Experimental details and laser beam specifications have been detailed earlier. The solutions of suitable concentrations were prepared by dissolving the samples in dimethyl formamide (DMF). Beam waist at focus and diffraction length z_0, both in the sample, were 13 μm and 1.5 mm respectively. The samples were taken in a cuvette of 1mm path length.

3. Nonlinear absorption in Pcs

A detailed discussion of excited states in Pcs is required to understand the results of open aperture Z-scan measurements. Excited states play a very important role in

determining the nonlinear and other photo-physical properties of Pcs and Ncs. Excited state dynamics in certain Pcs have been studied using femtosecond time resolved (transient) differential absorption (TDA) measurements in solution as well as in thin films. William et. al [24] have studied femtosecond excited state dynamics in polycrystaline / amorphous thin films of ClAlPc and FAlPc. Femtosecond excited state dynamics in PcS_4 and $ZnPcS_4$ in aqueous as well as in dimethyl sulphoxide (DMSO, organic solvent) solutions have been investigated by Howe et. al [25]. Femtosecond spectroscopy of VOPc has been studied by Terasaki et. al. [26]. Common observation is that nonlinear absorption takes place in solution and thin films of free base Pc (H_2Pc) and MPcs in the spectral region between their Q and S bands though, MPcs have been found to be better nonlinear absorbers than corresponding free base Pcs [27, 28]. This indicates that nonlinear absorption is a property of the Pc ring, though metal ions can modify it considerably. Femtosecond studies indicate that nonlinear absorption takes place in a time scale of sub-picoseconds. Considering the fast response time of nonlinear absorption, William et. al. [24] attributed the nonlinear absorption to TPA, which has been later identified to be STPA. Howe et. al [25] have measured the fluorescence in PcS_4 and $ZnPcS_4$, varying the wavelength of excitation from 390 nm to 670 nm. They could observe a red fluorescence (690 nm – 700 nm) for all the wavelengths of excitation, which indicated that fluorescence emission always occurred between the same levels, irrespective of the wavelength of excitation. They attributed this fluorescence to the $S_1 \leftarrow S_0$ transition. Upper excited singlet levels such as S_2 are short lived. Hence, even if atoms are initially excited to higher vibrational levels in S_2, they can immediately come back to S_1, the first excited singlet state in the time period of the pulse width of the laser. They could also detect a very weak fluorescence around 500 nm, which was attributed to the emission from S_2. However, it can be assumed that nearly all the molecules excited to S_2 and higher excited singlet states come back to S_1. Wei et. al [29] have studied the intensity dependence and fluence dependence of nonlinear absorption at 532 nm using picosecond pulses. It may be noted that pure

TPA depends purely on intensity, while ESA depends on the input fluence. By varying the pulse width, it is possible to make measurements at different intensity levels, keeping the fluence level the same. Wei et .al [29] observed that all the plots corresponding to the same fluence level had a perfect overlap, irrespective of the value of intensity. All these investigations have confirmed the fact that the mechanism of nonlinear absorption taking place in Pcs, in the wavelength region between their Q and S bands, is ESA. In this context, it is very relevant to point out that the mechanism of nonlinear absorption taking place in fullerenes (C_{60} and C_{70}) at 532 nm is also ESA [30–34]. Many researchers have investigated in detail the mechanism of ESA, both experimentally and theoretically [35-38]. These results indicate that ESA occurs when the absorption cross section of the excited states is higher than that of the ground state. SA occurs in all the other cases. It is important to note that ESA is different from TPA. TPA does not involve any real intermediate energy levels and two photons are absorbed simultaneously. On the other hand, ESA consists of two successive one-photon transitions involving real intermediate energy levels. The mechanism of ESA can be explained as follows.

Nonlinear absorption in macromolecules such as Pcs on irradiation with nanosecond and picosecond pulses can be explained using a five-level model shown in fig.1 [39-41]. S_n and T_n represent singlet and triplet manifolds (n = 0,1,2) respectively. Because of the very large size of these molecules, they will have a plethora of vibrational levels within each electronic level. At thermodynamic equilibrium nearly all the atoms occupy the lowest vibrational energy level (v = 0) of S_0. On irradiation with laser pulse, atoms in the lowest vibrational energy level of S_0 initially get excited to some upper vibrational energy level of S_1 through a one-photon transition. Subsequently, the excited atoms relax to the lowest vibrational energy level of S_1 (v = 0) through non-radiative decay within a few sub-picoseconds. Details of the non-radiative relaxation occurring in the vibrational levels of S_0, S_1 etc. are not relevant because it occurs in a time scale much less than the pulse width of the laser even for

picosecond excitation. From $S_1(v = 0)$ state, molecules again get excited to some vibrational levels of S_2. However, under nanosecond time scales, $S_2 \leftarrow S_1$ singlet transition does not deplete the population in S_1 appreciably as atoms excited to S_2 decay to S_1 $(v = 0)$ within picoseconds. It may be noted that the transitions $S_1(v = 0)$ $\leftarrow S_0(v = 0)$ and $S_2(v = 0) \leftarrow S_1(v = 0)$ are forbidden because of the even parity of the energy levels involved. Involvement of vibrational levels with appropriate parity is essential to preserve parity conservation in these transitions. From $S_1(v = 0)$, atoms can decay to T_1 $(v = 0)$ through intersystem crossing. Atoms can also go to S_0 through fluorescence. When excited with 532 nm, phthalocyanines exhibit only week fluorescence. Therefore, most of the atoms get de-excited to the first excited triplet state, viz., T_1 as a result of intersystem crossing.

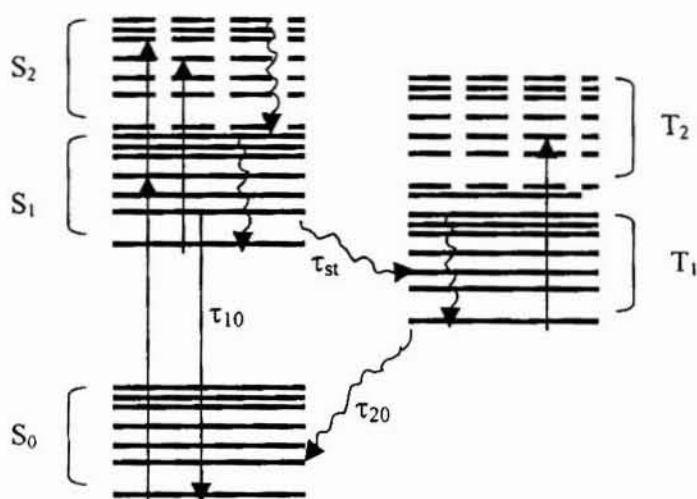Fig. 1 Five level energy diagram for Pcs
S_n (n = 0,1,2): Singlet levels; T_n(n = 1, 2): Triplet levels
Solid line: radiative; curved line: non-radiative

Intersystem crossing from S_1 to T_1 is a spin forbidden transition and hence it will occur comparatively slowly. Typical intersystem crossing rate is a few nanoseconds to nearly a hundred nanoseconds [42,43]. Besides, triplet states generally have a

lifetime higher than that of singlet states. A typical triplet state lifetime is also of the order of nanoseconds. Therefore, under picosecond excitation, intersystem crossing rate and triplet state populations are not relevant [39]. ESA under picosecond excitation takes place solely due to $S_2 \leftarrow S_1$ singlet transition [21]. Consequently, the explanation of ESA under picosecond excitation requires only three singlet energy levels viz., S_0, S_1 and S_2. However, under nanosecond excitation intersystem crossing rate and triplet state population are very significant. ESA observed in measurements using nanosecond pulses is attributed mostly to $T_2 \leftarrow T_1$ transition [44,45]. In short, Pcs can exhibit nonlinear absorption and hence optical power limiting, under nanosecond excitation through $T_2 \leftarrow T_1$ triplet transitions and under picosecond excitation through $S_2 \leftarrow S_1$ singlet transitions.

3.1. Effective nonlinear absorption coefficient

Though the original theory of Z–scan was derived for pure TPA, it has been shown that the same theory can also be used for ESA. However, in this case we have to properly redefine the nonlinear absorption coefficient β as β_{eff}. The present measurements have been taken using nanoseconds pulses and therefore, two assumptions can be made: (1) intersystem crossing [from $S_1(v = 0)$ to $T_1(v = 0)$] is fast compared to the laser pulse width and (2) intersystem crossing yield Φ_{isc} is nearly one i.e. virtually all the atoms excited from S_0 reach the first excited triplet state T_1. As mentioned previously, atoms then get excited from T_1 to T_2 as a result of ESA. Under these assumptions, intensity variation through the sample and population in the first excited triplet state T_1 are respectively given by following equations [18]

$$\frac{dI}{dz} = -\sigma_0 n_0 I - \sigma_t n_t I \tag{3.2}$$

$$n_t = \sigma_0 n_0 I \Phi_{isc}; \quad (\Phi_{isc} = 1) \tag{3.3}$$

Here σ_0, σ_t, n_0 and n_t are ground state absorption cross-section, first excited triplet state absorption cross-section, number of molecules in the ground state per ml and number of molecules in the first excited triplet state per ml respectively. (z' corresponds to sample length). From equations (3.2) and (3.3), the intensity dependent absorption coefficient $\alpha(I)$ and β_{eff} are given respectively by

$$\alpha(I) = \sigma_0 n_0 + \sigma_1 \sigma_0 n_0 I \qquad (3.4)$$

$$\beta_{eff} = n_0 \sigma_0 \sigma_1 \qquad (3.5)$$

It is clear that β_{eff} is intensity dependant for STPA through the factor n_0, whereas β is independent of intensity for pure TPA. β_{eff} is a measure of the over all absorptive nonlinearity present in the sample [43].

3.2. Rate equations

Dynamics of ESA can be described using rate equations. Under nanosecond excitation, amongst singlet excited states, population at S_1 alone is important. This is because of the fact that higher excited singlet states have a lifetime of the order of picosecond, which is less than the laser pulse width. Therefore, only the ground state (S_0), first excited singlet state (S_1) and first excited triplet state (T_1) are considered. If σ_g, σ_s and σ_t represent the absorption cross sections of S_0, S_1 and T_1 respectively, the rate equations for the populations in these energy levels may be written as [18]

$$\frac{dn_0}{dt} = -\frac{\sigma_0 I}{h\nu} n_0 + \frac{1}{\tau_{10}} n_1 + \frac{1}{\tau_{20}} \qquad (3.6)$$

$$\frac{dn_1}{dt} = \frac{\sigma_0 I}{h\nu} n_0 - \left(\frac{1}{\tau_{10}} + \frac{1}{\tau_{12}}\right) n_1 \qquad (3.7)$$

$$\frac{dn_2}{dt} = \frac{1}{\tau_{12}}n_1 - \frac{1}{\tau_{20}}n_2 \qquad (3.8)$$

Here n_0, n_1 and n_2 are the populations in S_0, S_1 and S_2 levels respectively. τ_{10}, τ_{12} and τ_{20} are the life times of $S_0 \leftarrow S_1$, $T_1 \leftarrow S_1$ and $S_0 \leftarrow T_1$ transitions respectively. Transmitted light intensity may be written in terms of total absorption coefficient, which is also a function of time. Eq. (3.9) and eq. (3.10), give total absorption coefficient and transmitted intensity respectively.

$$\alpha(t) = \sigma_0 n_0(t) + \sigma_1 n_1(t) + \sigma_2 n_2(t) \qquad (3.9)$$

$$\frac{dI}{dz} = -(\sigma_0 n_0 + \sigma_1 n_1 + \sigma_2 n_2)I \qquad (3.10)$$

The equations (3.9) and (3.10) can be numerically solved using the initial conditions, $n_0(t = -\infty, z) = N = n_0 + n_1 + n_2;$ $n_1(t = -\infty, z) = n_2(t = -\infty, z) = 0$. σ_1 and σ_2 are kept as adjustable parameters. In macromolecules the vibrational levels of excited singlet states (S_1 & S_2) and triplet states (T_1 & T_2) overlap in most cases. Intersystem crossing occurs in nanosecond time scales. Hence under picosecond excitation, S_2 level is considered instead of T_1. In the steady state conditions, the nonlinear absorption coefficient is written as [18]

$$\alpha = \alpha_0\left[\frac{1+KI'}{1+I'}\right] \qquad (3.11)$$

Here $I' = I/I_s$ where I_s is the saturation intensity and $K = \sigma_T/\sigma_0$. If K is greater than one, we get RSA and a value of K less than one, yields SA. In this chapter, β_{eff} is measured using two-photon absorption theory introduced by Sheik Bahae et. al [46].

4. Nonlinear Refraction

Closed aperture Z-scan experiment yields information regarding nonlinear refraction in the samples. However, as indicated earlier, closed aperture Z-scan experiments carried out in samples in solutions from will give the effect of nonlinear refraction due to thermals effects. In most of the cases cases, thermal nonlinearity is negative and it is characterized by a pre-focal maximum and a post-focal minimum as shown in the fig. 2. Thermal nonlinearity is totally different from electronic nonlinearity. It essentially arises from local heating of the sample due to release of thermal energy on nonradiative decay. Local heating results in local refractive index change. In the context of this thesis, we are interested in electronic contribution to nonlinearity alone.
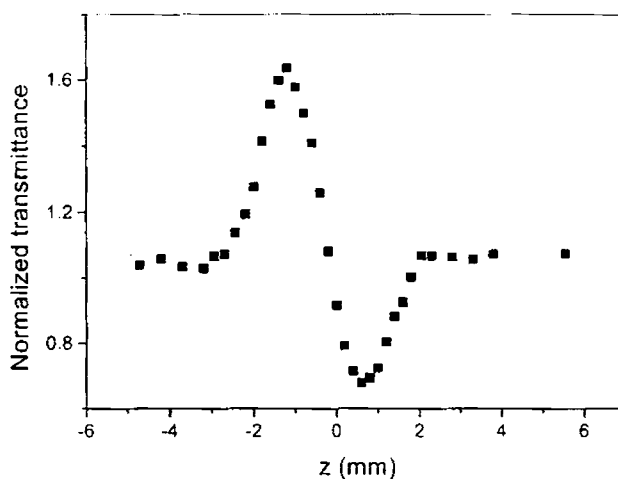
Fig. 2. Closed aperture Z-scan graph (thermal refraction)

$Eu(Pc)_2$ (0.12 mM)

5. Results and discussion

Open aperture Z-scan plots obtained for MoOPc and LaPc in presence of ESA are shown in fig. 3. These plots are typical of all samples exhibiting ESA. Transmittance is a minimum at the focus and increases steadily on both sides of the focus. β_{eff} is obtained by fitting the experimental open aperture Z-scan plot to the eq. (3.12) [46]

$$T(z) = \frac{C}{q_0 \sqrt{\pi}} \int_{-\infty}^{\infty} \ln(1 + q_0 e^{-t^2}) dt \qquad (3.12)$$

where

$$q_0(t) = \beta I_0(t) L_{eff} \qquad (3.13)$$

Here C is the normalizing constant, L_{eff} is the effective length and I_0 is the irradiance at focus. The measured values of β_{eff} for MoOPc and LaPc are given in table I, along with their concentration and irradiance at focus.

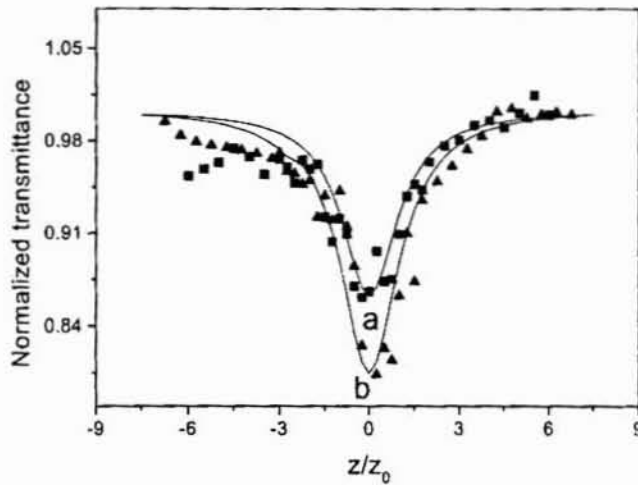Fig.3. Open aperture Z-scan curves
a. MoOPc (0.42 mM); b. LaPc (0.48 mM)

Table I: Values of β_{eff} for MoOPc and LaPc along with concentration and irradiance

Sample	Concentration (mM)	Irradiance(I_0) MW cm^{-2}	β_{eff} cm GW^{-1}
MoOPc	0.42	217	24.4
LaPc	0.48	183	44

β_{eff} is a measure of the strength of nonlinear absorption and optical power limiting [42]. β_{eff} of LaPc is nearly two times that of MoOPc. This indicates that nonlinear absorption is high in LaPc. Since β_{eff} is an effective quantity, it depends on intensity of excitation and concentration of the sample [45]. In the present case, LaPc and MoOPc have nearly identical concentrations (Table I). However the power levels of the experiments differ. Therefore, we can plot nonlinear transmission as a function of input fluence. Such plots can represent a better comparison of the nonlinear absorption or nonlinear transmission in these samples.
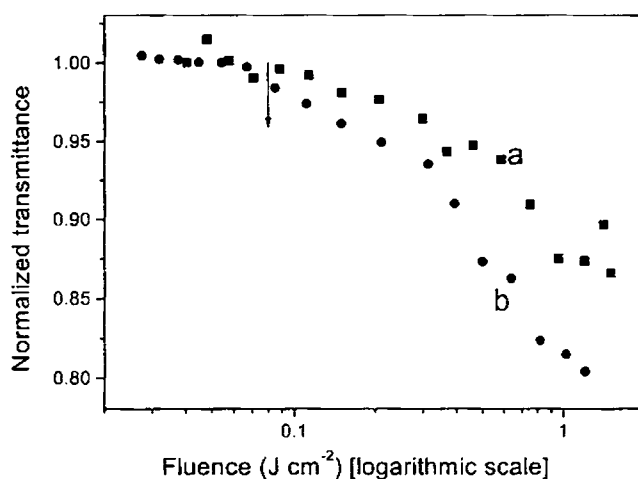
Fig. 4. Nonlinear transmission (fluence on logarithmic scale)
a. MoOPc (0.42 mM); b. LaPc (0.48 mM)

Fig. 4 shows the nonlinear transmission for MoOPc and LaPc. These plots were generated from Z-scan measurements. From the value of fluence at focus, fluence values at other sample positions (z) can be calculated using standard equations for gaussian beam waist. It can be seen that optical limiting property is high in the case of LaPc. The downward arrow indicates the approximate fluence level at which the transmission begins to deviate from linear transmission. It can be seen that these two samples have nearly identical fluence levels for the onset of optical limiting ($\approx$ 0.08 Jcm^{-2}).

Plots similar to those in fig. 3 were obtained for certain bis-Pcs viz. $Eu(Pc)_2$, $Sm(Pc)_2$ and $Nd(Pc)_2$ as well as for a bis-Nc viz. $Eu(Nc)_2$ using open aperture Z-scan technique. However, only the plots of nonlinear transmission generated from Z-scan graphs are presented here. It may be noted that the structures of mono Pcs [LaPc, MoOPc] differ from those of bis-Pcs [$Eu(Pc)_2$, $Sm(Pc)_2$ and $Nd(Pc)_2$] and bis - Ncs. Values of β_{eff} obtained for these samples are given in table II along with their irradiance at focus and concentrations.

Table II: β_{eff} values of $Eu(Pc)_2$, $Sm(Pc)_2$ and $Nd(Pc)_2$ along with concentration and irradiance

Sample	Concentration (mM)	Irradiance (MW cm^{-2})	β_{eff} (cm GW^{-1})
$Eu(Pc)_2$	0.22	89	126
$Sm(Pc)_2$	0.19	164	28
$Nd(Pc)_2$	0.17	164	29

β_{eff} values of $Eu(Pc)_2$ is much higher than those of $Sm(Pc)_2$ and $Nd(Pc)_2$. From the measured values of β_{eff}, it can be seen that $Eu(Pc)_2$ is a better nonlinear absorber and hence a good optical limiter than the other two samples. Fig. 5 shows the nonlinear transmission for these samples. The optical limiting property of $Sm(Pc)_2$ and $Nd(Pc)_2$ are nearly identical. The fluence level for optical power limiting of these samples is nearly 90 mJcm^{-2} as indicated by the arrow in fig 5. It is to be noted that $Nd(Pc)_2$ and $Eu(Pc)_2$ differ slightly in their concentration. Since values of β_{eff} depend on concentration it has to be verified whether the better optical limiting property of

Eu(Pc)$_2$ is due to its marginally higher concentration. Hence samples of identical concentration of Nd(Pc)$_2$ and Eu(Pc)$_2$ was prepared and experiment was repeated.

Fig.5. Nonlinear transmission in certain bis-Pcs
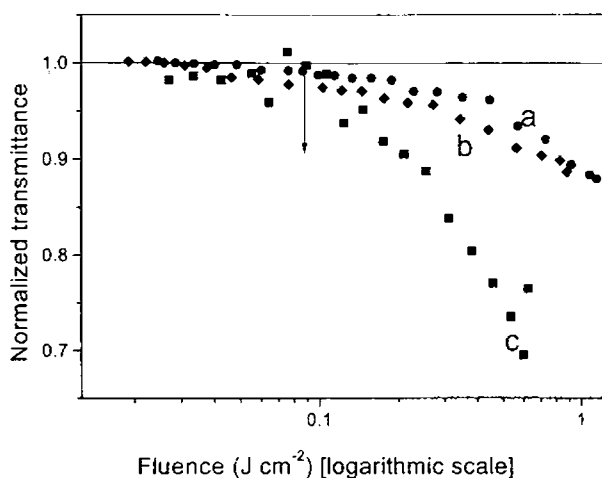
a. Nd(Pc)$_2$ (0.19 mM); b. Sm(Pc)$_2$ (0.17 mM); c.Eu(Pc)$_2$ (0.22 mM)
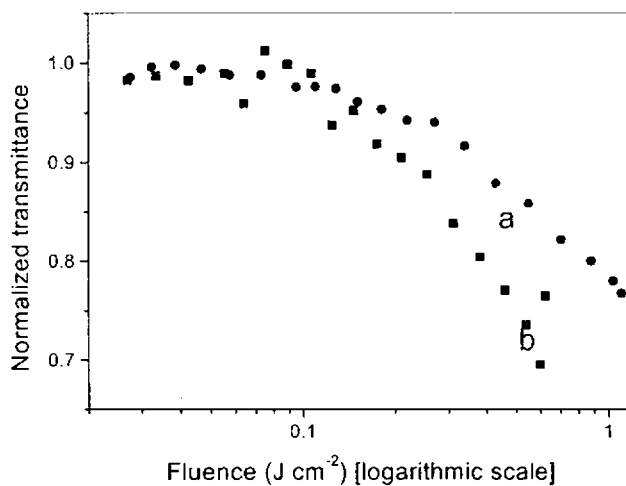
Fig. 6. Nonlinear transmission

a. Nd(Pc)$_2$ (0.24 mM); b. Eu(Pc)$_2$ (0.22 mM)

Fig. 6 shows the nonlinear transmission for solutions of $Nd(Pc)_2$ and $Eu(Pc)_2$, having nearly identical concentrations. It can be seen that optical limiting property is higher for $Eu(Pc)_2$ in this case also. Hence, it can be concluded that under nanosecond excitation optical limiting property of $Eu(Pc)_2$ is the highest amongst the bis-Pcs investigated here.

Fig. 7 shows the nonlinear transmission for a bis-naphthalocyanines, viz. $Eu(Nc)_2$. β_{eff} was obtained to be 39 $cmGW^{-1}$ for an irradiance of 152 MW cm^{-2} at focus. It can be seen that the fluence level for optical limiting is higher (≈ 0.4 Jcm^{-2}, arrow in fig.7) in the case of $Eu(Nc)_2$. The value of fluence for the onset of optical limiting in bis-Pcs is around 90 $mJcm^{-2}$.
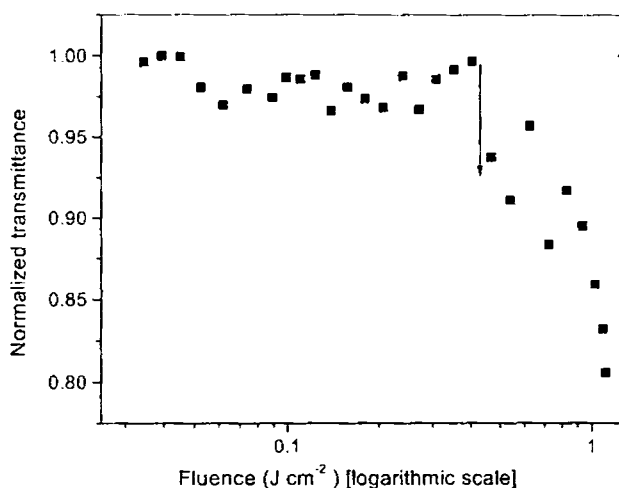
Fig. 7. Nonlinear transmission in $Eu(Nc)_2$ (0.2 mM)

Therefore, the fluence level for optical limiting for $Eu(Nc)_2$ is nearly four times higher than those of mono Pcs and bis –Pcs investigated here. A comparison of fig. 7 with fig. 4, fig. 5 and fig. 6 indicates that in the case of $Eu(Nc)_2$, beyond the threshold level, there is a comparatively faster decrease in the transmitted fluence. There are reports that Ncs undergo photochemical changes on laser irradiation [10,11]. Besides, it has also been reported that Ncs are better optical limiters at higher laser irradiance,

which is consistent with our observation. An advantage of Ncs is that they can act as optical limiters in the red region of the visible spectrum also, where Pcs absorb strongly, because the Q-bands of Ncs are considerably red shifted from those of Pcs.
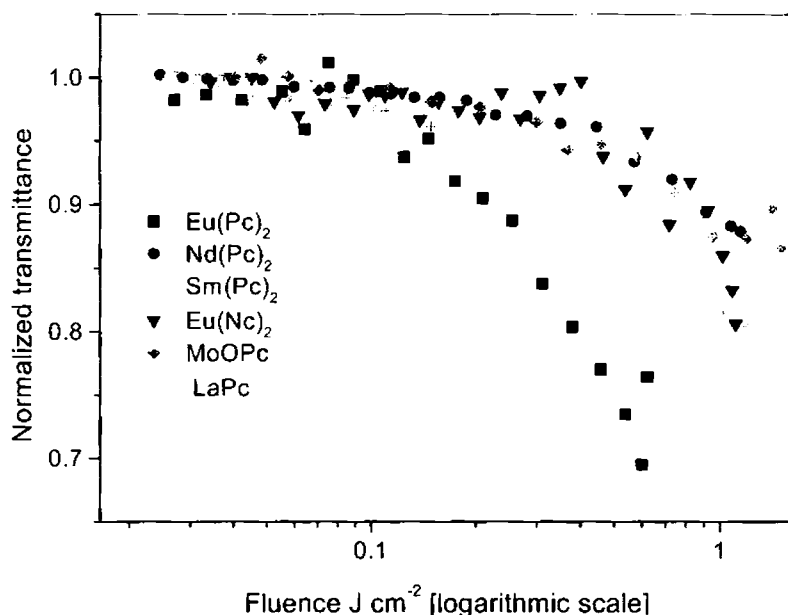
Fig. 8. Nonlinear transmission
Sm(Pc)$_2$ (0.17 mM), Eu(Nc)$_2$ (0.2 mM), Nd(Pc)$_2$, MoOPc (0.42 mM)
LaPc (0.48 mM), Eu(Pc)$_2$ (0.22 mM)

Fig. 8 shows the nonlinear transmission in all the samples discussed in the current investigation. Even though the concentrations are different, a comparison of their optical limiting property is very appropriate. In spite of its comparatively low concentration, Eu(Pc)$_2$ shows better optical limiting than MoOPc and LaPc, both of which have concentrations two times that of Eu(Pc)$_2$. The fluence level for optical limiting is the highest for Eu(Nc)$_2$ amongst all the samples studied.

Under nanosecond excitation, ESA and therefore, optical limiting occur as a result of T$_2$ ← T$_1$ transition [35]. Hence the strength of nonlinear absorption depends on

$\Phi_T \times \sigma_T / \sigma_g$, where Φ_T is the intersystem crossing rate [47]. Thus, under nanosecond excitation if the intersystem crossing rate is very small, the effect of nonlinear absorption can be less even if σ_T / σ_g is fairly high. While describing β_{eff}, it was assumed that $\Phi_T = 1$; however, in many cases intersystem crossing rate, which depends on a number of factors, is less than unity.

Rate of intersystem crossing is explained using eq. (3.14) [48]. The term $\langle \psi_S | H_{SO} | \psi_T \rangle$ gives the spin-orbit coupling and $|\langle \chi_S | \chi_T \rangle|^2$ is the Frank Condon factor. Delta function indicates that only the levels for which $E_T \approx E_S$ will contribute to the intersystem crossing rate.

$$k_{isc} = \left(\frac{2\pi}{\hbar} \right) |\langle \psi_S | H_{SO} | \psi_T \rangle|^2 \times \sum_T |\langle \chi_S | \chi_T \rangle|^2 \delta(E_S - E_T) \qquad (3.14)$$

If the central metal ion of MPcs has unfilled d-shell, there is good interaction between d electrons and delocalized π electrons of the Pc ring through spin–orbit coupling [24]. The net intersystem crossing rate will be high only if both spin-orbit coupling and vibrational overlap integral (Franck Condon factor) are sufficiently large. Therefore, it must be noticed that the observed results depend on the term $\Phi_T \times \sigma_T / \sigma_g$ and not on σ_T / σ_g alone. All the samples investigated here, except MoOPc, have rare earth metal ions.

Though the predominant mechanism of ESA under nanosecond excitation is $T_2 \leftarrow T_1$ transition, the possible contributions from S_1 to ESA can also taken into account by defining an effective excited state absorption cross section (σ_{exc}^{eff}) as $f_s \sigma_s + f_t \sigma_t$ [23, 48], where σ_s and σ_t correspond to absorption cross sections of S_1 and T_1 states respectively. f_s and f_t give populations in S_1 and T_1 respectively. The figure of merit of nonlinear absorption is given by (σ_{exc}^{eff})/ σ_g. Relative contributions to ESA from

levels S_1 and T_1 can be obtained from the ratio $f_s\sigma_s/ f_t\sigma_t$. If this ratio is of the order of unity, it means that both $S_2 \leftarrow S_1$ and $T_2 \leftarrow T_1$ transitions contribute to ESA. If this ratio is very large, implication is that $S_2 \leftarrow S_1$ transition is dominant. In the case of aza-substituted porphyrazine derivatives, it has been found that the dominant contribution to ESA comes from $S_2 \leftarrow S_1$ transition even under nanosecond excitation [48]. However in most of the MPcs, under nanosecond excitation, $T_2 \leftarrow T_1$ transition is the dominant contributor to ESA.

Like ESA, pure TPA (Two- Photon Absorption) can also be used for optical power limiting. Threfore, it is appropriate to compare the merits of these two process. ESA requires that samples should have a weak linear absorption. On the other hand, in the case of TPA, until the threshold is reached, there is near total transparency. Pure PTA has instantaneous response. The most important advantage of pure TPA is that it retains the optical quality of the beam after tranvesing through the sample [49]. However, in the case of ESA, transmitted pulse need not retain the incident pulse shape. The relaxation process of TPA is determined by the time required for the restoration of population in the ground state of the molecular systems.

5.1. Concentration dependence

Pcs can form dimers and oligomers at higher concentration due to aggregation of the molecules. In the absence of dimer formation, β_{eff} value increases linearly with concentration [34]. Hence, a study of the concentration dependence of nonlinear absorption in Pcs is required to verify if dimers are formed in the present experimental condition. Fig 9 shows the open aperture Z-scan curves obtained for $Nd(Pc)_2$ for different concentrations, at nearly identical irradiance values. Magnitude of nonlinear transmission gets increased as concentration of the samples is increased. Values of β_{eff} measured for different concentrations and the results obtained are given in Table III.
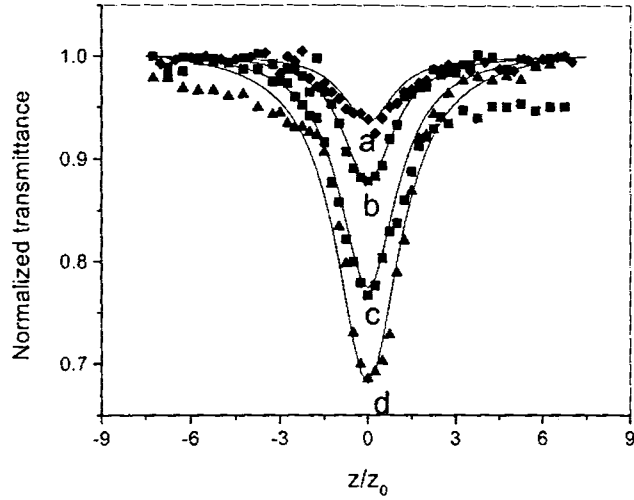
Fig. 9. Open aperture Z-scan curves for different concentration $Nd(Pc)_2$
a. 0.11 mM; b. 0.186 mM; c. 0.24 mM; d. 0.4 mM

Table III: β_{eff} for different concentrations for $Nd(Pc)_2$

Concentration (mM)	Incident power (MW cm^{-2})	β_{eff} (cm GW^{-1})
0.106	160.5	13.2
0.186	164	27.5
0.235	157	66.5
0.4	159	119.4

Fig. 10 shows the plot of β_{eff} against concentration. The plot is a straight line, which implies the absence of dimer formation up to a concentration of 0.4 mM. Slightly scattered nature of β_{eff} values in fig. 10 may be attributed to small variations in the input irradiance level, which arise because of pulse to pulse variation of laser pulse energy.
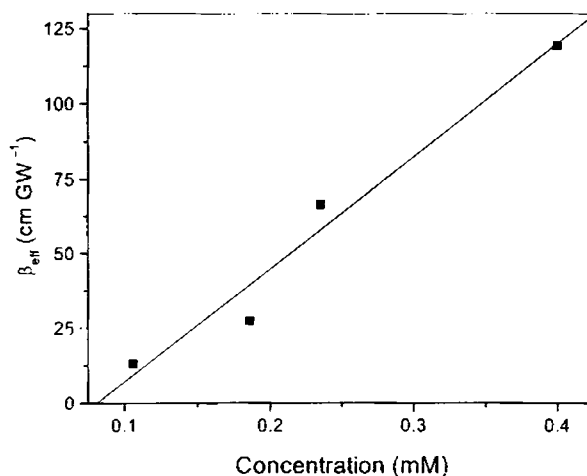
Fig. 10. Plot of β_{eff} values against concentration

Concentrations of all the samples used for Z-scan measurements are less than 0.4 mM and therefore, it can be assumed that dimer formation is not significant to affect the measurements in the present case. Fig. 11 shows the plots of nonlinear transmission for various concentrations. It can be seen that all the plots are similar except for the magnitude of nonlinear transmission. There is no any remarkable difference in the fluence level for the onset of optical limiting for different concentration of the samples. This implies that concentration does not influence the optical limiting considerably in these samples. It may be appropriate to compare the present results with those reported for fullerenes, C_{60}, which also exhibits ESA like Pcs under nanosecond and picosecond excitations [14,34]. Nonlinear transmission studies reported in C_{60} under nanosecond excitation shows concentration dependence, but
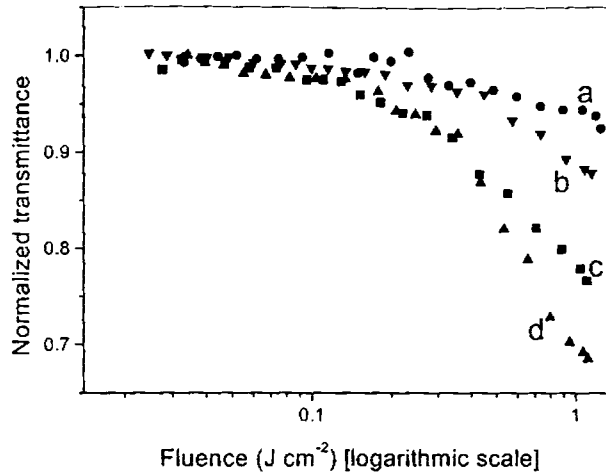
Fig. 11. Nonlinear transmission in $Nd(Pc)_2$ for different concentrations
a. 0.11 mM; b. 0.19 mM; c. 0.24 mM; d. 0.4 mM

such concentration dependence is absent under picosecond excitation. Riggs et. al [50] have attributed the concentration dependence of nonlinear transmission under nanosecond excitation to some bimolecular processes involving excited first triplet state T_1.

6. Conclusions

Nonlinear absorption in a number of Pcs viz., LaPc, MoOPc, $Eu(Pc)_2$, $Sm(Pc)_2$ and $Nd(Pc)_2$ and also in a bis-Nc viz. $Eu(Nc)_2$ was studied using open aperture Z-scan experiments. Nonlinear transmission and optical limiting were explained in terms of a five-level model. Values of β_{eff} were also determined. It was observed that among mono Pcs studied here viz. MoOPc and LaPc, LaPc was found to be a better NL absorber. Among bis-Pcs viz. $Eu(Pc)_2$, $Sm(Pc)_2$ and $Nd(Pc)_2$, $Eu(Pc)_2$ exhibited better nonlinear absorption. The transmission in these samples was found to deviate from linear transmission around a fluence level of 80-90 mJcm^{-2}. In the case of $Eu(Nc)_2$, nonlinear transmission was observed from an input fluence level of around 0.4Jcm^{-2}, which is nearly four times than those of other Pcs mentioned here.

References

[1] Y Kojima, T Matsuoka, N Sato and H Takahashi. Macromolecules **28** (1995) p. 2893

[2] B C Ozkul, F . Sanchev. Appl. Phys. B **68** (1999) p. 39

[3] J S Shirk, R G S Pong, F J Bartoli and A W Snow. Appl. Phys. Lett. **63** (1993) p. 1880

[4] M A Diaz, A Dogariu, D J Hagan, E W V Stryland. Chem. Phys. Lett. **226** (1997) p. 86

[5] S R Mishra, H S Rawat, M Lagate. Opt. Commun. **147** (1998) p. 328

[6] M Wittmann, A Penkofer. Appl. Phys. B. **65** (1997) p. 761

[7] Tai-Huei Wei, Tzer H Huang and M S Lin. Appl. Phys. Lett. **72** (1998) p.2505

[8] C R Mendonca, L Gaffo, L Misoguti, W C Moreira, O N OliveriaJr. S C Zilio.
Chem. Phys. Lett. **323** (2000) p. 300

[9] M Hanack, D Dini, M Barthel, S Vagin. The Chem. Record **2** (2002) p. 129

[10] M Hanack, T Schneider, M Barthel, J S Shirk, S R Flom, R G S Pong. Coord.
Chem. Revs. 219 – 221 (2001) p. 235

[11] D Dini, M Barthel and M Mahack. Eur. J. Org. Chem. (2001) p. 3759

[12] J E Riggs and Ya – Pin Sun. J. Chem. Phys. **112** (2000) p. 4221

[13] T C Wen, S P Chen, C Y Tsai. Synthetic Metals. **97** (1998) p. 105

[14] T H Wei, T H Huang, T T Wu, P C Tsai, M S Lin. Chem. Phys. Lett. **318** (2000) p. 53

[15] B L Justus, Z H Kafafi and A L Huston. Opt. Lett. **18** (1993) p. 1603

[16] F M Qureshi, S J Martin, X Long, D D C Bradley, F Z Henari, W J Blau, E C Smith, C H
Wang, A K Kar, H L Anderson. Chem. Phys. **231** (1998) p. 87

[17] G S He, G C Xu, P N Prasad, B A Reinhardt, J C Bhatt, A G Dillard. Opt. Lett.
20 (1995) p. 435

[18] C Li, L Zhang, M yang, H Wang, Y Wang. Phys. Rev. A **49** (1994) p. 1149

[19] G de la Torre, P. Vazquez, F A Lopez, T Torres. J. Mater. Chem. **8** (1998) p. 1671

[20] G. de la Torre, M. Nicolau and T.Torres in "Phthalocyanines: synthesis,
Supramolecular, organization and physical properties", in H.S. Nalwa (ed)
Supramolecular photosensitive and electroactive materials.   Chapter 1, p. 1-
111, Academic press (April 2001)

[21] M Pittman, P Plaza, MM Martin, Y H Meyer Opt. Commun. **158** (1998) p. 201

[22] M P Sing and S C Mehendale. IEEE J. OE. **34** (1998) p. 1867

[23] C Y Tsai, S P Chen, T C Wen. Chem. Phys. **240** (1999) p. 191

[24] V S Williams, S Mazumdar, N R Amstrong, Z Z Ho and Peyghambarian. J.
Phys. Chem. **96** (1992) 4500

[25] L Howe and J Z Zhang. J. Phys. Chem. A **101** (1997) 3207

[26] A Terasaki, M Hasoda, T Wada, H Tada, A Koma, A yamada, H sasabe, A F
Garito, T Kobayashi. J. Phys. Chem. **96** (1992) 10534

[27] K Dou, X Sun, X Wang, R Parkhill, Y Guo, E T Knobbe. Solid. State Commun. 107
(1998) p. 101

[28] J W Perry, K Mansour, S R Marder, K J Perry, D Alvarez Jr.I Choons. Opt. Lett. **19**
(1994) p. 625

[29] T H Wei, D J Hagan, M J Sence, E W Van Stryland, J W Perry and D R Coulter.
App. Phys. B. **54** (1992) p. 46

[30] J Shell, D Ohlman, D Brinkmann, R Levy, M Joucla and J L Rehspringer, B Horerlage J.
Chem. Phys. **111** (1999) p. 5929

[31] J E Riggs and Y P Sun. J. Phys. Chem. A **103** (1999)p. 485

[32] B L Justus, Z H Kafafi and A L Huston. Opt. Lett. **18** (993) p. 1603

[33] M Cha, N S Saricftci, A J Heeger, J C Hummelen. Appl. Phys. Lett. **67** (1995) p. 3850

[34] M Konstantaki, E Koudoumas, S Couris, J M Janot, H Eddaoudi, A Deratani, P Seta, S Leach. Chem. Phys. Lett. **318** (2000) p. 488

[35] T Xia, D J Hagan, A Dogariu, A A said and E W V Stryland. Appl. Opt. **36** (1997) p. 4110

[36] P A Miles, Appl. Opt. **33** (1994) p. 6965

[37] G R J Williams. Appl. Phys. B. **63** (1996) p. 47

[38] P K Milson. Appl. Phys. B **70** (2000) p. 593

[39] T H Wei, T H Huang and H D Lin. Appl. Phys. Lett. **67** (1995) p. 2266

[40] Dou, X Sun, X Wang, R Parkhill, Y Guo and E Knobbe. IEEE J. QE. **35** (1999) p. 1004.

[41] G R Kumar, M Ravikanth, S Banerjee, A Sevian. Opt. Commun. **144** (1997) p. 245

[42] H Stiel, A Volkmer, I Ruckmann, A Zeug, B Ehrenberg, B Roder. Opt. Commun. **155** (1998) p. 135

[43] K P Unnikrishnan, Jayan Thomas, Binoy Paul, A Kurian, P Gopinath, V P N Nampoori and C P G Vallabhan. J. Non. Opt. Phys. & Mater. **10** (2001) p. 113

[44] K P Unnikrishnan, Jayan Thomas, V P N Nampoori and C P G Vallabhan. Opt. Commun. **204** (2002) p. 385

[45] S Couris, E Koudoumas, A A Ruth and Leach. Phys. B, At. Mol. Opt. Phys. **28** (1995) p.4537

[46] M S Bahae, A A said, T H Wei, D J Hagan and E W V Stryland. IEEE J. QE **26** (1990) p. 760

[47] G L Wood, M J Miller and A G Mott. Opt. Lett. **20** (1995) p. 973

[48] T C Wen and C T Tsai. Chem. Phys. Lett **311** (1999) p. 173

[49] G H He, C Weder, P Smith and P N Prasad. IEEE J. OE **34** (1998) p.2279

[50] J E Riggs and Y P Sun. J. Phys. Chem. A **103** (1999) p. 485

4

Wavelength dependence of nonlinear absorption in certain bis–phthalocyanines

Abstract

Wavelength dependence of nonlinear absorption in three bis-phthalocyanines, viz., $Nd(Pc)_2$, $Sm(Pc)_2$ and $Eu(Pc)_2$, was studied using open aperture Z-scan technique in the blue side of their Q-band. The objective of the measurements was to determine the wavelength region over which the mechanism of nonlinear absorption changes from reverse saturable absorption (RSA) to saturable absorption (SA). Resonant enhancement of imaginary part of third order susceptibility was also investigated. It was observed that both $Nd(Pc)_2$ and $Eu(Pc)_2$ exhibited RSA at 604nm, while $Sm(Pc)_2$ exhibited SA at this wavelength. Besides, resonant enhancement effect was found to be the highest in $Nd(Pc)_2$ and the lowest in the case of $Eu(Pc)_2$.

1. Introduction

Phthalocyanines (Pcs), porphyrins and their different derivatives are known to exhibit nonlinear absorption at 532 nm [1-2]. Nonlinear absorption exhibited by many of the metal substituted Pcs was investigated in the previous chapter in detail. Most of the nonlinear absorption studies carried out in Pcs, porphyrins as well as in their derivatives have been confined to 532 nm [3-5] and 1.06 μm [6,7] alone, mainly due to the unavailability of a laser source having wavelength tunability in the desired spectral range. Investigation of the wavelength dependence of nonlinear absorption, particularly along the absorption band, becomes very important and highly desirable when optical limiting (OL) application of these samples is considered. It is highly desired that optical limiters have broad band spectral response [8]. Pcs and their different derivatives exhibit optical limiting property at 532 nm predominantly due to excited state absorption (ESA) [9,10]. ESA occurs when excited states have an absorption cross section higher than that of the ground state [11,12]. When the wavelength of excitation is shifted closer to the wavelength of one-photon resonant absorption, magnitude of ground state absorption cross section will increase steadily. Consequently, the mechanism of nonlinear absorption gradually changes from ESA to saturable absorption (SA). In the case of SA, transmitted intensity increases with respect to incident intensity [13,14]. SA is strongly a non-parametric process. Usually nonlinear optical process is described by a nonlinear polarization, which can be expressed as a power series in electric field strength [eq. (1.3) of chapter I]. However, owing to the strongly non-parametric nature of SA, which involves one–photon resonant transition between real energy levels, such a power series expansion is not valid. However, since SA is an intensity dependent absorption, SA is also considered to be a nonlinear phenomenon. In fact, SA is an example of resonant nonlinearity [15]. A salient feature of resonant nonlinearity is the considerable enhancement in the magnitude of nonlinear coefficients with respect to nonresonant quantity [16]. Therefore, the investigation of wavelength dependence of nonlinearity will also help to study the resonant enhancement effects in different samples. Resonant nonlinearity

is basically an absorptive nonlinearity and as its magnitude increases, magnitude of refractive nonlinearity decreases. At the peak of one-photon resonant absorption, refractive nonlinearity is zero and therefore observed nonlinearity is entirely absorptive [17]. In most of the experimental situations a combination of a weak resonant and a background nonresonant nonlinearity is observed instead of a completely resonant or completely nonresonant nonlinearity. A fundamental draw back of the resonant nonlinearity is its slow response [18], but its advantage is, its enormously large magnitude. Besides, in the context of Pcs, the wavelength region over which ESA gets changed to SA will set the wavelength limit for passive optical power limiting. Thus, the study of wavelength dependence of nonlinear absorption is also important in technological application. It may also be noted that SA is exploited in the passive mode locking of lasers [19]. Considering its importance, resonant nonlinearity in three bis-phthalocyanines viz., $Sm(Pc)_2$, $Eu(Pc)_2$ and $Nd(Pc)_2$ along their absorption band in the visible region was studied using open aperture Z-scan technique and the results obtained therein are included in this chapter. Wavelength over which the mechanism of nonlinear absorption changes from reverse saturable absorption (RSA) to ESA (and vice versa) in these samples to the red side of 532 nm was also identified. In fact, the wavelength at which the mechanism of nonlinear absorption changes from SA to ESA, loss of laser power due to nonlinear absorption in the sample is a minimum. In this region nonlinearity is predominantly refractive.

A large number of resonant transition, such as electronic, vibrational and rotational transitions, are possible in macromolecules with extensive π electron conjugation. Each of these transitions may produce resonance effects. The relative strength of different transitions varies over several orders of magnitude [16]. For example, the strength of spin forbidden singlet to triplet transition can be as low as 10^{-12}. The spin allowed transition (e.g. $\pi \rightarrow \pi^*$ transition) may have a (relative) strength, which is nearly equal to unity. Even for symmetry allowed transitions, the strength can vary by a few orders of magnitude. For example, both $\pi \rightarrow \pi^*$ transition and $n \rightarrow \pi^*$ transition

are allowed. The strength of $n \rightarrow \pi^*$ transition is much less than that of $\pi \rightarrow \pi^*$ transition because of very low overlap between the molecular orbitals in the case of $n \rightarrow \pi^*$ transition. The change in permanent dipole moment occurring in the sample on excitation need not necessarily be related to the strength of the transition [16]. Large changes in dipole moment are known to occur for both weak and strong transitions. The resonant absorption relevant in the context of present experiments is the $S_1 \leftarrow S_0$ electronic transition, which is a spin allowed $\pi \rightarrow \pi^*$ transition. The vibrational transitions taking place in S_0 and S_1 are very fast (picosecond time scale) and hence those transitions can be neglected in the present studies.

2. Experimental

Phthalocyanines such as $Sm(Pc)_2$, $Eu(Pc)_2$ and $Nd(Pc)_2$ with identical structures were selected for the investigation. The structure and absorption spectrum of these samples are given in chapter 1. Q-bands of $Eu(Pc)_2$ and $Sm(Pc)_2$ are doublet with two peaks, one at 628 nm and the second one at 672 nm. The second peak is very less prominent for $Eu(Pc)_2$ but for $Sm(Pc)_2$ this peak is very prominent and nearly as intense as that at 628 nm. The Q-band of $Nd(Pc)_2$ has only one peak and it is located at 632 nm. It is interesting to note that although all these samples have similar structures, Q-bands, which are characteristic of these samples, exhibit certain differences. Therefore, present investigation can reveal how the spectral differences among these samples are manifested in their absorptive third order nonlinearity. The samples were dissolved in dimethyl formamide (DMF). The solution had a concentration of 0.19 mM. A MOPO laser (Quanta Ray 710) was used as the laser source for investigating the wavelength dependence of nonlinear absorption. The wavelength of excitation was varied from the absorption peaks of these samples to lower wavelengths till clear RSA was observed. The wavelengths of excitation were so chosen that the difference in linear absorbance of selected successive wavelengths were about 0.5 cm^{-1}. Under nanosecond excitation, closed aperture Z-scan experiments in samples, taken in the solution form, will give only thermal nonlinearity. Hence, only open aperture Z-scan

measurements were carried out. The beam waist at the focus and diffraction length, both within the sample, varied from 15 μm to 19 μm and 1.5 mm to 1.8 mm respectively, depending on the wavelength of excitation.

3. Results

In the presence of SA, the intensity dependent nonlinear absorption coefficient is given by [20].

$$\alpha(I) = \frac{\alpha_0}{1 + \dfrac{I}{I_s}} \qquad (4.1)$$

where α_0 is the linear absorption coefficient, I is the excitation intensity and I_s is the saturation intensity. It is assumed that there is no two-photon absorption (TPA) taking place simultaneously with SA. If TPA is present along with SA, the eq. (4.1) is modified, by taking into account TPA coefficient β [13] as

$$\alpha(I) = \frac{\alpha_0 I_s + \beta I}{I + I_s} \qquad (4.2)$$

Transmitted intensity is obtained from eq. (4.3). z' corresponds to sample length. $\alpha(I)$ is given by eq. (4.1)

$$\frac{dI}{dz'} = -\alpha(I)I \qquad (4.3)$$

For pure TPA, intensity dependent nonlinear absorption coefficient is given by the equation

$$\alpha(I) = \alpha_0 + \beta I \qquad (4.4)$$

A comparison of the equations (4.1) and (4.4) shows that when the excitation intensity (I) is much less than the I_s, the saturation intensity, $(-\alpha/I_s)$ can be considered

as equivalent to TPA coefficient β. To a good approximation, in the case of SA, $(-\alpha/I_s)$ gives the nonlinear absorption coefficient. In presence of ESA, the nonlinear absorption coefficient β is obtained from open aperture Z-scan technique, as described in chapter 3. From measured values of β, $Im[\chi^{(3)}]$ can be calculated using the equation [17]

$$Im[\chi^{(3)}] = \frac{\lambda \varepsilon_0 n^2 c \beta}{4\pi} \qquad (4.5)$$

Typical open aperture Z-scan curve obtained in presence of SA for these samples is shown in fig. 1. Transmittance is a maximum at the focus (where incident intensity is also a maximum) and it steadily decreases on both side of the focus. Thus the nature of the curve is just opposite to that corresponding to ESA, discussed in the chapter 3.

It is also important to note that two different forms of eq. (4.1) are also used to explain SA depending on experimental conditions. In the case of two level system with inhomogeneous broadening and hole burning, the I_s can be described by the following equation [20]

$$\alpha(I) = \frac{\alpha_0}{(1 + \frac{I}{I_s})^{0.5}} \qquad (4.6)$$

Samac et. al [20] have used the following empirical equation to get good theoretical fit to SA exhibited by poly(indenofluorene), a picket-fence polymer, though the reason for using the empirical relation has not been clearly identified.

$$\alpha(I) = \frac{\alpha_0}{1 + (\frac{I}{I_s})^{0.5}} \qquad (4.7)$$

However, equations (4.6) and (4.7) did not give good theoretical fit to the experimental curves for the samples under investigation here. Therefore eq. (4.1) was used to interpret the results.

3.1. Wavelength dependence of nonlinear absorption in Nd(Pc)$_2$

Nd(Pc)$_2$ was found to exhibit SA from the peak of absorption spectrum (632 nm) down to 612 nm. However at 604 nm, the sample was found to exhibit a fairly good ESA. This implies that Nd(Pc)$_2$ act as an optical limiter upto a wavelength of 604 nm [8].
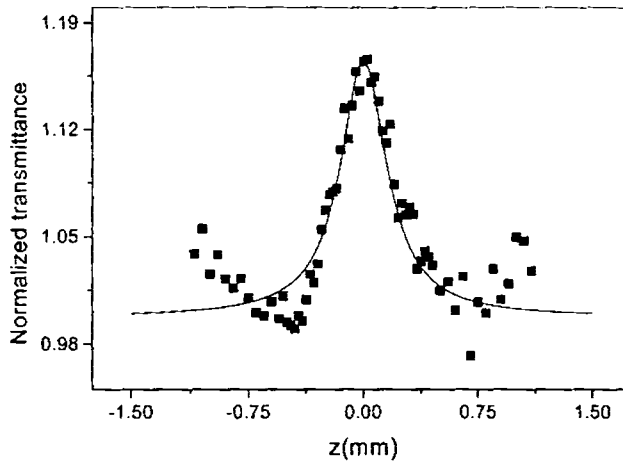
Fig. 1 Open aperture Z-scan curve indicating SA
Nd(Pc)$_2$ at 612 nm

Nonlinear absorption mechanism changes from RSA to SA in between 604 nm and 612 nm. Measured values of I$_s$, β and Im[χ$^{(3)}$] for Nd(Pc)$_2$ are given in table I along with linear absorption coefficient α$_0$ and excitation intensity at the focus, I$_0$. Excitation intensity in the focal region I$_0$ is less than measured value of saturation intensity I$_s$ for all the cases. We could get nearly identical values of I$_s$ for different values of I$_0$ whenever the value of I$_0$ is less than that of I$_s$. For example, we could

obtain values of I_s as 5.4 and 5.5 MWcm^{-2} respectively for an input irradiance of 2 MWcm^{-2} and 3.5 WMcm^{-2} (in the focal region) at 612 nm. It is evident that at sample positions other than the focus, excitation intensity I, is always less than the intensity at focus I_0. It can be seen that I_s increases as the wavelength of excitation is shifted away from resonance. Im[$\chi^{(3)}$] is a maximum at the absorption peak and it decreases steadily as the wavelength of excitation is shifted away from resonance. The value of Im[$\chi^{(3)}$] at 632 nm, which is the resonant wavelength, is nearly two orders of magnitude higher than that of 604 nm which indicates that resonant enhancement effect of Im[$\chi^{(3)}$] is fairly large.

Table I: Measured values of saturation intensity I_s, nonlinear absorption coefficient β^* and imaginary part of third order susceptibility Im[$\chi^{(3)}$]. I_0 is the excitation intensity at the focus.

λ (nm)	α_0 (cm^{-1})	I_0 MWcm^{-2}	I_s MWcm^{-2}	β^* cm GW^{-1}	Im[$\chi^{(3)}$] $\times 10^{-18}$ m^{2}V^{-2}
632	4.22	0.64	1.3	-	-8.86
624	3.85	0.65	2	-	-5.5
618	3.2	2.0	4.35	-	-2
612	2.6	2.0	5.5	-	-1.22
604	2	85	-	30	0.076

β^* values are given only for the case of ESA

3.2. Wavelength dependence of nonlinear absorption in Sm(Pc)$_2$

Sm(Pc)$_2$ was found to exhibit SA from its absorption peak at 628 nm down to 604 nm. At 596 nm, the sample exhibited RSA. Therefore Sm(Pc)$_2$ can act as an optical limiter upto 596 nm. Nonlinear absorption mechanism changes from RSA to SA in between 596 nm and 604 nm. The measured values of I$_s$, β and Im[χ$^{(3)}$] for Sm(Pc)$_2$ are given in table II along with linear absorption coefficient α$_0$ and excitation intensity at the focus I$_0$. In this case also excitation intensity is less than I$_s$ except at 604 nm [21].

Table II: Measured values of saturation intensity I$_s$, nonlinear absorption coefficient β* and imaginary part of third order susceptibility Im[χ$^{(3)}$] for Sm(Pc)$_2$. I$_0$ is the excitation intensity at the focus.

λ (nm)	α_0 (cm^{-1})	I_0 MWcm^{-2}	I_s MWcm^{-2}	β^* cm GW^{-1}	Im [χ$^{(3)}$] × 10^{-18} m^{2}V^{-2}
628	3.6	1.6	2.5	-	-4
620	3.3	1.66	3.25	-	-2.7
616	2.7	2	4.15	-	-1.7
610	2.2	7.2	12	-	-0.5
604	1.8	35	35	-	-0.14
596	1.4	143		31	0.06

β* values are given only for the case of ESA,

84

At 604 nm both I_0 and I_s are equal. Here also excitation intensity was found to increase as wavelength of excitation was shifted away from resonance. $Im[\chi^{(3)}]$ exhibited correspondingly a decreasing behaviour. $Im[\chi^{(3)}]$ exhibited a resonant enhancement of about seventy times.

3.3. Wavelength dependence of nonlinear absorption in Eu(Pc)$_2$

SA was observed in Eu(Pc)$_2$ from its absorption peak at 628 nm down to 610 nm, whereas at 604nm, the sample exhibited RSA. Therefore, it can be said that Eu(Pc)$_2$ can act as an optical limiter upto 604 nm to the blue side of its absorption maximum. Nonlinear absorption mechanism changes from RSA to SA in between 604 nm and 610 nm. Values I_s, β and $Im[\chi^{(3)}]$ obtained for Eu(Pc)$_2$ from Z-scan experiments are given in table III along with linear absorption coefficient α_0 and excitation intensity at the focus I_0.

Table III: Measured values of saturation intensity I_s, nonlinear absorption coefficient β^* and imaginary part of third order susceptibility $Im[\chi^{(3)}]$ for Sm(Pc)$_2$. I_0 is the excitation intensity at focus.

λ (nm)	α_0 (cm^{-1})	I_0 MWcm^{-2}	I_s MWcm^{-2}	β^* cm GW^{-1}	$Im[\chi^{(3)}]$ $\times 10^{-18}$ m^{2}V^{-2}
628	4.2	2.26	3.5	-	-3.2
616	3.2	2.7	6.5	-	-1.3
610	2.5	23.3	95	-	-0.07
604	2.0	83.5		50	0.12

β^* values are given only for the case of ESA

In this case also excitation intensity is less than I_s. Excitation intensity was found to increase as wavelength of excitation was shifted away from the resonance. $Im[\chi^{(3)}]$ exhibited correspondingly a decreasing behaviour. $Im[\chi^{(3)}]$ exhibited a resonant enhancement of about thirty times. Effective nonlinear absorption coefficient given in tables I, II and III for wavelengths corresponding to RSA are effective nonlinear absorption coefficient β_{eff}. It is a measure of over all absorptive nonlinearity. β_{eff} has been discussed in detail in chapter 3. A plot of $Im[\chi^{(3)}]$ against wavelength for $Sm(Pc)_2$, $Eu(Pc)_2$ and $Nd(Pc)_2$ is shown in fig. 2.
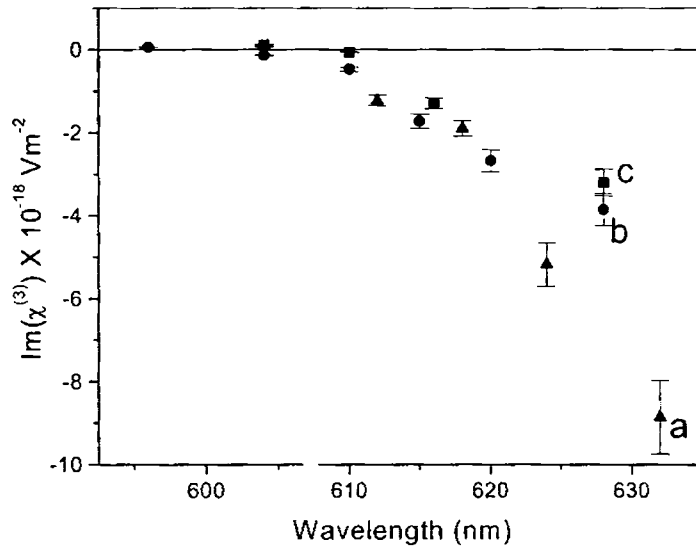
Fig. 2.Plot of $Im[\chi^{(3)}]$ against wavelength

a. $Nd(Pc)_2$; b. $Sm(Pc)_2$; c. $Eu(Pc)_2$

4. Discussion

A comparison of the values of I_s and magnitude of $Im[\chi^{(3)}]$ for the phthalocyanines investigated viz. $Nd(Pc)_2$, $Sm(Pc)_2$ and $Eu(Pc)_2$ yields the following results. It can be seen that in the region of SA, values of I_s are the lowest for $Nd(Pc)_2$, and the highest for $Eu(Pc)_2$. $Sm(Pc)_2$ shows I_s values in between those of $Eu(Pc)_2$ and $Nd(Pc)_2$. An I_s value as high as 95 $MWcm^{-2}$ is exhibited by $Eu(Pc)_2$ at 610 nm while $Nd(Pc)_2$ shows

an I_s value as low as 5.5 MWcm^{-2} at 612 nm. The wavelength dependence of I_s in these three samples are also reflected in the behaviour magnitude of $Im[\chi^{(3)}]$. Thus resonant enhancement was the highest (about hundred times) in the case of Nd(Pc)$_2$ and the lowest (approximately thirty times) in the case of Eu(Pc)$_2$. Sm(Pc)$_2$ showed a resonant enhancement, which is intermediate (about sixty times) to those of Nd(Pc)$_2$ and Sm(Pc)$_2$. The very high value of I_s exhibited by Eu(Pc)$_2$ indicates that it is a better reverse saturable absorber and hence better optical limiter. The plots in fig. 3 (to be discussed in coming paragraphs) are consistent with this observation. Apart from the variation in the degree of resonant enhancement of nonlinearity among these samples, it is also important to note the difference in the nature of nonlinear absorption exhibited by Sm(Pc)$_2$ at 604 nm from that of Eu(Pc)$_2$. While Eu(Pc)$_2$ exhibited RSA at 604 nm, Sm(Pc)$_2$ exhibited SA. Since all these samples have similar structure, the differences in the magnitude of nonlinearity as well as the nature of nonlinear absorption depend on the varying influence of metal ions. All these measurements were taken along the Q-bands of the absorption spectra, which is characteristic of these samples. Differences in the Q-band of these samples are an indication that the influences of these metal ions are not entirely identical.

Under nanosecond excitation, dynamics of RSA is explained considering a five level model [22] consisting of singlet and triplet states [S_n (n = 0, 1, 2) and T_n (n = 1, 2)]. Under picosecond excitation, ESA is explained singlet levels [S_n (n = 0, 1, 2) [9]. A minimum of three levels is essential to describe ESA. However, a two-level model consisting of singlet states S_0 and S_1 is sufficient to describe SA [23], which takes place because of the depletion of ground state population at S_0 due to spin allowed strong $S_1 \leftarrow S_0$ transition. In the context of this chapter, wavelength dependence of third order nonlinearity is of interest. Therefore details of rate equation describing the temporal evolution of populations in various energy levels are less significant and hence evaluation of $Im[\chi^{(3)}]$ using eq. (4. 5) is appropriate.
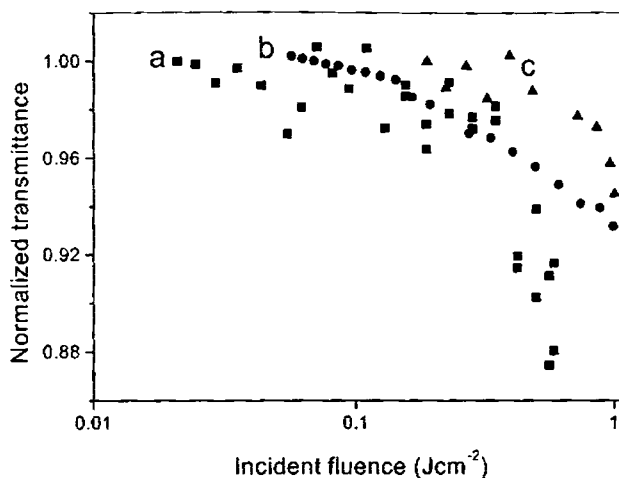
Fig. 3. Nonlinear transmission (fluence in logarithmic scale)

a. Eu(Pc)$_2$ (604 nm); b. Nd(Pc)$_2$ (604 nm); c. Sm(Pc)$_2$ (596 nm)

Fig. 3 shows the nonlinear transmission of the bis-Pcs investigated here at the wavelengths, for which RSA was observed. These plots were generated from respective Z-scan plots. All these samples have nearly identical concentration (0.19mM). It can be seen that Eu(Pc)$_2$ shows a better optical limiting property than the other two samples. Nonlinear absorption studies carried out at 532 nm discussed in chapter 3 also indicated that Eu(Pc)$_2$ has better optical limiting property than Nd(Pc)$_2$ and Sm(Pc)$_2$. Optical limiting (OL) property observed in the nanosecond excitation is the consequence of T$_2$ ← T$_1$ transition [11,24]. In the. present experimental conditions, OL property depends on the absorption cross-section of the first excited triplet state (T$_1$) as well as on the intersystem crossing rate, which were described in detail in the chapter 3.

It is appropriate to mention some important studies of wavelength dependence of third order nonlinearity in Pcs and in other organic materials using Z-scan technique. Raul et. al [15,17] have investigated optical nonlinearity in vandyl –phthalocyanine

(VOPc) crystal and also the nonlinearity in tetrakis(thiohexyl)vandyl –phthalocyanine along the absorption spectrum using picosecond pulses. Excited state dynamics in a mode locking dye (3, 3' – diethylloxadicarbocyanine iodide, DODCI) has been studied by Wittmann et. al [23]. Kandasamy et. al [13] have investigated optical nonlinearity in a porphyrin (T 3, 4, BCEMPP) doped in boric acid glass, using Z-scan techniques, at selected Ar^+ ion laser wavelengths.

5. Conclusions

Wavelength dependence of nonlinear absorption in solutions of three bis-Pcs, viz. $Nd(Pc)_2$, $Eu(Pc)_2$ and $Sm(Pc)_2$ were investigated using open aperture Z-scan in the blue side of their Q-band. Upper wavelength limit for optical limiting to the red side of 532 nm was identified. Saturation intensity I_s, effective nonlinear absorption coefficient β_{eff} and imaginary part of third order susceptibility were measured. Resonant enhancement of imaginary part of third order susceptibility was found to be the highest for $Nd(Pc)_2$ and the lowest for $Eu(Pc)_2$. Resonant enhancement in the case $Sm(Pc)_2$ was found to be about sixty times. Besides, at 604 nm, $Eu(Pc)_2$ exhibited fairly good ESA while $Sm(Pc)_2$ showed SA. Although these samples have similar structures, the observed differences in their nonlinear optical properties can be due to the varying influence of metal ions.

References

[1] J S Shirk, R G S Pong, F J Bartoli and A W Snow. Appl. Phys. Lett. **63** (1993) p. 1880

[2] C Li, L Zhang, M Yang, Hui Wang and Yuxiao Wang. Phys. Rev. B **49** (1994) p.1149

[3] T H Wei, D J Hagan, M J Sence, E W V Stryland, J W Perry and D R Coulter. Appl. Phys. B **54** (1992) p. 46

[4] G L Wood, M J Miller and A G Mott. Opt. Lett. **20** (1995) p. 973

[5] Y Kojima, T Matsuoka, N Sato and H Takahashi. Macromolecules. **28** (1995) p. 2898

[6] M A D Garcia, A Dogariu, D J Hagan, E W V Stryland. Chem. Phys. Lett. **266** (1997) p. 86

[7] S J Bentely, R W Boyd, W E Butler and A C Melissinos. **25** (2000) p. 1192

[8] K P Unnikrishnan, Jayan Thomas, V P N Nampoori and C P G Vallabhan. Appl. Phys. B 75 (2002) p. 871

[9] M Pittman, P Plaza, M M Martin, Y H Meyer. Opt. Commun. **158** (1998) p. 201

[10] M Hanack, D Dini, M Barthel, S Vagin. The Chem. Record. **2** (2002) 129

[11] T Xia, D J Hagan, A Dogariu, A A Said and E W V Stryland. Appl. Opt. **36** (1997) p. 4110

[12] P A Miles. Appl. Opt. **33** (1994) p. 6965

[13] K Kandasamy, K D Rao, R Deshpande, P N Puntambeker, B P Sing, S J Shetty, T S Srivastava. Appl Opt. B **64** (1997) p. 479

[14] Y M Cheung and S K Gayen. J. Opt. Soc. Am. B **11** (1994) p. 636

[15] R R Rojo, H Matsuda, H Hasai and H Nakanishi. J. Opt. Soc. Am. B. **17** (2000) p. 1376

[16] D S Chemla and J Zyss. Nonlinear Optical Properties of Organic Molecules and Crystals. Quantum Electronics. Principles and Applications. Academic Press (1987) Floroda

[17] R R Rojo, S Yamada, H Matsuda, H Hasai, Yuko Komai, S Okada, H Oikawa and H Nakanishi. Jpn. J. Appl. Phys. **38** (1999) p. 69

[18] R Philip, G R Kumar, M Ravikanth, G Ravindrakumar, Opt. Commun. **165** (1999) p. 91

[19] A Yariv. Optical Communications in Modern Electronics. Oxford University Press (1997) New York

[20] M Samoc, A Samoc, B L Davies, H Reisch and U Scherf. Opt. Lett. **23** (1998) p. 1295

[21] K P Unnikrishnan, Jayan Thomas, V P N Nampoori and C P G Vallabhan. Opt. Commun. **217** (2003) p 269

[22] T H Wei, T H Huang and H D Lin. Appl. Phys. Lett. **67** (1995) p. 2266

[23] M Wittmann and A Penzkofer. Appl. Phys. B 65 (1997) p. 761

[24] K P Unnikrishnan, J Thomas, V P N Nampoori and C P G Vallabhan. Opt. Commun. 204 (2002) p. 38

5

Degenerate four wave mixing studies in phthalocyanines and naphthalocyanines

Abstract

Degenerate four wave mixing studies were carried out in solutions of various metal substituted phthalocyanines and naphthalocyanines at 532nm under nanosecond excitation. Third order susceptibility $\chi^{(3)}$, figure of merit of third order nonlinearity F [F = $\chi^{(3)}/\alpha$, where α is the linear absorption coefficient] and second hyperpolarizability $\langle\gamma\rangle$ were measured. It was observed that many of these samples possessed fairly good $\chi^{(3)}$, F and $\langle\gamma\rangle$ values. Results obtained were explained taking into account the plausible effects of π electron conjugation, effect of central metal substituent and dimensionality of the molecules.

1. Introduction

Owing to the presence of delocalized and hence asymmetrically polarizable π electrons, organic compounds are considered to be good third order nonlinear optical (NLO) materials. Such materials possess fairly high bulk third order nonlinearity, $\chi^{(3)}$ and second hyperpolarizability $\langle \gamma \rangle$ values [1-2]. Unlike second order nonlinearity, third order nonlinearity is not constrained by any symmetry requirements and hence, it is present in all the samples in varying degrees of strength [3]. Apart from large and fast responding nonlinearity, organic materials have the added advantage of synthetic flexibility. Owing to synthetic flexibility, it is possible to tailor the structure of these materials suitably by introducing appropriate organic and inorganic substituents so as to maximize the nonlinearity [4-7]. In the case of centrosymmetric molecules, synthetic flexibility can be exploited to break the centrosymmetry by introducing appropriate substituents and thus inducing in the sample, second order NLO activity [8].

We require materials with fast acting nonresonant nonlinearity for technological applications such as optical switching [9]. There are several methods to increase the magnitude of third order nonlinear coefficients. One technique is to increase the π electron conjugation [10-13]. For example, naphthalocyanines (Ncs) are compounds with higher degree of conjugation in comparison to the corresponding phthalocyanines (Pcs) [14]. However, it has been observed that nonlinearity does not increase indefinitely with respect to π electron conjugation. For example, in the case of polydiacetylene, which possesses the highest value of $\langle \gamma \rangle$ among linear polymers, it has been observed that nonlinearity gets saturated after a definite degree of conjugation [15]. Hence there is limitation in maximizing $\langle \gamma \rangle$ by simply increasing π electron conjugation. There are a number of alternative and more efficient methods to enhance third order nonlinearity. One method is to substitute the samples with appropriate ligands at axial and peripheral positions. Some chemical species like NH_2 can donate electrons to a π electron system, while some other species like -COOH

have strong tendency to withdraw electrons from a π electron system. A chemical architecture consisting of an electron donating and an electron accepting group at opposite ends of a π electron system can increase hyperpolarizability of the materials considerably by effecting intramolecular charge transfer (ICT) mechanisms. Materials with such chemical architectures are called "push – pull" compounds [13,16-18].

Addition of suitable metal ions at the center of the Pc ring is the third method. In fact, more than sixty metal ions have been substituted in Pcs [19-21]. When metal ions are substituted, it can create additional levels in HOMO – LUMO gap resulting in a number of charge transfer (CT) mechanisms [12]. Another important factor that influences the magnitude of nonlinearity is the dimension of the molecules [4,22-24]. As dimensions of the molecule increases, effective conjugation length decreases resulting in a reduction in the magnitude of nonlinearity [25]. Besides, if the sample exhibits very good nonlinear absorption, it will also increase the nonlinearity [26]. However, enhancement of nonlinearity due to nonlinear absorption is not recommended for device applications, except in the case of optical limiting (OL). Nonlinearity due to absorption generally has a slow response time and also suffers from detrimental photothermal effects [27]. For technological applications, nonresonant instantaneous nonlinearity is required. Nonresonant nonlinear response is very fast but usually is small in magnitude, whereas resonant nonlinearity has large magnitude but very a slow response [28]. Resonant nonlinearity involves redistribution of population among different energy levels (excited states) and this is the reason for its slow response. Response time of the resonant nonlinearity is determined by the lifetime of the energy levels involved [29]. Experimental investigation of the influence of some of these factors on third order nonlinearity is very important and highly desirable. Work presented in this chapter is an attempt in this direction. Pcs and Ncs are suitable materials for this type of investigation because of their good nonlinearity, synthetic flexibility and thermal as well as chemical stability [5,6,30-32]. They also have a number of technological applications like

optical power limiting [33-35], wave-guide fabrication, photo-dynamic therapy [36] etc. Degenerate four wave mixing (DFWM) in optical phase conjugation (OPC) geometry was used as the experimental technique to probe these effects.

DFWM is a popular and advantageous method to measure third order susceptibility [$\chi^{(3)}$] of a variety of materials [37]. There are many factors to be considered when four wave mixing techniques are employed to measure $\chi^{(3)}$ values. For instance, if we measure $\chi^{(3)}$ with third harmonic generation (THG) technique, we get solely the electronic response [38]. No other effects (e.g. thermal effects in the case of absorbing samples and orientational effects in the case of asymmetric molecules) interfere with THG experiments. However, in THG technique, plausible effects of one photon, two-photon or three-photon resonant absorption at pump or signal frequencies have to be considered [39]. But in the case of FWM technique, signal can be generated due to orientational and thermal effects in addition to pure electronic response [40]. A good example is CS_2, which is considered as a standard third order NLO material in FWM experiments. The signal in the case of CS_2 arises from orientational response of CS_2 molecule under the influence of electric field of the laser light. Besides, in FWM experiments, both the refractive and absorptive components of nonlinearity can contribute to the measured $\chi^{(3)}$ values. However, it is also possible to separate real and imaginary parts of third order susceptibility in DFWM measurements by measuring the phase and amplitude of signal separately [41]. However, in the measurements presented in this thesis, phase of the signal is not measured and hence the real and imaginary parts are not separated. There are a number of advantages for FWM techniques over single beam Z-scan technique. It is possible to study the temporal evolution of nonlinearity using FWM technique by suitably delaying (optical delay) any one of the interacting beams. Maximum temporal resolution that can be attained is limited by the pulse width of the laser. For example, experiments under picosecond and sub picosecond excitations carried out by many other researchers have revealed that the typical response time of electronic

nonlinearity is of the order of a few picoseconds in many organic materials [42]. Since the measurements mentioned in this thesis were taken using nanosecond pulses, temporal evolution of nonlinearity is not easy to investigate.

2. The samples

A number of Pcs and Ncs with varying structures, dimensions and central metal ions were selected for experimental investigation. They include metal substituted (mono) phthalocyanines (MPcs), viz., LaPc, FePc, and MoOPc (Molybdenum oxy phthalocyanine); mono-naphthalocyanines (MNcs), viz., VONc (vandyl oxy phthalocyanines), ZnNc and MgNc; bis-phthalocyanines $M(Pc)_2$ viz., $Sm(Pc)_2$ and $Eu(Pc)_2$ and a bis-naphthalocyanines viz., $Eu(Nc)_2$. All these samples have different structures as well as varying degrees of π electron conjugation. Metal ions of all these samples are also different. Therefore, these samples provide good opportunity to investigate the effects of metal ions, structures etc. on third order nonlinearity. Structure and properties of these samples have been discussed in chapter 1. Those details are required to understand the results presented in this chapter.

Besides, Nalwa et. al [42] have observed from THG experiments carried out in thin films that peripheral substitution reduces the magnitude of $\chi^{(3)}$, if axial substituent is present in Pc systems, for example, as in the case of VOPc. They attributed the reduction in magnitude of nonlinearity to the effect of molecular stacking. Yamashita et. al [43] have measured $\chi^{(3)}$ values of VONc and VOPc using THG technique itself in thin films and found that the $\chi^{(3)}$ value of VONc is lower than that of VOPc. This observation is very interesting because of the fact that VONc has higher degree of π electron conjugation than that of VOPc. In the context of these reports, we got interested in the second hyperpolarizability $\langle\gamma\rangle$ value of VONc, obtained from DFWM measurements carried out in solution form. This result is compared with our DFWM measurements in other Pcs and Ncs as well as with the results of Nalwa et. al [42] and Yamashita et. al [43] from THG measurements. We could also obtain comparatively

very low value of ⟨γ⟩ for VONc from DFWM measurements. This coincidence is very interesting, as THG and DFWM are different processes involving third order nonlinearity. Since ⟨γ⟩ is a microscopic quantity, it can be said that low value of ⟨γ⟩ of VONc is an intrinsic property of the sample [44].

3.Experimental

Experimental details and theory of DFWM were discussed in detail in chapter 2. In brief, back scattering geometry of optical phase conjugation was used for making the measurements. As indicated earlier, an advantage of DFWM experiment is that we can select different components of third order susceptibility tensor by suitably choosing the polarizations of interacting beams [26,45]. This property is exploited to avoid thermal contribution occurring in experiments with nanosecond pulses. If the polarizations of all the interacting beams are the same, a thermal grating is formed under nanosecond excitation in an absorbing sample. In the absence of thermal grating (e.g. experiments with picosecond pulses) experiments with co-polarized laser beams give $\chi^{(3)}_{xxxx}$ component of the susceptibility tensor. If polarization of the probe beam is orthogonal to those of the pump beams, $\chi^{(3)}_{xyxy}$ component of the susceptibility tensor is obtained. Also if the polarization of any one of the interacting beams is orthogonal to those of the other beams, a polarization grating is formed in their interaction region instead of intensity (thermal) grating [46,47] even under nanosecond excitation. In the present experiment, polarizations of the interacting beams were so chosen that measurements gave only electronic response. The two pump beams were vertically polarized and the probe beam was horizontally polarized. The polarization of the phase conjugate beam is same as that of pump beam.

3.1 Calibration

Dependence of third order susceptibility tensor components on polarizations of interacting beams was exploited in the present measurements to standardize the

experimental setup. CS_2, is considered as a standard third order nonlinear optical material as it possess completely nonresonant Kerr nonlinearity due to orientational response. The experimental setup was calibrated by measuring the ratio of $\chi^{(3)}{}_{xyxy}$ to $\chi^{(3)}{}_{xxxx}$ for CS_2. This value was obtained to be 0.695, which is very close to accepted value of 0.706 given in the literature [48]. Fig. 1 shows the log-log plot of OPC signal intensity against pump beam intensity for CS_2, when polarization of the probe beam was orthogonal to those of the pump beams. This is a straight line with slope equal to 2.8, which is very close to the theoretical value of three. This also indicates that there is no saturation of nonlinearity. Similar plots were obtained when all the beams were of identical polarization.
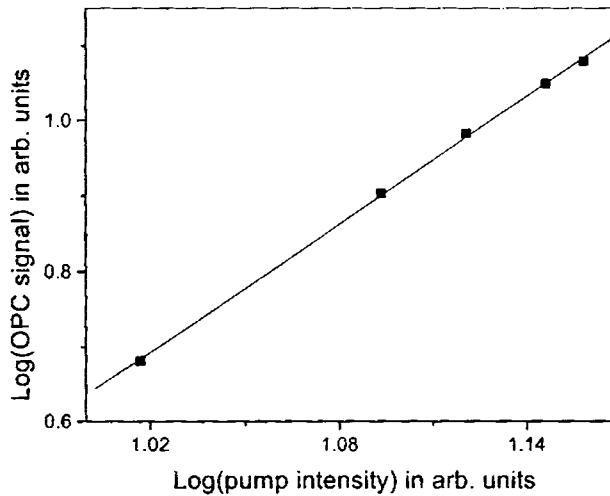

Fig. 1. log-log plot of OPC signal against pump beam intensity

CS_2 (slope = 2.8)

4. Results

Detailed discussion of the theory of DWFM is given in chapter 2. Only relevant equations are given in this section. With respect to the reference sample CS_2, third order susceptibility can be calculated using the equation [28]

$$\chi^{(3)} = \chi^{(3)}_{ref} \left[\frac{\left(\frac{I}{I_0} \right)}{\left(\frac{I}{I_0} \right)_{ref}} \right]^{\frac{1}{2}} \left[\frac{n}{n_{ref}} \right]^2 \frac{l_{ref}}{l} \frac{\alpha l}{\left(1 - e^{-\alpha l} \right) e^{-\frac{\alpha l}{2}}} \tag{3.1}$$

$\chi^{(3)}_{ref}$ was taken to be 2.73 x 10^{-13} esu [48]. Here n is the refractive index, l is the sample length, I and I_0 are respectively OPC signal and pump beam intensity and α is the linear absorption coefficient. In absorbing samples the quantity of interest is the figure of merit (F) of nonlinearity. It is defined as the ratio $\chi^{(3)}/\alpha$. It is a measure of the maximum nonlinearity that can be achieved for a given absorption loss. Samples with higher F values are considered to be better NLO materials. F values are very often used to compare third order nonlinearity of different absorbing materials. Second hyperpolarizability $\langle \gamma \rangle$ can be calculated using the equation [12]

$$\langle \gamma \rangle = \frac{\chi^{(3)}_{solution} - \chi^{(3)}_{solvent}}{L^4 N_{solute}} \tag{3.2}$$

$L = (n^2 + 2)/3$ is the Lorenz local field correction factor [3] and N_{solute} is the number density of solute molecules per ml.

4.1. Third order susceptibility of the solvent

$\chi^{(3)}$ is a measure of bulk nonlinearity of the sample. Therefore, $\chi^{(3)}$ of the solvent, dimethyl formamide (DMF) was measured under the same experimental condition to evaluate the solvent contribution to third order observed susceptibility of these samples. Fig. 2 shows the log-log plot of OPC signal against pump beam intensity for DMF. Slope of the straight line is 2.8, which is nearly equal to theoretical value of three. This indicates the third order nature of the process involved. Using eq. (5.1), $\chi^{(3)}$ of the DMF was obtained to be 0.35 x 10^{-13} esu
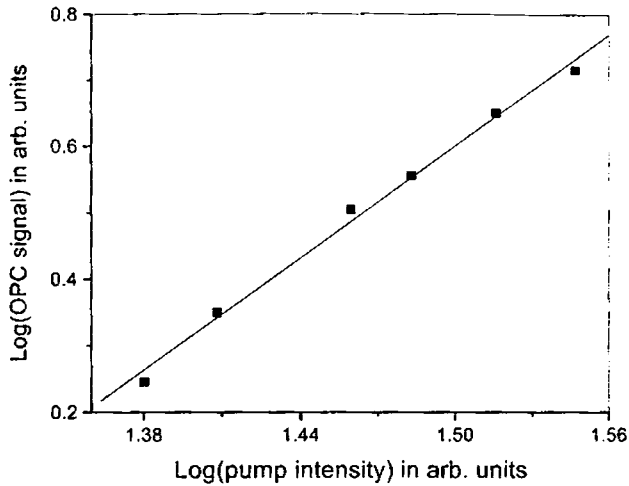
G 85 12

Fig. 2. Log-log plot of OPC signal against pump intensity DMF (slope = 2.8)

4.2. Third order nonlinear coefficients of the samples

Figures 3, 4, 5 and 6 show the log – log plots of phase conjugate intensity against pump beam intensity for (mono) Pcs, (mono) Ncs, bis-Pcs and bis-Nc respectively. All these plots are straight lines with slopes nearly equal to the theoretical value of three. (Exact slope of each plot is shown in the figure caption). A slope of three indicates the third order nature of the process involved as well as the absence of saturation of nonlinearity in measurements. A competing process that can take place during DFWM measurements is TPA. The effect of TPA in DFWM experiments has been investigated in detail both theoretically and experimentally and the results show that in the presence of TPA, OPC signal is related to pump intensity through its fifth power instead of cubic dependence [49,50]. Slope of three in the present investigation indicates that TPA contribution is practically zero. Since experiments were carried out in samples taken in solutions form, it is possible to evaluate microscopic molecular property viz. second hyperpolarizability $\langle\gamma\rangle$. (Brackets indicates that we get isotropically averaged quantities). Measured values of third order $\chi^{(3)}$, figure of merit

$F = \chi^{(3)}/\alpha$ and $\langle\gamma\rangle$ are given in table I along with extinction coefficients of these samples. The extinction coefficient ε can be evaluated using the eq.(3.3) [51].
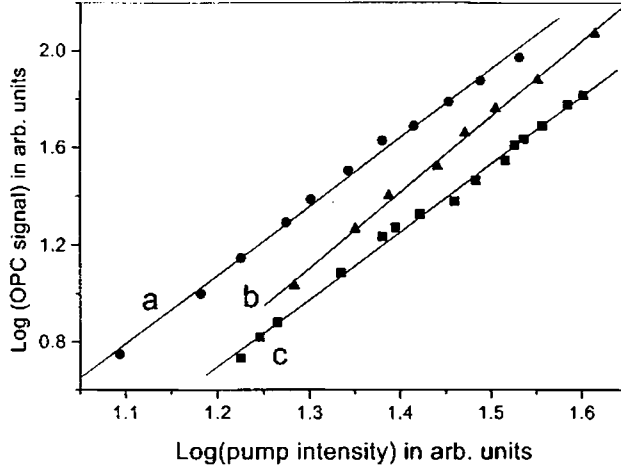
Fig. 3. Log-log plots of OPC signal against pump beam intensity

a. MoOPc (slope: 2.8); b. FePc (slope: 2.8); c. LaPc (slope:3.1)
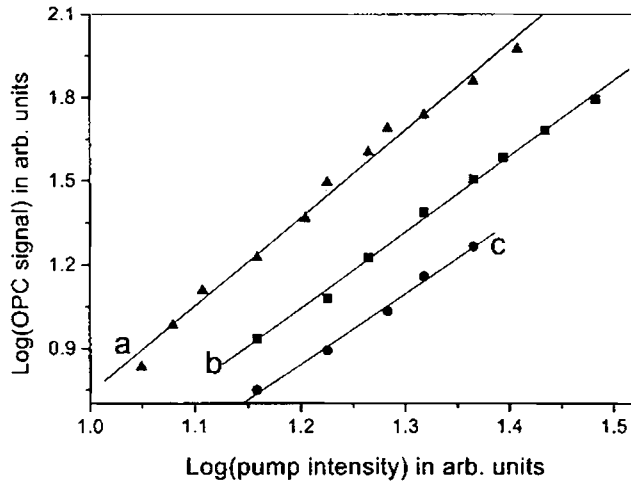
Fig. 4. Log-log plot of OPC signal against pump intensity

a. ZnNc (slope: 3.1); b. MgNc (slope: 2.7); c.VONc (slope: 2.6)

$$\varepsilon = 10^{-3} \times \sigma N_A \Big/ _{\ln(10)} \tag{3.3}$$

where σ is the absorption cross section and N_A is the Avagadro number.
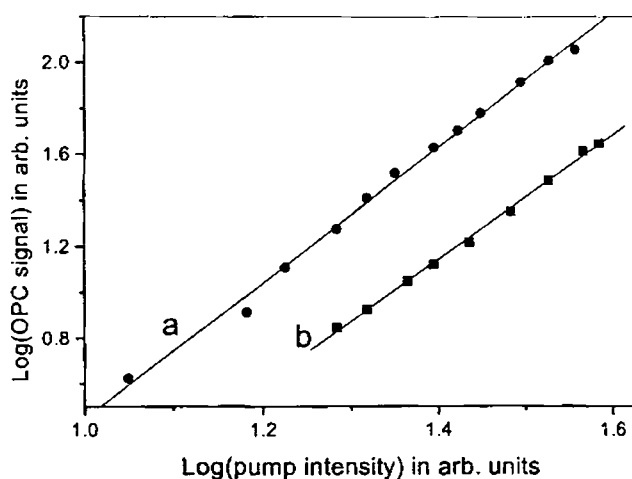
Fig. 5. Log-log plot of OPC signal against pump beam intensity
a. Sm(Pc)$_2$ (slope: 2.9); b. Eu(Pc)$_2$ (slope: 2.7)
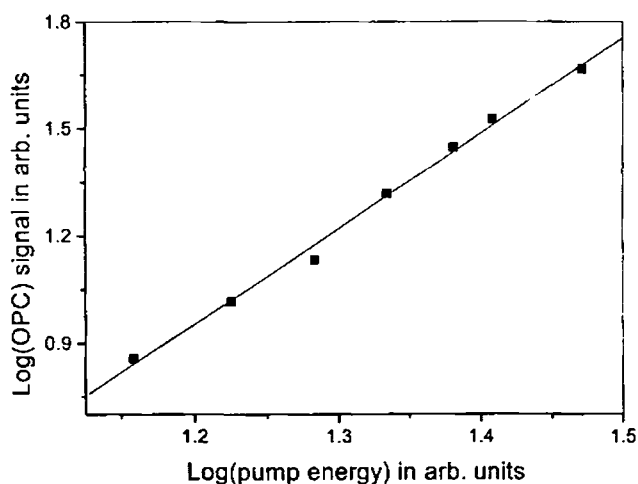
Fig. 6 log-log plot of OPC signal against pump intensity
Eu(Nc)$_2$ (slope: 2.7)

Table I

Measured values of $\chi^{(3)}$, figure of merit $F = \chi^{(3)}/\alpha$ and $\langle\gamma\rangle$ are given in the table along with extinction coefficients ε of these samples.

Sample	$\varepsilon \times 10^3$ ltr cm^{-1} mol^{-1}	$\chi^{(3)}$ ($\times 10^{-13}$ esu)	F ($\chi^{(3)}/\alpha$) esu-cm	$\langle\gamma\rangle$ ($\times 10^{-32}$ esu)
FePc	0.4	1.14	3.8	13
LaPc	0.62	1.4	4.6	24
MoOPc	0.9	1.86	3.72	31
MgNc	0.24	1.72	6.37	20.7
VONc	0.36	1.36	6.2	17
ZnNc	1.6	2.7	4.0	65.6
Sm(Pc)$_2$	1.3	1.8	3.75	43.6
Eu(Pc)$_2$	1.1	1.8	3.25	41
Eu(Nc)$_2$	2.1	1.6	2.9	55
DMF (solvent)	-	0.35		

$\chi^{(3)}$ of the solvent (DMF) is also given.

From the Table, it can be seen that all the samples posses a $\chi^{(3)}$ value, which is three times (or higher) than that of the solvent. MgNc and VONc exhibit the highest but nearly identical F values. The lowest F value was observed for Eu(Nc)$_2$. Most of the other samples possessed moderate F values. In the case of absorbing samples, those, which possess higher F values, have better NLO materials. Amongst them VONc and MgNc gave maximum nonlinearity for a given absorption loss. In this investigation, the highest $\langle\gamma\rangle$ value was obtained for ZnNc, followed by Eu(Nc)$_2$ and FePc exhibited the lowest $\langle\gamma\rangle$ value. $\langle\gamma\rangle$ values of Eu(Pc)$_2$ and Sm(Pc)$_2$ were nearly identical.

Nonlinearity due to parametric processes, which are extremely fast (sub-picosecond response time), obey very selective phase matching conditions. Non-parametric processes involve light induced changes in the energy level populations of the systems [52]. In this case phase matching conditions are not applicable. Since all the samples investigated here have weak absorption at the wavelength of our interest viz., 532nm and also due to the fact that these samples exhibit excited state absorption (ESA) at this wavelength, observed nonlinearity may not exclusively be due to parametric processes. Non-parametric processes have comparatively low response time. A good example for non-parametric nonlinearity is the passive optical power limiting.

5. The important parameters determining the $\langle\gamma\rangle$ values

Values of $\langle\gamma\rangle$ depend on a number of factors. In the case of organic molecules, it is known that $\langle\gamma\rangle$ values depend on the extent of π electron conjugation and therefore, these values are usually higher if π electron conjugation is high. However, it has been observed in one- dimensional polydiacetylenes that $\langle\gamma\rangle$ values get saturated after a finite degree of conjugation [15]. Apart from π electrons, there are many other factors that can influence the $\langle\gamma\rangle$ values considerably. For examples, $\langle\gamma\rangle$ values depend on the oscillation strength (f) [12,53,54] such that $\langle\gamma\rangle$ values are large if oscillation strength

is high. Oscillation strength is related to extinction coefficient ε through the relation [54]

$$f = \left(\frac{1}{n}\right) \times 4.319 \times 10^{-9} \int \varepsilon d\upsilon \qquad (3.4)$$

Apart from the oscillation strength and the extent of π electron conjugation, in the context of the samples investigated here, the other important parameters determining $\langle\gamma\rangle$ values are, (1) the nature of metal substituent [12,55-58], (2) dimensionality of the molecules [4, 22-24] and (3) the effect of axial substituent [13,16-18,42,59,60]. $\langle\gamma\rangle$ values mentioned here are influenced by many of these factors simultaneously and hence, the measured values have a cumulative contribution from these parameters, which are discussed below.

5. 1. Effect of metal ions

Many investigators have explored the effect of metal ions on nonlinear and spectroscopic properties of Pcs. Here, only the influence of metal ions on third order nonlinearity is discussed. Other effects of metal ions like shift of peak wavelength of Q-band etc. have been explained in chapter 1. Nearly 60 metal ions can be incorporated in Pc ring without compromising on their other properties like thermal and chemical stability [19-21]. Metal substitution, in many occasions, improves the magnitude of nonlinear optical response through the polarizable valence electrons. Among a number of metal ions, transition metal with incompletely filled d-shells, have been found to be very effective in enhancing the third order nonlinear properties [2,12]. In free base form, Pcs have D_{2h} symmetry. When metals ions are incorporated at the center, the symmetry changes to D_{4h} [61]. The substitution of transition metal ions in the phthalocyanine ring can perturb the π electron system and thus influence the spectral features. It can induce a number of low-lying states in the highest occupied molecular orbital – lowest unoccupied molecular orbital (HOMO – LUMO) gap via charge transfer (CT) mechanisms. CT mechanism means the interaction of the

valence electrons of the metal ions with π electrons of the Pc ring. Possible CT mechanisms include metal – ligand charge transfer (d→ π*, MLCT), ligand metal charge transfer (π* → d, LMCT) and metal- metal charge transfer states. The location of the CT states depends on the overlap between the orbitals and separation between filled and unfilled states [12,60]. CT mechanisms are rarely observed in MPcs if transition metal ions possess filled d shells. Generally, if metal ions have completely filled states, interaction between electrons of the metal ions and those of Pc ring is very weak. Hence, such metal ions do not considerably influence the nonlinearity through CT mechanisms. Apart from non-transition metal, there are a number of MPcs with rare earth ions as their metal substituent. Unlike the case of Pcs with transition metal ions, no remarkable change in nonlinear property was observed in rare earth metal ion substituted Pcs. Second hyperpolarizability ⟨γ⟩ of a number of rare earth ion substituted bis-Pcs and their anions had been measured at 1.06 μm using DFWM technique [56]. ⟨γ⟩ values of the anions $[M(Pc)_2^{-1}]$ were nearly identical. Differences in the ⟨γ⟩ values of neutral species were attributed to resonance effects arising from intervalence transitions around 1.06 μm. $Sc(Pc)_2$ exhibited strong resonant enhancement of nonlinearity due to intervalence transition at 1.06 μm [56].

5.2. Effect of dimensionality

Dimensionality of the molecules influences their linear and nonlinear polarizability considerably. This has been investigated both experimentally and theoretically [4,22-24]. For example, in one-dimensional systems like polyacetylene, electron confinement occurs in one dimension along the chain length and microscopic susceptibility is predominantly due to $⟨γ⟩_{xxxx}$. Here, all electric fields are aligned along the chain axis. When dimensions of the molecules are increased effective conjugation length available for an electron to respond to applied optical field decreases and consequently ⟨γ⟩ values exhibit a reduction in magnitude [25]. Conjugation length refers to the minimum size of a box in which electrons can be squeezed without

altering its states and response to external field. However, as dimensionality of the molecules is increased the number of susceptibility components increases. In one-dimensional molecules like polyacetylene, there is only one component for $\langle\gamma\rangle$, viz., $\langle\gamma\rangle_{xxxx}$. But in planar molecules like cyclooctatetraene, there are a number of components for $\langle\gamma\rangle$, $\langle\gamma\rangle_{ijkl}$. Many investigators have derived qualitative relations between $\langle\gamma\rangle$ and the dimensionality of the molecules. It is assumed that the most important contribution to $\langle\gamma\rangle$ come from the valence electrons. Swell has derived the following equation [24]

$$\gamma = \frac{3555}{16} a_0^7 \qquad (3.5)$$

where a_0 is the Bohr radius. Calculations in Unsold approximation by Ducuing give the relation [24]

$$\gamma \propto \frac{L^{10}}{N^3} \qquad (3.6)$$

where L is the delocalization length and N is the number of electrons. For one-dimensional systems, $N \propto L$ and thus $\gamma \propto L^7$. For two-dimensional systems, $N \propto L^2$ and hence $\gamma \propto L^4$. Evidently, if all the other parameters remain the same, polarizability is high in one-dimensional molecules. Calculation for one dimensional electron gas by Rustagi and Ducuing [24] as well as calculation by Agarwal [24] for polydiacetylene using tight binding approximation gave dependence of $\langle\gamma\rangle$ on L as L^5 and L^6 respectively. These calculations predict a weaker dependence cf $\langle\gamma\rangle$ on L in comparison with calculations of Swell. However, all these calculations point to the fact that $\langle\gamma\rangle$ values depend significantly on dimensionality of the molecules [24]. Kumar et. al [23] have measured $\chi^{(3)}$ values of basket handled porphyrins and observed a decrease in third order nonlinearity due to the deviation from planarity of molecules.

5.3. Effect of axial and peripheral substituent

In the samples investigated here, oxygen atom may be considered as an axial substituent in MoOPc and VONc, as oxygen atom projects outside the plane of Pc and Nc rings [55]. Because of synthetic flexibility, it is possible to incorporate electron donating (D, donor; e.g. NH_2) and electron accepting (A, acceptor; e.g. -COOH) chemical groups at appropriate positions of these molecules. Such compounds are called Push-Pull compounds. Such compounds have D - π - A structure. As in the case of metal ions, the axial and peripheral substituents also can enhance $\langle\gamma\rangle$ by introducing intramolecular charge transfer (ICT) mechanisms. ICT processes are associated with change in dipole moment $\Delta\mu$ between the ground state and the first excited state. Hammett free energy relationships are used to describe how substituents alter the electronic structure of the molecules. Hammmmett free energy is usually expressed using the equation [13]

$$\log K = \log K_0 + \rho\sigma \qquad (3.7)$$

K and K_0 denote equilibrium constants for substituted and unsubstituted compounds respectively. σ is the characteristic of the substituents indicating its behaviour as an electron donor or electron acceptor. ρ is a measure of the sensitivity of the processes to alteration in the substituents. For the samples investigated here, effect of substituents is very less in comparison with those of metal ions and dimensionality of the molecules. In the context of the influence of different factors on $\langle\gamma\rangle$ values, plausible reasons for the results obtained may be explained as follows.

6. Discussion

MoOPC, LaPc and FePc are the (mono) Pcs investigated here for their $\langle\gamma\rangle$ values. These samples have more or less similar structures. π electron density is also the same in these samples. Therefore, differences in their $\langle\gamma\rangle$ values can be explained in

terms of the influence of metal ions and other parameters like oscillation strength as follows. Among mono Pcs, MoOPc has the highest $\langle\gamma\rangle$ value and FePc has the lowest $\langle\gamma\rangle$ value. LaPc has a $\langle\gamma\rangle$ value in between MoOPc and FePc. Fe and Mo are transition metal ions. Therefore, there is a possibility that CT processes occur in these samples [12]. In the case of MoOPc, the oxygen atom lies outside the Pc plane, giving rise to pyramidal structure [55]. Such compounds have an axial component for polarizability, which enhances the $\langle\gamma\rangle$ value. CT processes together with pyramidal structure due to axial oxygen atom of the MoOPc can be one reason for the high value of $\langle\gamma\rangle$ for MoOPc. Among mono Pcs, MoOPc has the highest oscillation strength because of its large value of ε. This can also partly contribute to its $\langle\gamma\rangle$ value [53,54]. Therefore, the observed highest value of $\langle\gamma\rangle$ for MoOPc among mono Pcs may be attributed to the combined contribution of CT process, oscillation strength and influence of axial substituent. FePc does not have any axial substituent like MoOPc. It has the lowest value of ε, indicating a low value for oscillation strength. However, since Fe^{2+} is a transition metal ion with unfilled d shells there can be some CT processes, which alone can influence $\langle\gamma\rangle$ [12]. Therefore $\langle\gamma\rangle$ value of FePc may be attributed to the presence of π electrons and influence of transition metal ion Fe^{2-}. In the case of LaPc, CT process are very unlikely to occur, because La^{2+} is a rare earth metal ion. From the optical limiting studies given in chapter 2, it can be seen that LaPc is a better nonlinear absorber in comparison with MoOPc. If nonlinear absorption is high, it can enhance the imaginary part of third order susceptibility as well as $\langle\gamma\rangle$ by non-parametric process. In fact, increased value of third order nonlinearity due to enhanced nonlinear absorption has been reported [26]. Besides, LaPc has a value of ε higher than that of FePc. This also favours a higher value of $\langle\gamma\rangle$ for LaPc with respect to FePc. Therefore higher value of $\langle\gamma\rangle$ of LaPc with respect to FePc may be due to the combined contribution from nonlinear absorption and its higher value of ε.

It is very appropriate to compare the present results with those reported previously. Reji et. al [28] have measured $\langle\gamma\rangle$ value of FePc using DFWM measurements at 532 nm under picosecond excitation. They got a $\langle\gamma\rangle$ value of 27 × 10^{-32} esu without subtracting the $\chi^{(3)}$ value of the solvent. Without eliminating the solvent contribution, $\langle\gamma\rangle$ value of the FePc obtained from present measurements is 19 × 10^{-32}, which is less than the value obtained by Reji et. al [28] for FePc. Difference between these two measurements can partly be due to the experimental conditions. Reji et. al [28] made measurements using 35 ps pulses with co-polarized beams. Measurements reported here have been made using nanosecond pulses (7 ns). In Pcs, nonlinear and spectroscopic properties depend on the excited states as well. When pulse width changes from picoseconds to nanoseconds, the behaviour of excited states will vary. Under picosecond excitation singlet states are important, whereas under nanosecond excitation, influence of triplet states becomes important. Besides, polarizations of interacting beams in the case of picosecond excitation were different from those in present case [62].

Ncs are molecules with greater number of π electron conjugation [17]. Therefore, in the case of Ncs higher values of $\langle\gamma\rangle$ are expected in comparison with those for corresponding Pcs. However, results obtained indicate that such an enhancement need not necessarily occur for all the samples. The results obtained for VONc, ZnNc and MgNc, Nc samples investigated here, are explained as given below. MgNc exhibited a $\langle\gamma\rangle$ value higher than that of FePc, but less than those of MoOPc and LaPc. Mg^{2+} is a non-transition metal ion without any unfilled states. Therefore, no CT processes can occur in MgNc [12,2]. This implies that that Mg^{2+} ion does not perturb the electronic distribution of Nc ring appreciably. Besides, MgNc has the lowest value of ε, indicating weak oscillation strength. Therefore, it can be assumed that observed $\langle\gamma\rangle$ value of MgNc is mostly due to π electron conjugation. In this context higher value of

$\langle\gamma\rangle$ for MgNc with respect to FePc must be resulting from its higher degree of π electron conjugation.

The lowest $\langle\gamma\rangle$ value was observed for VONc. As in the case of MoOPc, VONc has an oxygen atom as axial substituent. Therefore, the structure of VONc is pyramidal [55]. Vandyl oxy ion is a transition metal ion with unfilled d – shells. In spite of the presence of a transition metal ion with unfilled d – shells, axial substituent and increased degree of π electron conjugation, VONc exhibited the lowest $\langle\gamma\rangle$ value. This result can be easily understood if we compare this result with certain previous reports. It has been observed by H S Nalwa et. al [42]from THG in thin films that $\chi^{(3)}$ value of vandyl oxy phthalocyanine (VOPC) significantly decreased when peripheral groups were substituted. Similar results have been observed for TiOPc as well. On the other hand, the case of CuPc and NiPc, peripheral substituents enhanced $\chi^{(3)}$ values [42]. General observation is that in the case of Pcs, peripheral substitution is not recommended to increase the nonlinearity if axial substituents are present in the molecules, for example, as in the case of VOPc and MoOPc. Nalwa et. al [42] attributed the reduction in magnitude of $\chi^{(3)}$ of Pcs with axial and peripheral substituents to the possible effects of molecular stacking. Yamashita et. al [43] have also reported very low value of $\chi^{(3)}$ for VONc with respect to VOPc using THG at 1.6 µm. According to their measurements, the ratio of $\chi^{(3)}$ values of VONc to VOPc is 0.081. This observation is very interesting because of the fact that VONc has greater π electron conjugation than that of VOPc with no other structural difference, but no proportionate enhancement in $\chi^{(3)}$ was observed. From a comparison of the structures of VOPc and VONc, we can see that higher degree of π electron conjugation in VONc with respect to VOPc results from the presence of additional benzene rings at its lateral position. It is also to be noted that unlike $\chi^{(3)}$, $\langle\gamma\rangle$ is a microscopic quantity. Present DFWM measurements have been made in samples taken in solution form. Moreover, THG and DFWM are fundamentally different processes. Nevertheless the

significantly low value of $\langle\gamma\rangle$ for VONc is in good qualitative agreement with those of Nalwa et. al [42] and Yamashita et. al. [43]. This coincidence indicates that reduction in magnitude of nonlinearity of VONc can be due to some intrinsic property of the sample and not necessarily due to molecular stacking alone [44].

ZnNc has the highest $\langle\gamma\rangle$ value among all the samples. Zn^{2+} is a transition metal ion, but it does not have unfilled d states. Therefore, CT processes are very unlikely [12]. Very high value of $\langle\gamma\rangle$ for ZnNc can partly be due to its large value of extinction coefficient, which implies increased oscillation strength [12,53,54]. Extinction coefficient of ZnNc is nearly eight times that of MgNc and five times that of VONc. Secondly, ZnNc has increased π electron conjugation in comparison with (mono) Pcs. Besides, dimensionality of the molecules can influence the $\langle\gamma\rangle$ values considerably in the case of ZnNc, as discussed below.

Sm(Pc)$_2$, Eu(Pc)$_2$ and Eu(Nc)$_2$ are bis-Pcs and bis-Ncs respectively. They have increased π electron conjugation in comparison with mono Pcs and mono Ncs. Both mono Ncs as well bis-Pcs and bis-Ncs have greater π electron conjugation with respect to mono Pcs. However, in the case of the former, π electron conjugation increases in the same plane, whereas in the case of the later, π electron conjugation increases because of addition of molecules in a different plane. In other words, bis-Pcs and bis-Ncs are not strictly planar like ZnNc, MgNc and FePc and hence the effect of dimensionality is very important as will be discussed later. Nearly identical values of $\langle\gamma\rangle$ for Sm(Pc)$_2$ and Eu(Pc)$_2$ indicate that rare earth ions do not influence the nonlinearity as transition metal ions with unfilled states do. Intervalence transition observed by Shirk et. al [56] around 1.06 μm in certain bis-Pcs are unlikely to influence measurements made at 532 nm. Eu(Nc)$_2$ has a $\langle\gamma\rangle$ value higher than those of Sm(Pc)$_2$ and Eu(Pc)$_2$. This can mainly be due to the increased level of π electron conjugation present in Eu(Nc)$_2$ with respect to that in Sm(Pc)$_2$ and Eu(Pc)$_2$ [62].

112

$Eu(Nc)_2$ has an extinction coefficient, which is nearly double those of $Sm(Pc)_2$ and $Eu(Pc)_2$. This may also partly contribute to the $\langle\gamma\rangle$ value of $Eu(Nc)_2$.

If we consider π electron conjugation and extinction coefficients alone, $Eu(Nc)_2$ should have the highest $\langle\gamma\rangle$ value. But highest $\langle\gamma\rangle$ value was observed for ZnNc. This can be explained considering the dimensionality of the molecules. In mono Ncs, degree of π electron conjugation increases in the same plane with respect to mono Pcs. But in the case of bis-Pcs and bis-Ncs, π electron conjugation increases not in the same plane, but in two distinct planes. Therefore, bis-Pcs and bis-Ncs are not planar like LaPc or MgNc. Proportionate enhancement in $\langle\gamma\rangle$ can be observed with respect to increased π electron conjugation only if it is achieved without increasing the dimension of the molecular systems. Kumar et. al [23] have investigated basket handled porphyrins using DFWM at 532 nm under picosecond excitation. They too have observed a decrease in third order nonlinear response due to the deviation of molecular structure from planarity.

It may be appropriate to mention the other important reports on nonlinearity of phthalocyanines and related compounds. Bulk third order nonlinearity $\chi^{(3)}$ of a large number of Pcs has been studied in amorphous, crystalline and polycrystalline films using third harmonic generation technique as well as DFWM at a number of wavelengths [43,55,63]. The work by Nalwa et. al [42] and Yashamita et. al [43] have been already mentioned. THG measurements carried out in thin films of a number of axial substituted Pcs like ClAlPc, FalPc, VOPc, TiOPc and MoOPc [64] at NIR wavelengths indicate that, MoOPc possesses higher value of $\chi^{(3)}$, which is consistent with our result of the highest value of $\langle\gamma\rangle$ for MoOPc among mono Pcs [62]. In fact values of NLO coefficients measured in thin films of Pcs and Ncs depend on the nature of films (amorphous, crystalline or polycrystalline), excitation wavelength [39] (which decides if one-photon / multi photon resonant absorption is possible) and

techniques used for making measurements [65]. Nevertheless, main trends of our results are in agreement with those of others.

7. Conclusions

DFWM studies were carried out in solutions of a number of metal substituted mono-Pcs, mono-Ncs, bis-Pcs and bis-Ncs at 532 nm under nanosecond excitation. Polarizations of the interacting beams were so chosen that electronic response is obtained. Third order susceptibility $\chi^{(3)}$, figure of merit of third order nonlinearity F, defined as $\chi^{(3)}/\alpha$, where α is the absorption coefficient and second hyperpolarizability $\langle \gamma \rangle$ were measured. MgNc and VoNc exhibited the highest values of F indicating that these two materials possess maximum third order nonlinearity for a given absorption loss. $Eu(Nc)_2$ exhibited the lowest F value. $\langle \gamma \rangle$ values were explained taking into account the extent of π electron conjugation, effect of central metal ion, influence of oscillation strength and effect of dimensionality. It was observed that ZnNc exhibited the highest value of $\langle \gamma \rangle$, followed by $Eu(Nc)_2$. $\langle \gamma \rangle$ value of ZnNc is attributed to the combined effect of dimensionality and its high value of oscillation strength. FePc exhibited the lowest value of $\langle \gamma \rangle$. VONc showed a very low value of $\langle \gamma \rangle$ despite the presence of a transition metal ion with unfilled d-shells. $\langle \gamma \rangle$ values of $Eu(Pc)_2$ and $Sm(Pc)_2$ were nearly equal.

References

[1] Akira Terasaki, Masahiri Hosoda, Tutsuo Wada, Hirokazu Tada, Atushi Koma, Akira Yamada; Hiroyuki Sasabe, Anthony F garito, Takayoshi Kobayashi. J. Phys. Chem. **96** (1992) p. 10534

[2] V S Williams, S Mazumdar, N R Amstrong, Z Z Ho and N Peyghambarian. J. Phys. Chem. **96** (1992) p. 4500

[3] Y R Shen. Principles of Nonlinear Optics. Y R Shen. John Wiley & Sons (1991) Singapore

[4] H S Nalwa and S Kobayashi. J. Porphyrins and Phthalocyanines. **2** (1998) p. 21

[5] G de la Torre, P. Vazquez, F Agullo – Lopez and T Torres, J. Mater. Chem **8** (1998) p.1671

[6] G. de la Torre, M. Nicolau and T.Torres in "Phthalocyanines: synthesis, supramolecular, organization and physical properties", in H.S. Nalwa (ed) Supramolecular photosensitive and electroactive materials. Chapter 1, p. 1-111, Academic press, San Diego (April 2001)

[7] J H Chou, M E Kosal, H S Nalwa, N A Rakow and K S Suslick; The Porphyrin Handbook. K Kadish, K Smith, R Guilard (Ed) Academic Press. New York (2000) vol. 6 ch. 4. p.43 131

[8] K S Suslick, N A Rakow, M E Kosal and J H Chou. J. Porphyrins and Phthalocyanines. **4** (2000) p.407

[9] B L Davies and M Samoc. Current Opinion in Solid State and Material Science (Optical and Magnetic Materials) (1997) p. 213

[10] S R Marder, W E Torruellas, M B Desce, V Ricci, G I Stegeman, S Gilmour, J Luc Bredas, Jun Li, G U Bublitz, S G Boxer Science 276 p. 1233

[11] S A Hambir, D Wolfe, G J Blanchard and G L Baker. J. Am. Chem. Soc. **119** (1997) p. 7367

[12] K Kandasamy, S J Shetty, P N Puntambekar, T S Srivastava, T Kundu and B P Sing. J. Porphyrins and Phthalocyanines 3 (1999) p. 81

[13] A Sastre, M A Diaz-Garcia, D del Rey, C Dhenaut, J Zyss, I Ledoux, F Agullo Lopez and T Torres. J. Phys. Chem. A **101** (1997) p. 9773

[14] H S Nalwa, M hanack, G Pawlowski, M K Engel. Chem. Phys.245 (1999) p. 17

[15] M K Cassetevens, M Samoc, J Pfleger and P N Prasad. J. Chem. Phys.92 (1990) p. 2019

[16] K S Suslick, C T Chen, G R Meredith, and L T Cheng. J. Am. Chem. Soc. **114** (1992) p. 6928

[17] B K Mandal, B Bihari, A K Sinha and M Kamath. Appl. Phys. Lett. 66 (1995) p. 932

[18] A K Sinha, B Bihari and B K Mandal. Macromolecules. **28** (1995) p.5681

[19] M O Wolf. Adv. Mater. **13** (2001)p. 545

[20] R Kubiak, J Janczak. Cryst. Res. Technol. **36** (2001) p. 1095

[21] W D Cheng, D S Wu, H Zhang and J T Chen. 64 Phys. Rev. B. (2001) p.125109 -1

[22] Ifor. D W Samuel, I Ledoux, C Delporte, D L Pearson and James M Tour. Chem. Mater. **8** (1996) p. 819

[23] G R Kumar, M Ravikanth, S Banergee, Armen Sevian. Optic. Commun. **144** (1997) p. 245

[24] D S Chemla, J Zyss. Nonlinear Optical Properties of Organic Molecules and Crystals. Quantum Electronics. Principles and Applications. Academic Press (1987) Florida

[25] M Hosoda, T Wada, A Yamada, A F garito and Hiroyuki Sasabe. Jpn. J. Appl.

Phys. **30** (1991) p. 1715

[26] J R G Thorne, S M Kuebler, R G Denning, I M Blake, P N Taylor, H L Anderson. Chem. Phys. Lett. **248** (1999) p. 181

[27] J G Breitzer, D D Dlott, L K Iwaki, S M Kirkpatrick and T B Rauchfuss. J. Phys. Chem. A **103** (1999) p.6930

[28] R. Philip, M Ravikanth, G R Kumar, Optic. Commun. **165** (1999) p. 91

[29] P C de Souza, G Nader, T Catunda, M Muramatsu and R J Horowicz. Opt. Commun. **163** (1999) p. 44

[30] N Ishikawa, Y Kaizu. Coord. Chem. Rev.**226** (2002) p. 93

[31] N Kobayashi. Coord. Chem. Rev.**227** (2002) p. 129

[32] M K Engel, Report Kawamura Inst. Chem. Res. (1997) 11-54

[33] D Dini, M Barthel and M Hanack. Eur. J. Org. Chem.(2001) p. 3769

[34] H Hanack, T Schneider, M Barthel, J S Shirk, S R Flom, R G S Pong. Coord. Chem. Rev. **219-221** (2001) p. 235

[35] M Hanack, D Dini, M Barthel, S Vagin. The Chemical Record. **2** (2002) p. 129

[36] F F Alonso, P Marovino, A M Paoletti, M Righini, G Rossi. Chem. Phys. Lett. **356** (2002) p. 607

[37] R de Nalda, R del Coso, J R Isidro, J Olivares, A S Garcia, J Solis and C N Afonso. J. Opt. Soc. Am. B **19** (2002) p. 289

[38] M A Diaz Garcia, F A Lopez, W E Torruellas, G I Stegeman. Chem. Phys. Lett. **235** (1995)p. 535

[39] M A Diaz- Garcia, J M Cabrera, F A Lopez, J A Duro, G de La Torre, T Torres, F F Lazaro, P Delhaes and C Mingautod. Appl. Phys. Lett. 69 (1996) p. 293

[40] A Costela, I G Moreno. Chem. Phys. Lett. **249** (1996) p.373

[41] D Faccio, P Di Trapani, E Borsella, F Gonella, P Mazzoldi and A M Malvezzi. Europhys. Lett **43** (1998) pp. 213 – 218

[42] H S Nalwa, A Kakuta. Thin Solid Films. **254** (1995) p.218

[43] A Yamashita, S Matsumoto, S Sakata, T Hayashi, H Kanbara. Optic. Commun. **145** (1998) p.141

[44] K P Unnikrishnan, Jayan Thomas, V P N Nampoori and C P G Vallabhan. Communicated to Synthetic. Metals

[45] Jun Ichi Sakai. Phase Conjugate Optics. Mc. Graw Hill (New York)

[46] D W Neyar, Larry A Rahan, D W Chandler, J A Nunes and W G Tong. J. Am. Chem. Soc. **119** (1997) p. 8293

[47] J A Nunes, W G Tong, D W Chandler and L A Rahn. J. Phys. Chem. A **101** (1997) p. 3279

[48] R A Fischer (Ed.) Optical Phase Conjugation Academic Press (New York) 1983

[49] S Wu, X C Chang and R L Fork. Appl. Phys. Lett. **61** (1992) p. 919

[50] M Zhao, Y Cui, M Samoc and P N Prasad. J. Chem. Phys. **95** (1991) p. 3991

[51] T H Wei, D J Hagan, M L Sence, E W V Stryland, J W Perry and D R Coutler. Appl. Phys. B. 54 (1992) p. 46

[52] W Werncke, M Pfeiffer, A Lau, W Grahn, H H Johannes, L Dahne. J. Opt. Soc. Am. B. **15** (1998) p. 863

[53] M G Kuzyk and C W Dirk. Phys. Rev. A **41**(1990) p. 5098

[54] I Renge, H Wolleb, H Spahni and U P Wild. J. Phys. Chem. A 101 (1997) p. 6202

[55] A Yamashita, S Matsumoto, S Sakata and T Hayashi., H Kanbara J. Phys. Chem. B **102** (1998) p. 5165

[56] J S Shirk, J R Lindle, F J Bartoli and M E Boyle. J. Phys. Chem. **96** (1992) p. 5847

116

[57] K Kamada, M Ueda, T Sakaguchi, K Ohta and T Fukumi. J. Opt. Soc. Am. B **15** (1998) p. 838

[58] M Koshino, H Kurata, S Isoda and T Kobayashi. ICR Annual Report. **7** (2000) p. 6

[59] K Kandasamy, S J Shetty, P N Puntambekar, T S Srivastava, T Kundu anf B P Singh. Chem. Commun. (1997) p. 1159

[60] H Kanbara, T Maruno, A Yamashita, S Matsumoto, T Hayashi, H Konami, N Tanaka. J. Appl. Phys. 80 (1996) p. 3674

[61] T Kimura, M Sumimoto, S Sakaki, H Fujimoto, Y Hashimoto, S Matsuzaki. Chem. Phys. 253 (2000) p. 125

[62] K P Unnikrishnan, Jayan Thomas, V P N Nampoori and C P G Vallabhan. Chem.Phys. **279** (2002) p. 209-213

[63] S Fang, H Hoshi, K Kohama and Y Maruyama. J. Phys. Chem. 100 (1996) p. 4104

[64] H S Nalwa, M K Engel, M Hanack and G Pawlowski. Appl. Phys. Lett. **71** (1997) p. 2070

[65] M F Yung and X Y Wong. Appl. Phys. B 66 (1998) p. 585

6

Nonlinear optical absorption studies in silver nanosol using Z-scan technique

Abstract

Nonlinear optical absorption in silver nanosol was investigated at three selected wavelengths (456 nm, 477 nm and 532 nm) using open aperture Z-scan technique. It was observed that nature of nonlinear absorption is sensitive to both input fluence and excitation wavelength. The present sample was found to exhibit both reverse saturable absorption (RSA) and saturable absorption (SA) at these wavelengths depending entirely on excitation fluence. Results are explained in terms of the electron dynamics taking place in metal nanoparticles following the excitation. RSA is attributed mainly to enhanced absorption resulting from photochemical changes. SA observed for fluence values lower and higher than those corresponding to RSA are respectively attributed to plasmon bleach and saturation of RSA.

1. Introduction

Nanomaterials, which include metal [1,2] and semiconductor nanoparticles [3], carbon nanotubes [4,5], nanowires [6] etc. are a new class of technologically important nonlinear optical (NLO) materials. Nanophotonics and nanotechnology are relatively new and rapidly developing areas of science and technology, wherein the unique properties of confined electron in nanostructures are exploited. Metal nanoparticles may be considered as typical examples of nanomaterials, which form an intermediate region between the domain of atomic and molecular physics and that of condensed matter [7]. In a non-interacting cluster of N atoms, there exists N fold degeneracy for each energy level. Interatomic interaction lifts degeneracy. Consequently, these energy levels spread to form a band. In the bulk metal, the details of interaction between individual atoms are less important in comparison with density of states, which decides their properties. However, in the case of nanoparticles, both electron level distribution and density of states determine optical properties. It may be noted that density of states is related to the inverse of energy level spacing averaged over electron level distribution [7]. Though remarkable advances in nanotechnology occurred only in the recent past, the idea of quantum confinement is rather old.

Optical and electrical properties of metal nanoparticles are considerably different from those of the bulk. Unique properties of electrons in nanostructures are due to quantum and dielectric confinement effects, which appear on reduction in the particle size down to nanometer and sub nanometer range. Quantum confinement (QC) increases the spacing between energy levels, which leads to a system of discrete energy levels in an otherwise continuos band. However, QC effects are practically important only if the particle size is of the order of sub nanometer range (<1 nm) [8]. On the other hand, dielectric confinement effects can be observed even in particles of bigger size. In fact, dielectric confinement is present in all the nanoparticles. Condition for dielectric confinement is that particle size should be less than wavelength of light. When particle size is reduced, plasmon frequency of the bulk

metal, which usually occurs in the deep UV region, gets down shifted in energy, to visible or near UV region. This leads to the formation of surface plasmon resonance (SPR) band [8-11]. SPR band is a characteristic feature of metal nanoparticles. In the case of metal nanoparticles optical measurements are particularly sensitive to SPR band, which depends on both the size and collective interaction between individual particles as well as the interaction with the matrix that supports them [7,12]. SPR is the collective mode of oscillations of free electrons in the conduction band, which occupy energy levels immediately above Fermi energy [13]. When particles size is reduced the lattice periodicity is lost and hence the concept of free electrons moving in an infinite and periodic lattice is not fully valid [10]. In semiconductor nanoparticles exciton bands are observed instead of SPR.

In dipole or quasi-static approximation (i.e. if particle size is less than wavelength of incident light), SPR band is independent of particle size [13]. Concept of a particle immersed in a spatially uniform but temporally varying electric field is sufficient to describe behaviour of nanoparticles under this approximation. However, dipole approximation is valid only for small particles (< 30 nm) [14]. In larger particles, size-dependent SPR features are clearly observed. It has been found both experimentally and theoretically that the peak, width and shape of SPR band depend on the size, shape and environment of nanoparticles. SPR band broadening and a red shift of the peak are usually observed with respect to increase in particle size. This observation is in agreement with the concept of limitation of electron mean free path by scattering on the particle surface. Mie theory and Maxwell-Garnet theory explain the SPR peak in terms of higher moment oscillations and particle size [15]. However, in most cases small deviations are observed between theory and experiments. This can be due to fact that conditions assumed in theory, like defect free lattice, are not fully satisfied.

In comparison with bulk materials, nanoparticles posses large surface to volume ratio, which is exploited in many of their spectroscopic and analytical applications. The small size shortens the average diffusion time of charge carriers to migrate on to surface, which leads to an increase in the efficiency and the yield of charge transfer and surface reactions [16]. Besides, at plasmon resonance frequency a large enhancement of local field can be realized. The local field is given by the formula [17]

$$E_i = 3\varepsilon_d(\omega)E_0 / [\varepsilon_m(\omega) + 2\varepsilon_d(\omega)] = f_i(\omega)E_0 \qquad (6.1)$$

where $\varepsilon_m = \varepsilon'_m + i\varepsilon''_m$ is the dieletric constant of the metal particles, ε_d is the dielectric constant of the matrix and $f_i(\omega)$ is the local field factor. Because of enhanced local field and large surface to volume ratio, nanoparticles are widely used for surface enhanced Raman scattering [18], surface second harmonic generation (SSHG) [19] etc. Molecular species adsorbed at surface of nanoparticles exhibit both species and surface specificity, which make selective excitation of adsorbed molecules possible. Therefore adsorbed materials on nanoparticle surfaces are considered to be an ideal specimen to study metal-liquid heterogeneous interface. For example, in the bulk isotropic materials, second order nonlinearity is zero; however, when such molecules are adsorbed on the nanoparticle surface, isotropy is lost and second order effects like SHG is observed, even if the two materials are individually isotropic [20].

Synthetic flexibility of organic materials can also be incorporated in nanoparticles by modifying their surface appropriately with suitable methods. Synthetic flexibility in metal nanoparticles can be achieved by forming an organic thin film on them [21] by dipping nanoparticles in suitable chemical reagent. These unimolecular organic films are called self-assembled monolayers (SAMs). Formation of SAMs is an easy route for surface functionalization with both appropriate aromatic and aliphatic organic

units. SAMs are also useful in the design of molecular assemblies, capable of performing electronic functions such as switching, gating and logic operations. If a single molecule can perform electronic operations, its size makes it possible to utilize 10^{13} units cm^{-2} in comparison with present level of 10^8 units cm^{-2}. Therefore, proposed nanodevices consisting of single molecules can enhance the memory capacity tremendously. Biological compounds like DNA can also be attached to nanoparticles making the way for bio-photonics rather easy. SAMs are formed by chemiadsorption of organic films on nanoparticle surface and hence they are thermodynamically more stable than physi-adsorbed layers. SAMs are also protective in nature. Nanoparticles are isolated from the surroundings by SAMs and thus growth and agglomeration by air oxidation and other forms of degradation are prevented. However, there is a limitation that SAM can be formed only on the surface of certain substrates like Au, Ag, Pt , Cu, GaAs. There are also constraints on the choice of anchoring group [22].

Most of the applications of nanoparticles make use of their nonlinear and spectroscopic properties. Hence investigation of NLO properties of nanomaterials is very relevant. Nanoparticles have been used in ultrafast switching [23], data storage [24] and optical limiting [25]. In this chapter, nonlinear absorption and refraction in a representative noble metal nanoparticle (silver nanosol) is investigated using Z-scan technique. Nonlinear optical properties of nanoparticles arise because of the SPR. There are two possible contributions to nonlinear properties of metal nanoparticles [10]. They are (1) interband transitions from filled d–states to conduction band, (2) intraband transitions of electron in the conduction band. However, in silver nanoparticles interband transition frequency is outside the SPR band (above 4eV) and therefore, the contribution from interband transitions to nonlinearity can be neglected. As far as silver nanoparticles are concerned, main contribution to optical properties is from intraband transition.

124

2. Sample preparation and characterization

Silver nanosol was prepared by standard reduction technique, which is also called hydrosol method [7]. This method is well suited for the preparation of silver nanosol, which is an aqueous solution of silver nanoparticles. For sample preparation, 10 ml of 1 mM $AgNO_3$ solution was added drop wise to 30 ml of 2.0 mM $NaBH_4$ solution. The solution was stirred well and was kept at a temperature of zero degree. The sample was characterized by spectroscopic method. The absorption spectrum of the sample is shown in fig. 1. SPR peak was observed at 416 nm.
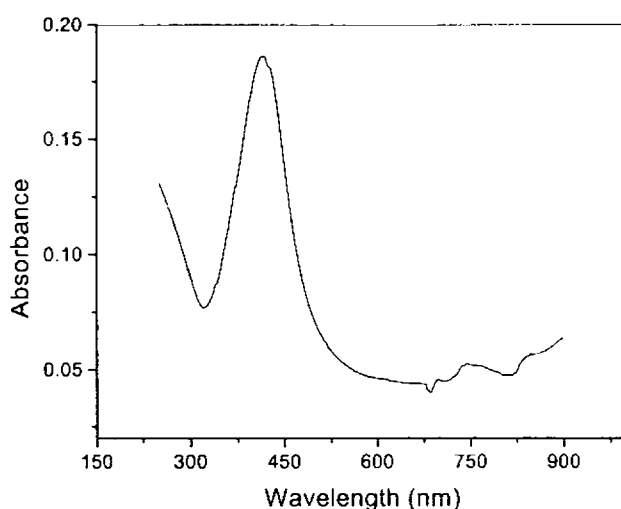

Fig. 1. Absorption spectrum of silver nanosol

The SPR peak of silver nanoparticles mentioned in many other previous reports is around 420 nm. P V Kamat et. al [15] reported SPR peak of silver nanoparticles produced by reduction technique using sodium citrate as 420 nm. Ya– Pin Sun et. al [23] has also observed SPR peak for silver nanoparticles around 420 nm. Our observation is consistent with these results. In the case of gold nanoparticles, the SPR peak occurs around 520 nm [13]. Typical size of silver nanoparticles formed by sodium citrate reduction technique is about 40-60 nm [15]. Roberti et. al [16] have synthesized the silver nanosol using silver nitrate and sodium borohydride at zero

temperature. They could obtain the silver particles of average size of 10 nm with an SPR peak around 390 nm. They could also obtain nanoparticles of around 4 nm size with a SPR peak at 400 nm by varying the rate of reaction. It is interesting to note that Roberti et. al [16] observed a marginal blue shift of SPR peak with increasing particle size, which was attributed to the environment of nanoparticles. The width of SPR band was attributed to coupling of plasma oscillations to individual electronic states and also to non-uniform particle size distribution. There are several other methods to synthesis nanoparticles, like ion implantation. Out of them, hydrosol method produces particles of lower size [7].

3. Experimental

Wavelength dependence of nonlinear absorption in silver nanosol is the theme of our interest. Therefore, open aperture Z-scan experiments were carried out at three selected wavelengths near SPR band, which include 456 nm, 477 nm and 532 nm. It can be seen that 456 nm is well inside the SPR band, 477 nm is on the edge of the SPR band and 532 nm is outside the SPR band. Hence, nonlinear absorption in three different regions of SPR band is investigated. Closed aperture Z-scan measurements were also carried out at 532 nm. Measurements at 532 nm were taken with second harmonic of Nd: YAG laser while the measurements at other two wavelengths were taken using a MOPO.

4. Electron dynamics in metal nanoparticles

With femtosecond and picosecond pulses, it is possible to study in real time the electron dynamics taking place in metal nanoparticles following laser excitation. Electron dynamics refers to processes involving excitation of electrons due to laser irradiation and subsequent thermalization. There are several techniques to study electron dynamics such as laser flash photolysis and transient reflectivity measurements. Among the different types of nanoparticles, electron dynamics in noble metal nanoparticles like Ag and Au as well as Au-Ag alloy has been studied in

126

detail by earlier researchers. Their results are very relevant in the context of present measurements. Roberti et. al [16] have studied electron dynamics in aqueous silver colloid using femtosecond pulses. Kamat et. al [15] have investigated electron dynamics in aqueous silver using picosecond pulses. Picosecond dynamics of colloidal gold nanoparticles has been investigated by Ahmadi et. al [13]. Electron dynamics in silver–gold alloys has been investigated by Link et. al [12]. It can be said that fairly good understanding of electron dynamics in noble metal nanoparticles evolved from these investigations.

An advantage of metal nanoparticles is that we can separate electron and lattice specific heat capacities. The concept that electron and lattice specific heat capacity can be separated forms the foundation of two-temperature model (TTM) [12,13]. The electronic heat capacity is less than lattice heat capacity and hence, electrons can be selectively excited without heating the lattice. Let T_i, T_e, and T_l be the initial temperature, the electronic temperature and the lattice temperature respectively. Before laser excitation, $T_i = T_e = T_l$ and hence system is in fairly good thermodynamic equilibrium and hence electrons have a Fermi distribution. When nanoparticles are irradiated with laser pulse the SPR band gets excited and higher order (quadrupole, octopole etc) oscillations are induced, in addition to dipole oscillations. These oscillations can couple with the applied electric field through the surface. The electrons that are excited possess energy higher than Fermi energy and are called hot electrons. Hot electrons have a non-thermalized, non-Fermi distribution [12]. During this process, electrons can occupy higher energy levels of conduction band. Consequently, SPR frequency of excited atoms differs from that of unexcited atoms. A higher temperature results in broadening of the plasmon band and a decrease in its intensity. The consequence is that SPR band can no longer absorb around the peak of original SPR, which leads to SPR bleach [13,15]. Fig. 2 shows the typical plasmon bleach in gold nanoparticles, reproduced from ref. [13]. Spectrum of plasmon bleach (solid line in fig.2) is a mirror image of plasmon band (dashed line in

fig. 2). Kamat et. al. [15] have investigated energy dependence of plasmon bleach for silver nanoparticles, using picosecond pulses, at 355 nm. For lower energy values, a plot of differential absorption against incident energy gave a straight line with slope one. This indicates that plasmon bleach is a mono photonic process. Bleaching of the absorption occurs in ultrafast. time scale and is accompanied by the appearance of broad transient absorption on red and blue side of the bleached region.
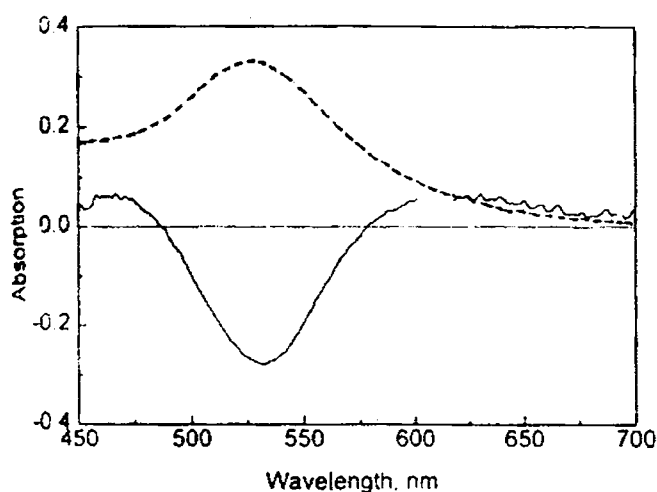

Fig. 2 Plasmon bleach in gold nanoparticles (reproduced from ref.[13])

Dotted line: plasmon band; solid line: plasmon bleach

Hot electrons get subsequently thermalized by dissipating excess energy through successive processes of electron–surface scattering, electron-electron scattering, electron-phonon scattering [10-13,15,16]. Fermi liquid theory says that electron – electron scattering rate is proportional to the square of the energy difference between the excited state and Fermi energy. It is possible to achieve different non-thermal (non Fermi) distribution by changing the wavelength of excitation. Scattering rate is higher for highly excited electrons, greater number of energy levels are available for these electrons in momentum space. Similarly scattering rate is very low for an electron distribution, close to Fermi level. Exact time scales of all these phenomena
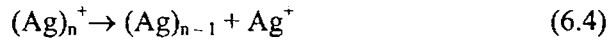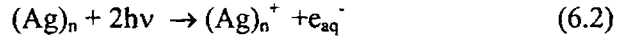
may vary according to type and environment of nanoparticles. During thermalization process heat energy is eventually transferred to the surrounding medium viz., solvent in the case of nanoparticle solutions and substrate in the case of nanoparticle films.

Excess thermal energy can increase the temperature of surrounding medium, which in turn influence the SPR. Full recovery of plasmon bleach is delayed and transient absorption is observed until the process of thermalization of hot electrons is complete. The electron-electron scattering is very fast and occurs in sub picosecond time scale. Depending on the experimental conditions as well as on the type of nanoparticles, the broad transient absorption may consist of two components with different time scales viz. a fast picosecond component and a comparatively slow one lasting for a few nanoseconds. For example, in gold nanoparticles, recovery of plasmon band takes place in a time scale slightly greater than 50 picoseconds with a double exponential kinetic fit, consisting of two temporal components (2.5 ps and $\approx$ 50 ps) [13]. In the case of silver nanoparticles, transient absorption often satisfies a double exponential fit with a fast (100 ps) and a slow (1.5 ns) components for transient absorption, probed at 440 nm after exciting with 355 nm [15]. However, only longer component was observed when transient absorption was probed with 600 nm. Transient absorption spectra measurements on silver nanoparticles have shown that though strong bleaching of the plasmon band occurs in sub nanosecond time scale, full recovery of plasmon bleach is delayed up to a few nanoseconds ($\cong$ 2 ns) [15]. Component of transient absorption present in picosecond time scale is due to broad transient absorption taking place on red and blue side of bleached region of SPR.

The component of transient absorption taking place in nanosecond time scale is mainly due to photochemical change induced absorption occurring in the sample as a result of photo-ejection of electrons on laser irradiation. Photo-ejection of electrons is a multi photon process. The ejected electrons can charge the nanoparticle surface electrically, leading to aggregation, which results in a transient state (Ag^+e^-), through

photo-induced intraparticle charge separation [15]. During this transient period, aggregation can occur leading to formation of large nanoparticle clusters with very broad plasmon band. All these processes take place in nanosecond time scale. These phenomena also result in transient absorption. Study of energy dependence of transient absorption occurring, in longer time scale has been described in ref [15]. They got a straight line with a slope equal to two which indicated that that photo-ejection of electrons is a two-photon process. Some possible chemical reactions occurring in the samples are given below.

$$(Ag)_n + 2h\nu \rightarrow (Ag)_n^+ + e_{aq}^- \qquad (6.2)$$

$$(Ag)_n^+ + e_{aq}^- \rightarrow (Ag)_n \qquad (6.3)$$

$$(Ag)_n^+ \rightarrow (Ag)_{n-1} + Ag^+ \qquad (6.4)$$

Eq. (6.1) shows the photo ejection of electron through a two-photon process. Some of the silver ions thus generated can undergo recombination and this is shown in eq. (6. 2). Remaining silver ions can form aggregates.

Besides, ejection of electrons creates holes, which act as free carries and effect free carrier absorption (FCA). It may thus be noted that slow component (ns) of transient absorption is due to FCA and photochemical change induced absorption, while the fast (ps) component is due to thermalization of hot electrons. Optical limiting property of silver as well as in silver halides nanoparticles under nanosecond excitation were explained based on the slow component [26,27]. The results obtained in the present experiment are explained considering the SPR band bleach, photochemical change induced absorption and particle size–selective excitation.

5. Results and discussion

Plots "a" and "b" in fig.3 show the open aperture Z-scan curves obtained at 532 nm for fluence values (at focus) of 0.08 Jcm^{-2} and 0.5 Jcm^{-2} respectively. Plot "a"

corresponds to reverse saturable absorption (RSA) whereas plot "b" indicates saturable absorption (SA). Obviously as energy is increased, RSA changes to SA. RSA (plot "a" in fig. 4) can be due to enhanced absorption resulting from photochemical change induced absorption. FCA is also an alternative mechanism for RSA. However, since present system of nanoparticles is uncapped, there is greater probability for photochemical changes. Since SA is observed for fluence values higher than those corresponding to RSA, it is attributed to saturation of RSA. It has been shown in earlier reports that SA can occur when RSA gets saturated [28,29].
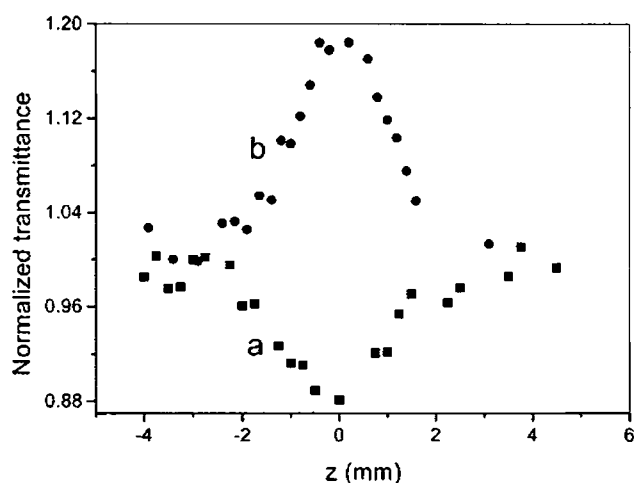

Fig. 3. Open aperture Z-scan graphs at 532 nm

a. 0.2 Jcm^{-2}; b. 0.5 Jcm^{-2}

Fig. 4 shows the open aperture Z-scan curves obtained at 477 nm for fluence values (at focus) of 0.08 Jcm^{-2} and 0.44 Jcm^{-2}. In Z-scan experiments, fluence is a maximum at the focus and it continuously decreases in regions away from the focus. Therefore, plot "a" in fig. 4 indicates that for lower values of fluence, the sample exhibits SA, but as fluence is increased, SA changes to RSA. In this case, SA takes place for lower values of fluence than those corresponding to RSA and hence SA observed is of different origin from the case observed at 532 nm. In the present case, SA can be due

to SPR bleach. SA has been observed for lower values of fluence than those corresponding to RSA previously, in Z-scan experiment [16]. RSA, as in the case of 532 nm, is attributed to enhanced absorption due to photochemical changes.
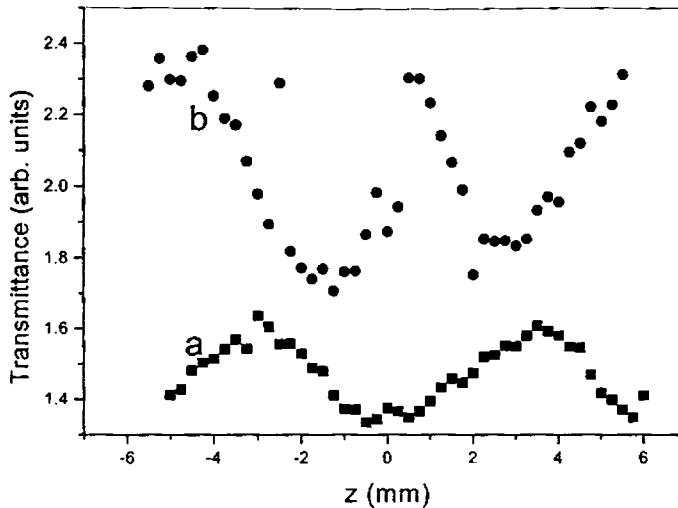

Fig. 4. Open aperture Z-scan curves at 477 nm

a. 0.08 Jcm^{-2}; b. 0.44 Jcm^{-2}

Each point in plot "b" of fig. 4 corresponds to a fluence value, about five times higher than that of plot "a". It is interesting to note that plot b is a mirror image of plot a. SA observed in plot b around the focus occurs for higher fluence values after the observation of RSA and hence it arises due to saturation of RSA. From fig. 4 it is evident that both the SA and RSA are very sensitively dependent on input fluence. Hence the plots in fig. 4 were not normalized to linear transmittance. Fig. 5 shows the open aperture Z-scan curves obtained for a fluence value of 0.22 Jcm^{-2} at focus. In this case only SA is observed.

Plots a, b and c of fig. 6 shows the open aperture Z-scans curves obtained at 456 nm for input fluence (at focus) of 0.1 Jcm^{-2}, 0.2 Jcm^{-2} and 0.6 Jcm^{-2} respectively. SA, in

132

plot "a" of fig. 6, corresponds to lower values of fluence than those corresponding to RSA. Therefore, SA observed here could be due to plasmon bleach.
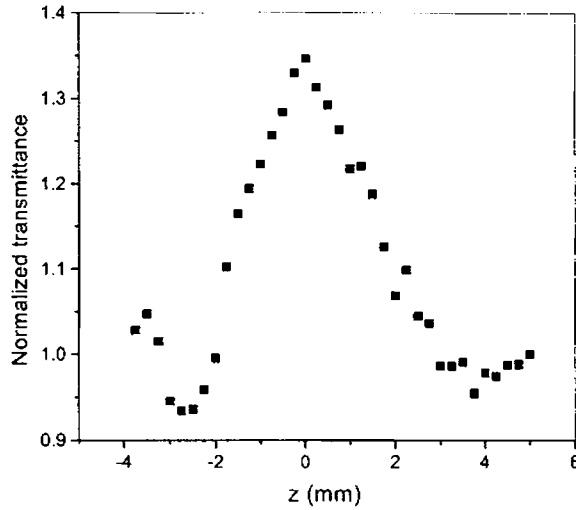

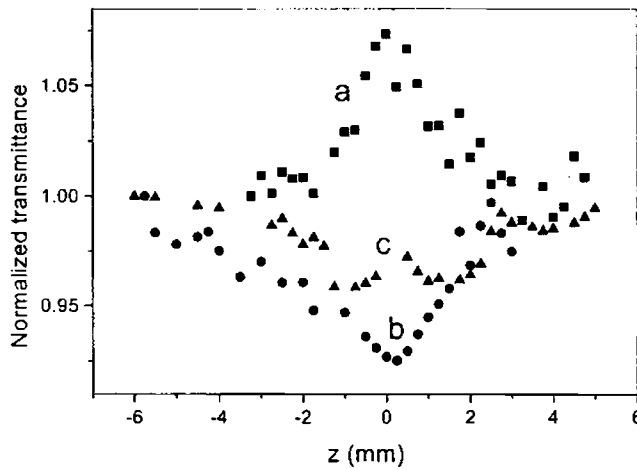Fig. 5. Open aperture Z-scan curve at 477 nm (0.22 Jcm^{-2})

Fig. 6 Open aperture Z-scan curves at 456 nm
a. 0.1 Jcm^{-2}; b. 0.2 Jcm^{-2}; c.0.6 Jcm^{-2}

When fluence is increased to 0.2 Jcm^{-2} SA changes to RSA, which can be attributed to enhanced absorption resulting from photochemical changes. When fluence is further increased to 0.6 Jcm^{-2} a clear sign of emergence of SA is observed at focus, which can be due to saturation of RSA. General hehaviour of nonlinear absorption at both 456 nm and 477 nm remains the same. Therefore SA observed here could be due to plasmon bleach. When fluence is increased to 0.2 Jcm^{-2} SA changes to RSA, which can be attributed to enhanced absorption resulting from photochemical changes. When fluence is further increased to 0.6 Jcm^{-2} a clear sign of emergence of SA is observed at focus, which can be due to saturation of RSA. General hehaviour of nonlinear absorption at both 456 nm and 477 nm remains the same.

A comparison of figures 3, 4, 5 and 6 yields the following important results; (1) no plasmon bleach was observed at 532 nm. 532 nm is out side the SPR band and hence probability for plasmon bleach can be less; (2) dynamic range of RSA at 477 nm is considerably less than those at 456 nm and 532 nm; (3) threshold level for plasmon bleach, as well as for RSA is very low at 477 nm in comparison with 456 nm. Observed lower threshold for plasmon bleach at 477 nm may be explained if we assume that there is close correspondence between SPR band and number density of particles with specific size. Results of picosecond electron dynamics studies carried out by Kamat et. al [15] show that when silver nanoparticles were excited with 355 nm, plasmon bleach observed was a mirror image of normal SPR spectrum. However, when the same sample was excited with 532 nm, plasmon bleach was observed around 532 nm and in the region of original plasmon band (around 420 nm) broad transient absorption was observed. This observation is a very clear indication of size selective excitation of nanoparticles by varying the wavelengths. Similar results have also been observed in the study of electron dynamics in gold nanoparticles described in ref [13]. Number density of nanoparticles that are excited at 456 nm can be higher than that excited at 477 nm. Consequently, number of photons (greater fluence) may be required for plasmon bleach to occur at 456 nm. However, it must be

said that plasmon bleach was not observed at 532 nm in the present experiments even though such results have been observed under picosecond excitation by some earlier researchers [28]. The reason for very low threshold as well as dynamic range of RSA at 477 nm is not clear from the present measurements. Further studies under picosecond and femtosecond excitations may be required in this direction to reach definite conclusions.

In nanoparticle systems, nonlinear scattering is a viable alternative process that can mimic nonlinear absorption. Optical limiting due to nonlinear scattering has been reported in gold nanoparticles. Nonlinear scattering is a size dependent mechanism. Francois et. al [30] have observed that particles of bigger size are better optical limiters. Strong optical limiting property due to nonlinear scattering has also been reported in carbon black suspension (CBS). In CBS, optical limiting is due to nonlinear scattering by the micro plasma generated at the focal region. In CBS optical limiting property has been observed only under nanosecond excitation [31,32]. Under picosecond excitation, micro plasma generated will not expand sufficiently to scatter incident light to effect optical limiting. In the context of measurements mentioned here, fluence dependent switching between SA and RSA observed at nearly all the wavelengths of excitation indicates that nonlinear scattering is highly unlikely.

Fig. 7 and fig. 8 show the nonlinear transmission for silver nanosol at 532 nm and 456 nm respectively. The fluence level for optical limiting at both 532 nm and 456 nm is around 0.17 Jcm^{-2}. Limiting threshold of silver nanoparticles in POP polymer stabilized ethanol suspension has been reported to be 0.18 Jcm^{-2}. Similarly, limiting threshold of AgS nanoparticles was found to be around 0.23 Jcm^{-2} [26]. The limiting threshold reported and those obtained from our measurements are in fairly good agreement. Optical limiting property was found to be high in silver nanoparticles as well as in other silver containing nanoparticles (e.g. AgS).
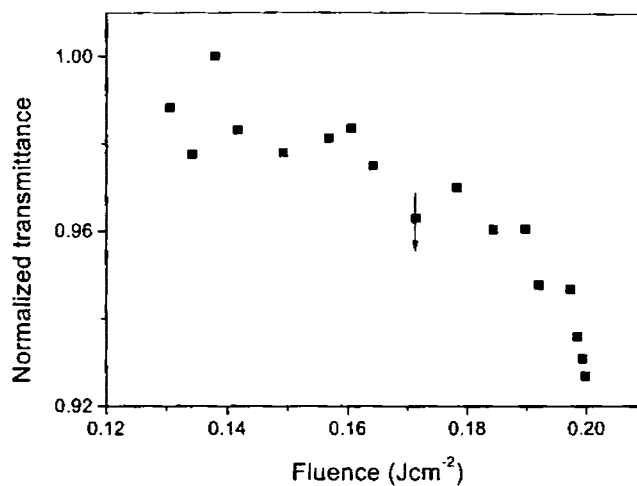
Fig. 7. Nonlinear absorption in silver nanosol (456 nm)
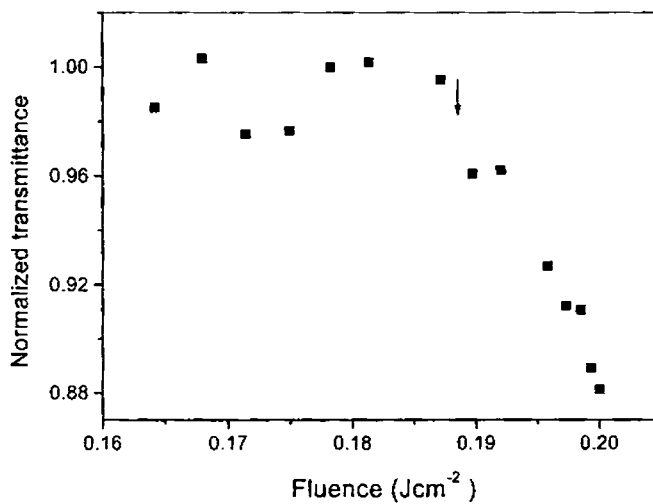
(Arrow indicates the threshold region)

Fig 8. Nonlinear absorption in silver nanosol (532 nm)

(Arrow indicates the threshold region)

6. Closed aperture Z-scan measurement

Closed aperture measurements were carried out in silver nanosol at 532 nm to know whether nonlinear refraction is present. Fig. 9 shows the divided Z-scan graph obtained at 532 nm. [Divided Z-scan curve is obtained when closed aperture Z-scan curve is divided by open aperture Z-scan curve]. Fig. 9 shows that there is no significant change from linear transmittance, which indicates that the sample does not exhibit nonlinear refraction, either positive or negative. Absence of negative nonlinearity implies that there is no thermal lensing effect in the sample.
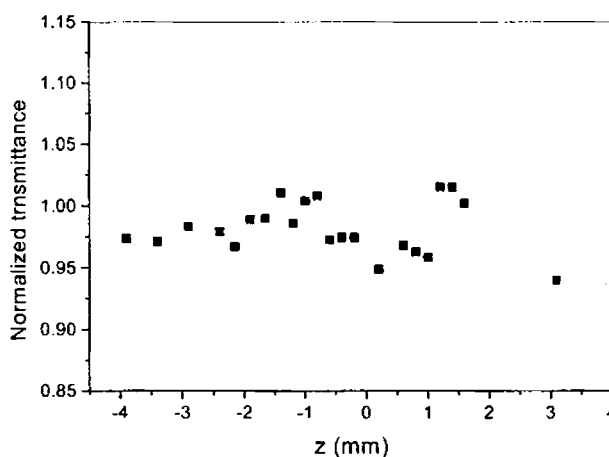

Fig. 9. Divided Z-scan curve (532 nm)

Absence of thermal lensing effect can be due to very low linear absorption at 532 nm. Since the wavelength of excitation is far away from plasmon resonance, there might be positive nonlinear refraction due to electronic contribution. The absence of positive nonlinear refraction in the measurements may be due to the fact that most of part of thermalization process occurs in the picosecond time scale. Detailed studies under picosecond and femtosecond excitations are required to arrive at definite conclusions.

It may be relevant to mention important works in nanoparticles other than optical limiting studies. One of such reports is four-wave mixing in silver nanoparticles around SPR region [33], where $\chi^{(3)}$ spectrum was found to follow the SPR band. Other such reports include degenerate four wave mixing studies in colloidal gold [14] as well as copper and gold in the glass matrix [17] as a function of particle size.

7. Conclusions

Nonlinear absorption in silver nanosol was investigated at selected wavelengths (456 nm, 477 nm and 532 nm) in the red side of the SPR peak using nanosecond pulses. Results were explained taking into account electron thermalization processes and plausible photochemical changes which could occur in the sample on laser irradiation. An interesting observation is that the sample can act as a saturable absorber as well as a reverse saturable absorber at the same wavelength entirely depending on incident laser fluence. This is an important observation because unlike the present sample, organic NLO materials very rarely show SA and RSA at the same wavelength. Besides, at certain wavelengths (e.g. 477 nm) mechanism of nonlinear absorption was found to be very sensitive on laser fluence. General trend of nonlinear absorption is that as incident fluence is increased, the sample first exhibits SA, then RSA and finally saturation of RSA giving rise to SA. SA occurring at lower values of fluence (than those corresponding to RSA) is attributed to the bleaching of plasmon band. RSA is attributed to enhanced absorption resulting from photochemical changes occurring in the samples. RSA can take place due to FCA as well, but present systems of nanoparticles are uncapped and hence possibility is higher for photochemical change induced absorption. Closed aperture Z-scan measurements were also carried out in at 532 nm, but it did not reveal any sign of nonlinear refraction. Absence of nonlinear refraction may be due to the fact that the process is too fast to be observed under nanosecond excitation. Detailed investigation under picosecond and femtosecond excitation is required in this direction.

138

References

[1] W C Huang and J T Lue. Phys. Rev. B **49** (1994) p. 17279

[2] P Pell and D R Penn. Phys. Rev. Lett. **50** (1983) p.1316

[3] E J C Dawnay, M A Fardad, M Green and E M Yeatman. J. Mater. Res. **12** (1997) p. 3115

[4] P Chen, X Wu, X Sun, J. Lin, W Ji and K L Tan. Phys. Rev. Lett. **82** 12 (1999) p. 2548

[5] M Bockrath, D H Cobden, P L McEuen, N G Chopra, A Zettl, A Thess and R E Smalley. Science **275** (1997) p. 1922

[6] C N R Rao and A Govindaraj. Proc. Indian Acad. Sci. (Chem. Sci.) **113** (2001) p. 375

[7] W P Halperin. Rev. Mod. Phys. **58** (1986) p. 533

[8] S. Stagira, M Nisoli, S De Silvestri, A Stella, P Tognini, P Cheyssac, R Kofman Chem. Phys. **251** (2000) p. 259

[9] Gunter Schmid and Lifeng F Chi. Adv. Mater. **10** (1998) p. 515

[10] N D Fatti, F vallee, C Flytzanis, Y Hamanaka, A Nakamura. Chem. Phys. **251** (2000) p. 215

[11] J Y Bigot, V Halte, J C Merle, A Daunois. Chem. Phys. **251** (2000) p.181

[12] S Link, C Burda, Z L Wang and M A El-Sayed. J. Chem. Phys. **111** (1999) p. 1255

[13] T S Ahmadi, S L Logunov and M A El-Sayed. J. Phys. Chem. **100** (1996) p.8053

[14] M J Bloemer, J W Haus and P R Ashley. J Opt. Soc. Am. B 7 (5) (1990) p. 790

[15] P V Kamat, M Flumiani and G V Hartland. J. Phys. Chem. B **102** (1998) p.3123

[16] T W Roberti, B A Smith, and J Z Zhang. J. Chem. Phys. **102** (9) (1995) p. 3860

[17] K Uchida, S Kaneko, S Omi, C Hata, H Tanji, Y Ashahara and A J Ikushima. J. Opt. Soc. Am. B 11 (1994) p. 1236

[18] Shuming Nie and S R Emory. Science **275** (1997) p. 1102

[19] S Chen. J. Phys. Chem. B **104** (2000) p. 663

[20] R Antoine, P F Brevet, H H Girault, D Bethell and D Schiffrin. Chem. Commun (1997) p. 1091

[21] R Antoine, M Pellarin, B Palpant, M Broyer, B Prevel, P Galletto, P F Brevet and H H Girault. J. Appl. Phys. **84** (1998) p. 4532

[22] N K Chaki, M Aslam, J Sharma, K Vijayamohan. Proc. Indian Acad. Sci. (Chem. Sci.) **113**. (5 & 6) (2001) p. 659

[23] H Inouye, K Tanaka, I Tanahashi, and H Nakatsuka. Jpn. J. Appl. Phys. **39** (2000) p. 5132

[24] H Ditlbacher, J R Krenn, B Lamprecht, A Leitner and F R Aussenegg. Opt. Lett. **25** (2000) p. 563

[25] M R V Sahyun, S E Hill, N Serpone, R Danesh and D K Sharma. J. Appl. Phys. **79** (1996) p. 8030

[26] Y P Sun, J E Riggs, H W Rollins and R Gurudu. J. Phys. Chem. B **103** (1999) p. 77

[27] M Y Han, W Huang, C H Chew and L M Gan. J. Phys. Chem. B **102** (1998) p. 1884

[28] R Philip, G R Kumar, N Sandyarani and T Pradeep. Phys. Rev. B. **62** (2001) p. 481

[29] X Deng, X Zhang, Y Wang, Y Song, S Liu and C Li. Opt. Commun. **168** (1999) p. 207

[30] L Francois, M Mostafavi, J Belloni, J F Delouis, J Delaire and P Feneyrou. J. Phys. Chem. B. **104** (2000) 6133

[31] K Mansour, M J Soileau, and E W V Stryland. J. Opt. Soc. Am. B 9 (7) (1992) p. 1100

[32] Y P Sun, J E Riggs, K B Henbest and R B Martin. J. Nonl. Opt. Phys. Mater. **9** (2000) p. 481

[33] D Faccio, P Di Trapani, E Borsella, F Gonella, P Mazzoldi and A M Malvezzi. Europhys. Lett **43** (1998) p. 213

7

Conclusions and future prospects

1. Conclusions

Materials that are very useful for light based applications such as optical switching, data storage, optical limiting, frequency conversion are collectively called photonic materials. Most of the technological applications exploit nonlinear NLO properties of these materials in one way or other. Hence, investigation of NLO properties of different types of photonic materials becomes important in the frontier area of research. In this context, study of NLO properties certain photonic materials, which include organic systems and nanostructures, were chosen as the topic of the research work.

Metal substituted phthalocyanines (MPcs), naphthalocyanines (MNcs) and silver nanosol are the materials chosen for the present studies. Third order nonlinear optical properties of these materials were investigated using degenerate four wave mixing (DFWM) and Z-scan techniques. Pcs and Ncs are organic semiconductors. Nonlinear absorption and optical limiting properties of the samples were investigated using open aperture Z-scan technique. Second hyperpolarizability $\langle \gamma \rangle$ of Pcs and Ncs were obtained from DFWM. Some of the essential requirements of good photonic materials are large and fast acting nonlinearity, synthetic flexibility and ease of processing. It is noteworthy that Pcs and Ncs satisfy many of these requirements. Large and fast responding nonlinearity of organic materials comes mainly from the presence of delocalized π electrons. On the other hand, surface plasmon resonance (SPR) band determines the optical properties of silver nanosol. Linear and nonlinear

optical properties of silver nanosol are totally different from those of organic compounds. Thus two distinct classes of materials were studied for their nonlinear optical properties.

Interest in nonlinear absorption of Pcs at 532nm arises from the fact that these samples have potential applications as passive optical power limiters for sensor and human eye protection against laser irradiation. Optical limiting refers to a phenomenon in which the throughput of the sample remains constant beyond certain threshold input fluence level. Excited state absorption (ESA) is the mechanism of nonlinear absorption in Pcs and Ncs at 532 nm. Wavelength dependence of nonlinear absorption of certain bis-Pcs was also carried out in the blue side of the absorption peak of the Q-band. Studies on wavelength dependence of nonlinearity are not commonly reported. Application of these materials as broad band passive optical power limiters also requires knowledge of wavelength dependence of nonlinear absorption. Besides, these studies also gave some important results regarding the extent of resonant enhancement of $Im[\chi^{(3)}]$ in the selected samples. The wavelength region in which the mechanism of nonlinear absorption changes from reverse saturable absorption to saturable absorption was also identified.

Second hyperpolarizability $\langle\gamma\rangle$ is a microscopic parameter and it gives the magnitude of third order polarizability of molecules. $\langle\gamma\rangle$ values of various molecules depend on a number of structural and spectral parameters of the sample. Some of the parameters relevant in the context of Pcs and Ncs are (1) the extent of electron conjugation, (2) nature of metal substituents and (3) effect of axial and peripheral substituents. $\langle\gamma\rangle$ values were measured for a number of metal substituted Pcs and Ncs, having different structures, using DFWM techniques. This work was partly motivated by the interest to investigate the combined influence of many of the above mentioned factors on third order nonlinearity. Secondly, third harmonic generation (THG) experiment performed in certain samples like VONc by earlier researchers indicated some

interesting results. Measurements made using DFWM reported here were helpful to know whether such interesting results, reported by earlier researchers from THG measurements, reappear in DFWM as well, as these two processes are fundamentally different.

Nanomaterials are relatively new class of photonic materials. Such materials have unique properties that are different from those of the bulk. Nonlinear absorption of silver nanosol (aqueous solution of silver nanoparticles) was studied at well-chosen wavelength near surface plasmon resonance (SPR) and results obtained were explained in terms of the electron dynamics and enhanced absorption arising from plausible photochemical changes. The sample was prepared by reduction technique using silver nitrate and $NaBH_4$. SPR peak of the sample was observed to be at 416nm. This study was motivated by the fact that many of the previous nonlinear absorption studies carried out in silver and other nanomaterials are mainly confined to 532nm. During the course of these measurements, it was observed that the silver nanosol could act as reverse saturable absorber and saturable absorber at the same wavelength depending entirely on the input fluence.

2. Future prospects

In the context of technological applications, organic–inorganic hybrid systems, i.e. organic materials – nanomaterials composite, have been identified to be promising class of photonic materials. Hybrid materials do posses the synthetic flexibility of organic compounds. Recently, these hybrid systems have been identified to be essential ingredient of nanodevices. Good deal of work is being carried out the world over in this area. For a better understanding of fundamental mechanism and evolution of nonlinearity, time resolved measurements, laser flash photolysis experiments etc under picosecond and femtosecond excitations are required in many of the photonic materials.

G 8 5 12